

## The Composition of Liquids from Coals of Different Rank

G. P. Sturm, Jr., J. E. Dooley, J. S. Thomson,  
P. W. Woodward, and J. W. Vogh

U.S. Department of Energy, Bartlesville Energy  
Technology Center, P. O. Box 1398  
Bartlesville, Oklahoma 74003

### INTRODUCTION

Eight coal liquids prepared from six coals (9,10) of widely differing rank were characterized by procedures previously developed for petroleum (3,4,7) and by ASTM methods. The liquids were prepared and upgraded by hydrogenation in a batch autoclave under conditions intended to minimize cracking of the hydrocarbons (especially those of cyclic and aromatic structure) and yet produce most of the liquid hydrocarbons potentially obtainable from a given coal. The extent of the hydrogenation/hydrogenolysis (henceforth referred to as hydrogenation) of the raw coal liquids was adjusted as required to decrease the nitrogen content to about 0.2 to 0.3 weight-percent with the additional intent of providing a predominantly hydrocarbon liquid for analysis. Details of the coal liquid preparations have been reported previously (9,10). This report covers the characterization of the coal liquids and possible implications in relation to refining.

Among the many reports in the literature on coal liquefaction, several indicate a relationship between the rank of the coal and the complexity of the hydrocarbon groups in the coal and in its liquefaction products. This subject was reviewed in some detail in our previous reports (9,10) and will only be summarized and updated here. Early German work indicated that the lower-rank brown coals (lignite) were more reactive, requiring less hydrogen pressure, and produced smaller polynuclear hydrocarbon units (18) than bituminous coals. Also, the asphaltene content of the coal liquids decreased with the coal rank to a minimum for sub-bituminous coals. Early work by the U.S. Bureau of Mines produced similar results (14). Low rank coals were found to be so reactive that, at a reaction temperature of 430° C, high hydrogen pressure was required to prevent repolymerization of reactive fragments to coke. More recent studies have shown that the product from the liquefaction of a Utah sub-bituminous coal with hydrogen donor solvent (6) contained less benzene insoluble material than that from Pittsburgh bituminous coal.

Although the literature suggests that the complexity of hydrocarbon groups in coal and coal liquefaction products can differ substantially with the rank of the coal, specific data are sketchy and sometimes appear to be contradictory. A recent report on the comparison of solvent-refined lignite and solvent-refined sub-bituminous and bituminous coals (2) indicates hardly any difference among the products in terms of gross combustion analysis, acid and basic titres, molecular weight, and nuclear magnetic resonance, ultraviolet and electron spin resonance spectra. Only the nitrogen content of the coal was reflected in the solvent-refined products. However, in another recent study of a lignite, a bituminous coal, and an anthracite coal, analysis of the organic compounds trapped in the coals and contained in the products of selective oxidation indicated an increased condensation of aromatic rings with increasing rank (8). Analysis was performed by gas chromatography/time-of-flight mass

spectrometry and high resolution mass spectrometry. Furthermore, an extensive, detailed study revealed compositional differences in the pyridine extracts of three coals of different rank and also in their liquefaction products produced by the Synthoil process (1). For example, larger quantities of saturates and higher percentages of lower ring number saturate compound types were observed in the two higher rank coal extracts. However, the ring distributions of the aromatic fractions from the coal extracts indicated slightly higher average ring numbers for the higher rank coals.

Similar results were obtained in a study characterizing liquid products obtained from six coals of different rank by treatment of the coals with NaOH-alcohol for one hour at 300° to 350° C (11). Characterization by elemental analysis, molecular weight determination, and proton NMR indicated that the younger (lower-rank) coals gave simpler products with primarily tetralin-type nuclei and more abundant ether linkages than the higher rank bituminous coals which yielded products with five to six rings, about two of which were naphthenic. Similarly, in Japanese studies of pyridine extracts of coals of different rank (17), analysis by proton NMR indicated more condensed aromatic rings with less substitution and shorter aliphatic chains in the higher rank coal extracts. Extracts from bituminous coals contained an average of four or five aromatic rings with side chains averaging three or four carbons in length, whereas a lignite extract had an average of one or two aromatic rings with seven- or eight-carbon, aliphatic side chains. Finally, a study using carbon-13 NMR to characterize a hard-coal-tar pitch and a brown-coal-tar pitch indicated a predominance of fused aromatic ring systems with small amounts of methyl and hydroaromatic methylene groups for the hard-coal-tar pitch (5). The results for the brown-coal-tar pitch indicated primarily long, straight-chain aliphatics estimated at 25 to 40 carbon atoms in length.

The coal liquids characterized at the Bartlesville Energy Technology Center to date have come from different projects in which the primary objective was the development of a specific process. This precluded a systematic study of the relationship of coal rank to coal liquid composition, which is the objective of this study.

#### EXPERIMENTAL PROCEDURES

The upgraded coal liquids were distilled with a metal-mesh-spinning-band still under vacuum to produce cuts at 200°, 325°, and 425° C. Asphaltenes were then precipitated from each >425° C residuum dissolved in benzene by addition of 50 volumes of normal pentane (12). Further distillations on the asphaltene-free materials, at 202° C and 4 micron pressure using a wiped-wall molecular still, produced 425°-540° C distillate cuts and residua fractions. After removal of acids and bases from the <200° C distillates by extraction methods (16), an additional chromatographic separation with silica gel provided a check for the presence of olefins. No olefins were detected; thus, the acid- and base-free distillates were analyzed by ASTM D2789-71, Standard Method of Test for Hydrocarbon Types in Low Olefinic Gasoline by Mass Spectrometry.

The higher-boiling distillates were characterized by methods adapted from the characterization of heavy ends of petroleum (3,7). A schematic of the procedure is depicted in Figure 1. Details of the procedures have been reported previously (3,7,15,16). Analyses of subfractions of aromatic concentrates separated by gel-permeation chromatography (GPC) were performed on a low-resolution CEC 21-103 C

mass spectrometer (MS) using low-ionizing energy electrons to produce predominantly molecular ions. Compound-type assignments were made by means of previously established GPC-MS correlations and high-resolution mass spectral data for selected fractions. High-resolution, 70 eV, mass spectra were obtained on an AEI MS 3074 mass spectrometer. High- and low-resolution field-ionization spectra of selected fractions, primarily polyaromatic-polar concentrates, were obtained at Oklahoma State University on a CEC Model 21-110 B mass spectrometer fitted with a razor blade source (13).

## RESULTS

Descriptions and analyses of the six coal samples used to prepare the coal liquids are summarized in Table 1. Physical and chemical property data for the eight coal liquids prepared from the six coals are summarized in Table 2. Included in Table 2 are data for repeat runs on Illinois No. 6 and Wyodak coals. The repeat run for the Illinois No. 6 coal was made because of changes in the procedure instituted during the first liquefaction run, Illinois No. 6 run 1. The changes involved a switch from CoMo to NiMo catalyst and a decrease in the maximum temperature from 425° to 400° C (9). Also, upgrading of the first Illinois crude liquid fell short of the targeted value of 0.2 to 0.3 percent nitrogen. The second Wyodak coal liquid was prepared from the same crude liquid as the first by upgrading according to the time-temperature profile used for the Illinois No. 6 run 2 liquid. It was noted previously, that the lower-rank coals reacted more readily and under milder conditions than those of higher rank for both the initial liquefaction and the upgrading of the raw coal liquids (9). Thus, the second Wyodak run was made to determine possible effects of the extent of upgrading upon liquefaction-product composition.

Distillation results for the upgraded coal liquids are also summarized in Table 2. The results showed no large differences for the liquids, except for the extensively upgraded second Wyodak liquid which had a higher percentage of low-boiling material. Asphaltene content of the six "normally" upgraded liquids ranged from about 1 to 7 percent. Inclusion of the second Wyodak and first Illinois liquids extended the ranges of asphaltene content from 0.1 to 14 percent. The asphaltene content correlated with the nitrogen content of the liquids, thus supporting the use of nitrogen content to monitor the extent of coal-liquid upgrading.

Table 3 lists the specific gravity, nitrogen content, and sulfur content of the various distillation fractions obtained from each of the eight coal liquids. Nitrogen content increased for the higher-boiling distillates as expected. All sulfur values were low as expected. Nitrogen contents of the asphaltenes from the bituminous-coal liquids were higher than those from the lower-rank-coal liquids.

Results from the dual silica-gel/alumina-gel adsorption chromatography separations of the 200°-325° C, 325°-425° C, and 425°-540° C coal-liquid distillates are summarized in Table 4. Data for the acid and base extracts of the polyaromatic-polar adsorption fractions are also included in Table 4. Detailed results from the analyses of the saturate concentrates and the fractions from the GPC separations of the aromatic concentrates are not reported here but will be published elsewhere. Compound type assignments and the quantitative results for selected fractions from the GPC separations were checked by high-resolution electron-impact MS and by high- and

low-resolution FI/MS. The results were consistent except for the indication of very small amounts of additional compound types containing S, NO, NO<sub>2</sub>, and O<sub>2</sub>.

The characterization results from all fractions for each coal liquid were combined and expressed in terms of compound types containing the same number of total rings (aromatic and naphthenic). This scheme was chosen because of the different degree of saturation of aromatic rings in the upgrading of the crude liquids from different coals, and the fact that liquefaction and upgrading reaction conditions were chosen to minimize hydrocarbon ring cracking reactions. The results are summarized in Tables 5 and 6.

## DISCUSSION

Examination of the data in Table 5 shows the coal liquids to be more alike than different with regard to distribution by ring number. Differences among the liquids from the several coals doubtless were minimized because the upgrading was adjusted to eliminate heteroatoms to about the same level in most of the liquids. The greater reactivity of the lower-rank coals and the lesser required upgrading of their crude liquids was clear from the previously reported preparations (9). Some scatter in compositional data could be expected because of the variation of details of individual preparations. However, since conditions generally were such as to avoid cracking of hydrocarbons, especially hydrocarbon ring structures, differences or similarities in basic hydrocarbon structures should be valid. One of the largest uncertainties, is the extent of hydrogenation of aromatic hydrocarbon rings originally present in the coal. Total consumption of hydrogen was approximately constant, independent of coal rank (9), so that hydrogen consumed by reaction with high-combined oxygen in lower rank coals was counterbalanced by increased saturation of aromatic rings in the coals of higher rank. With the catalyst and conditions used, many of the polynuclear aromatic structures originally present could be expected to hydrogenate partially to yield hydroaromatics in the upgraded liquids. The uncertainty in the extent of hydrogenation of aromatics is circumvented in part by counting total rings per molecule in the several distillate fractions.

Comparison of the data from the two Illinois No. 6 liquefaction and upgrading runs summarized in Table 6 indicate very little difference in the products in terms of ring number distributions especially in the lower-ring-number compounds. The largest effect in switching from CoMo to NiMo catalyst and decreasing the maximum reaction temperature from 425° to 400° C appears in the compound types containing four or more rings and in the asphaltene content. The second Illinois run with NiMo at 400° C maximum temperature produced more >4-ring compound-type material at the expense of the asphaltenes.

As seen in Table 6, the ring-number data for the two Wyodak runs show that the extent of upgrading was an important factor in final product composition. The more extensive upgrading (Wyodak run 2) produced considerably higher yields of low-ring-number compound types. This was due only in part to more complete conversion of heteroatomic-ring compounds to hydrocarbons. Beyond that, some hydrocarbon cracking must have occurred.

Comparison of the data for the Illinois run 2 and Wyodak run 2 shows significantly higher yields of low-ring-number compound types for the liquid from the lower-rank Wyodak coal. However, since the

Wyodak coal was more reactive, the extent of upgrading as seen in the nitrogen contents was much greater for the Wyodak coal even though the same upgrading temperature-time profile was followed in each case. These differences were in contrast to the data from the six coal liquids in Table 5 which were upgraded to about the same nitrogen content, and for which no clear trend in terms of yields of compounds of equal ring number as a function of coal rank was evident.

## CONCLUSIONS

On the whole, the compositional studies showed the coal liquids upgraded to about the same level of nitrogen removal were much more alike than different. There was some scatter in the compositions in terms of number of rings per molecule but no consistent trend with the rank of coal. Although the ranks of the coals used in this study covered the full range of practical interest for liquefaction, selection of additional coal samples covering an even greater range of coal rank might be of value in determining any possible dependence of coal liquid composition upon coal rank.

The extent of upgrading influenced the ring-number distribution for liquids from a given coal. More extensive upgrading produced larger amounts of low-ring-number compound types, due in part to greater removal of heteroatoms and to additional cracking of alkyl linkages between ring systems.

Finally, taking the results of this compositional study in conjunction with the results of the preparation of the coal liquids, liquids from lower-rank coals were more easily upgraded and somewhat more cracking to lower molecular weight components occurred at a given severity of upgrading.

## ACKNOWLEDGMENTS

We are indebted to Dr. John B. Green and Steve Holmes for assistance in preparation of the coal liquids, and Janet Porter, Lois Karasa, Bob Vrana, Faye Cotton and Ed Zagula for their assistance in acquisition and reduction of the mass spectral data. We thank Dr. W. C. Lanning for discussions helpful in interpretation of the data. Also, we gratefully acknowledge the assistance of Drs. Q. Grindstaff and S. E. Scheppele of Oklahoma State University for providing the field-ionization mass spectra of selected fractions.

## REFERENCES

1. Aczel, T., R. B. Williams, R. J. Pancirov, and J. H. Karchmer, Final Report to U.S. Department of Energy, MERC-8007-1 (Pt. 1) (1976).
2. Baltisberger, R. J., R. A. Kaba, K. J. Klabunde, K. Saita, W. Sukalski, V. I. Stenber, and N. F. Woolsey, *Fuel*, 57, 529 (1978).
3. Coleman, H. J., J. E. Dooley, D. E. Hirsch, and C. J. Thompson, *Anal. Chem.*, 45 (9), 1724 (1973).
4. Dooley, J. E., D. E. Hirsch, C. J. Thompson, and C. C. Ward, *Hydrocarbon Processing*, 53 (11), 187 (1974).
5. Fischer, P., J. W. Standelhofer, and M. Zander, *Fuel*, 57 (6), 345 (1978).
6. Gorin, E., C. J. Kulik, and H. E. Lebowitz, *ACS Div. Fuel Chem. Preprints*, 20 (1), 79 (1975).

7. Haines, W. E., and C. J. Thompson, U.S. ERDA, LERC/RI-75/5-BERC/RI-75/2 (1975).
8. Hayatsu, R., R. E. Winans, R. G. Scott, L. P. Moore, and M. H. Studier, Fuel, 57, 541 (1978).
9. Lanning, W. C., J. B. Green, and J. E. Dooley, U.S. Department of Energy, BETC/RI-78/10 (1978).
10. Lanning, W. C., J. B. Green, and J. E. Dooley, ACS Div. Fuel Chem. Preprints, 23 (1), 62 (1978).
11. Makabe, M., and K. Ouchi, Fuel, 58 (1), 43 (1979).
12. Mima, M. J., H. Schultz, and W. E. McKinstry, U.S. ERDA, PERC/RI-76/6 (1976).
13. Scheppele, S. E., P. L. Grizzle, G. J. Greenwood, T. D. Marriott, and N. Perreira, Anal. Chem., 48, 2105 (1976).
14. Storch, H. H., C. H. Fisher, C. O. Hawk, and A. Eisner, U.S. BuMines, Tech. Paper 654 (1943).
15. Sturm, G. P., Jr., P. W. Woodward, J. W. Vogh, S. A. Holmes, and J. E. Dooley, U.S. Department of Energy, BERC/RI-78/4 (1978).
16. Sturm, G. P., Jr., P. W. Woodward, J. W. Vogh, S. A. Holmes, and J. E. Dooley, U.S. ERDA BERC/RI-75/12 (1975).
17. Takeya, G., Pure and Appl. Chem., 50, 1099 (1978).
18. Wu, W. R. K., and H. H. Storch, U.S. BuMines Bull. 633 (1968).

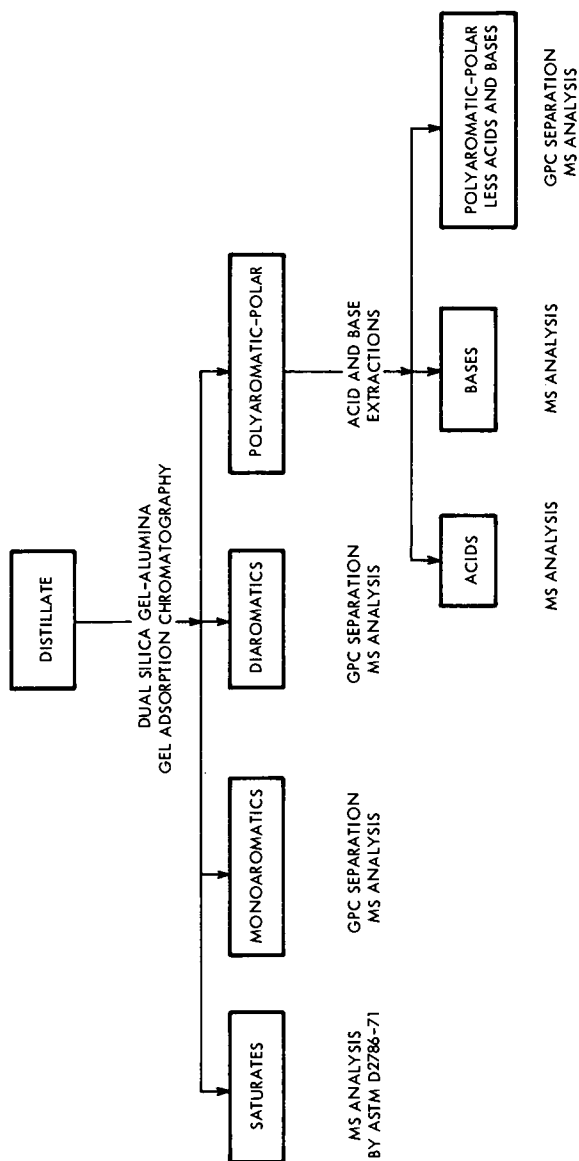


FIGURE 1. - Characterization scheme for 200-325° C, 325-425° C, and asphaltene-free 425-540° C coal liquid distillates.

TABLE I. - Analysis of coals, (weight percent)

Source	PA-WV	Illinois	W. KY	Montana	Wyoming	N. Dakota
Seam	Pittsburgh	No. 6	--	(Colstrip)	(Wyodak)	Beulah Std. II
Rank	hvb A	hvb B/C	hvb B/C	subb. A	subb. C	Lignite
Proximate analysis, (as received)						
Moisture.....	1.7	7.8	2.9	4.2	10.9	28.0
Volatile matter	35.9	34.2	38.4	34.4	39.5	31.0
Fixed carbon ..	55.1	51.4	48.8	48.5	42.7	33.3
Ash .....	7.3	6.6	9.9	12.9	6.9	7.7
Ultimate analysis, (moisture free)						
Hydrogen .....	5.1	4.9	4.9	4.3	4.8	4.5
Carbon .....	76.9	75.2	70.2	65.2	66.8	63.5
Nitrogen .....	1.5	1.6	1.4	0.6	1.0	0.9
Sulfur .....	1.6	1.5	4.3	1.8	0.5	1.3
Oxygen (diff) .	7.6	9.7	8.8	14.5	19.2	19.1
Ash .....	7.4	7.1	10.2	13.5	7.8	10.7

hvb B/C -- high volatile bituminous B or C

subb. -- subbituminous

TABLE 2. - Properties of crude and upgraded coal liquids

Coal	Pittsburgh	Illinois No. 6		W. Ky.	Colstrip	Wyodak	Lignite		
		Run 1	Run 2						
Nitrogen, wt-pct..... Oxygen, wt-pct..... Sulfur, wt-pct.....	0.44 .59 <.01	1.45 - 0.17	1.10 1.34 <0.01	1.28 2.09 0.02	0.64 1.61 <0.01	0.48 1.08 <0.01	0.43 1.55 <0.01		
	Crude Liquids								
	Upgraded Liquids								
Spec. gr., 60/60° F... SSU vis. @ 100° F.... SSU vis. @ 130° F.... Pour point, ° F..... Carbon, wt-pct..... Hydrogen, wt-pct..... Sulfur, wt-pct..... Nitrogen, wt-pct..... Oxygen, wt-pct.....	0.993 441 189 +5 89.2 10.8 <0.01 .20 .28	1.006 129 65 <+5 90.1 9.9 0.03 .444 .50	0.992 126 86 <+5 88.6 10.3 0.02 .250 .19	0.989 89 - <+5 88.2 10.7 0.02 .287 .32	0.987 263 123 +20 88.1 10.6 <0.01 .192 .34	Run 1 0.955 96 - +70 88.9 11.0 <0.01 .095 .17	Run 2 0.922 56 - +65 88.0 11.9 <0.01 .008 .04	0.983 181 123 +45 89.0 10.8 <0.01 .250 .61	
	Distillation, wt-pct:								
	10.0 21.7 20.3 26.6 16.2	12.3 27.3 20.7 19.1 6.4	11.4 27.9 22.5 23.7 7.5	16.6 26.1 22.8 19.7 9.3	11.5 21.5 21.1 20.9 18.4	13.9 26.7 21.3 25.2 11.2	18.3 30.3 19.1 25.3 6.3	12.3 24.0 20.7 21.0 15.0	
									<200° C.....
									200°-325° C....
									325°-425° C....
									425°-540° C <sup>a</sup> ..
	>540° C <sup>a</sup> .....								
	Asphaltenes, wt-pct ...	4.7	14.3	6.8	5.2	6.6	1.2	0.1	6.7

<sup>1</sup> Upgraded on same temperature-time program as Illinois No. 6 Run 2.

<sup>a</sup> Asphaltenes removed from >425° C residuum.

TABLE 3. - Distillation fractions of upgraded coal liquids

Coal	Pittsburgh	Illinois No. 6Run 1	Illinois No. 6Run 2	W. Ky.	Colstrip	Wyodak Run 1	Wyodak Run 2	Lignite
<200° C distillate:								
Spec. gr. ....	0.829	0.825	0.827	0.832	0.822	0.819	0.810	0.822
Sulfur, wt-pct. ....	<.01	.02	<.01	<.01	<.01	<.01	<.01	<.01
Nitrogen, wt-pct.	.003	.068	.001	.096	.023	.003	<.001	.007
200°-325° C:								
Spec. gr. ....	.915	.937	.926	.919	.918	.909	.897	.916
Sulfur, wt-pct. ....	<.01	.03	<.01	.02	<.01	<.01	<.01	<.01
Nitrogen, wt-pct.	.016	.102	.021	.062	.030	.012	.002	.104
325°-425° C:								
Spec. gr. ....	.983	1.018	1.001	.993	.982	.972	.952	.983
Sulfur, wt-pct. ....	<.01	0.01	<0.01	.02	<.01	<.01	<.01	<.01
Nitrogen, wt-pct.	.076	.396	.159	.200	.119	.072	.004	.304
425°-540° C <sup>1</sup> :								
Spec. gr. ....	1.045	1.079	1.061	1.049	1.032	1.026	1.001	1.032
Sulfur, wt-pct. ....	<0.01	<0.01	<0.01	<0.01	<0.01	<0.01	<0.01	<0.01
Nitrogen, wt-pct.	.272	.594	.415	.415	.233	.176	.029	.412
>540° C resid <sup>1</sup> :								
Nitrogen, wt-pct.	.420	.709	.576	.565	.348	.275	.052	.518
Asphaltenes:								
Nitrogen, wt-pct.	.722	1.104	1.004	1.036	.579	.393	.194	.714
>425° C resid:								
Sulfur, wt-pct. ....	<0.01	.01	<.01	0.04	.02	<.01	<.01	<.01
Nitrogen, wt-pct.	.374	.829	.56	.573	.332	.219	.024	.501
Asphaltenes, wt-pct	9.9	35.9	17.9	15.3	14.3	3.3	.4	15.7

<sup>1</sup> Asphaltene-free.

TABLE 4. - Fraction yields from adsorption chromatography and acid-base separations (weight percent)

Coal Fraction \ Liquid	Pittsburgh		Illinois No. 6 Run 1		Illinois No. 6 Run 2		Western Kentucky	
	Crude	Distillate	Crude	Distillate	Crude	Distillate	Crude	Distillate
200 - 325° C Distillate								
Saturates	11.91	54.9	7.92	29.0	11.75	42.1	11.82	45.3
Monoaromatics	7.77	35.8	15.02	55.0	13.81	49.5	12.01	46.0
Di aromatics	1.36	6.3	2.37	8.7	1.54	5.5	1.31	5.0
Polyaromatic-Polar	.36	1.7	2.00	7.3	.80	2.9	.65	2.5
Loss	.30	1.3	0.0	0.0	0.0	0.0	.31	1.2
325 - 425° C Distillate								
Saturates	5.44	26.8	2.11	10.2	3.87	17.2	4.92	21.6
Monoaromatics	10.17	50.1	6.91	33.4	9.70	43.1	9.46	41.5
Di aromatics	2.52	12.4	6.42	31.0	5.09	22.6	4.47	19.6
Polyaromatic-Polar	2.13	10.5	5.26	25.4	3.67	16.3	3.97	17.4
PAP Hydrocarbons	1.93	9.53	4.82	23.3	3.40	15.10	3.58	15.7
PAP Acids	.11	.56	.11	.51	.11	.47	.11	.47
PAP Bases	.05	.24	.14	.66	.10	.43	.09	.38
Loss	.08	.40	.19	.90	.23	1.10	.17	.80
425 - 540° C Distillate								
Saturates	2.26	8.8	.53	3.2	.80	3.6	2.17	11.8
Monoaromatics	5.76	22.4	1.30	7.9	1.80	8.1	2.36	12.8
Di aromatics	5.78	22.5	3.60	21.8	4.82	21.7	4.36	23.7
Polyaromatic-Polar	11.87	46.2	11.06	67.0	14.79	66.6	9.27	50.4
PAP Hydrocarbons	11.77	45.8	10.91	66.1	14.54	65.5	9.05	49.2
PAP Acids	.07	.29	.08	.50	.13	.59	.10	.55
PAP Bases	.05	.18	.07	.40	.10	.45	.04	.21
Loss	.01	.03	.01	.10	.01	-	.32	1.7

Coal Fraction \ Liquid	Calstrip		Wyodak Run 1		Wyodak Run 2		Lignite	
	Crude	Distillate	Crude	Distillate	Crude	Distillate	Crude	Distillate
200 - 325° C Distillate								
Saturates	10.75	50.0	15.06	56.4	22.73	75.0	11.71	48.8
Monoaromatics	8.92	41.5	10.12	37.9	6.24	20.6	10.13	42.2
Di aromatics	1.01	4.7	1.01	3.8	.51	1.7	1.02	4.2
Polyaromatic-Polar	.77	3.6	.51	1.9	.48	1.6	1.15	4.8
Loss	.05	.2	0.0	0.0	.34	1.1	0.0	0.0
325 - 425° C Distillate								
Saturates	5.84	27.7	6.99	32.8	11.77	61.6	5.22	25.2
Monoaromatics	8.52	40.4	8.48	39.8	4.22	22.1	7.87	38.0
Di aromatics	3.19	15.1	3.11	14.6	1.64	8.6	3.29	15.9
Polyaromatic-Polar	3.42	16.2	2.73	12.8	1.47	7.7	4.06	19.6
PAP Hydrocarbons	3.17	15.0	2.56	12.0	1.34	7.0	3.62	17.5
PAP Acids	.09	.41	.08	.37	.10	.52	.16	.76
PAP Bases	.08	.37	.03	.13	.01	.03	.18	.88
Loss	.21	1.0	.05	.25	.02	.15	.36	1.7
425 - 540° C Distillate								
Saturates	3.15	15.6	4.96	19.7	8.86	35.0	2.70	13.8
Monoaromatics	3.47	17.2	4.96	19.7	5.46	21.6	2.88	14.7
Di aromatics	4.38	21.7	4.79	19.0	3.74	14.8	3.49	17.8
Polyaromatic-Polar	9.19	45.5	10.48	41.6	7.24	28.6	10.29	52.5
PAP Hydrocarbons	8.79	43.5	10.21	40.5	6.93	27.4	10.09	51.5
PAP Acids	.12	.59	.09	.34	.14	.55	.11	.58
PAP Bases	.03	.14	.03	.11	.02	.06	.11	.54
Loss	.26	1.2	.16	.63	.15	.60	.22	1.1

TABLE 5. - Comparison of six coal liquids based on  
ring number, and asphaltene and  
residuum content (weight percent -  
total coal liquid basis)

No. of Rings \ Coal Liquid	Pittsburgh	Illinois No. 6 Run 2	Western Kentucky	Colstrip	Wyodak Run 1	Lignite
0	1.8	1.9	4.8	4.4	5.7	3.6
1	12.1	12.2	15.7	11.7	16.9	14.4
2	12.9	17.4	16.9	13.8	17.0	15.0
3	15.2	17.1	15.8	14.8	15.6	15.3
Sum 0 to 3	42.0	48.6	53.2	44.7	55.2	48.3
>4	32.2	31.9	27.9	27.6	29.6	24.5
Asphaltenes	4.7	6.8	5.2	6.6	1.2	6.7
>540° C Resid	16.2	7.5	9.3	18.4	11.2	15.0
Acids	.2	.2	.2	.2	.2	.3
Bases	.1	.2	.1	.1	.1	.3
Other <sup>1</sup>	4.6	4.8	4.1	2.4	2.5	4.9

<sup>1</sup> Includes unknowns, material not analyzed due to insufficient sample, and material lost in separations.

TABLE 6. - Ring number distributions for coal liquids produced  
from Illinois No. 6 and Wyodak coal using  
different processing conditions

No. of Rings \ Coal Liquid	Illinois No. 6 Run 1	Illinois No. 6 Run 2	Wyodak Run 1	Wyodak Run 2
0	2.1	1.9	5.7	6.2
1	11.4	12.2	16.9	21.6
2	16.1	17.4	17.0	20.1
3	17.3	17.1	15.6	16.9
>4	27.0	31.9	29.6	26.4
Asphaltenes	14.3	6.8	1.2	.1
>540° C Resid	6.4	7.5	11.2	6.3
Acids	.2	.2	.2	.2
Bases	.2	.2	.1	tr
Unknown and Losses	5.0	4.8	2.5	2.2

CHEMICAL COMPOSITION OF RAW AND UPGRADED  
ANTHRACENE OIL AND THE CHEMISTRY OF COAL  
LIQUIDS UPGRADING(1)

S. E. Scheppele(2)\*, G. J. Greenwood\*,  
R. J. Pancirov\*\*, and T. R. Ashe\*\*

Department of Chemistry\*, Oklahoma State University, Stillwater, OK 74074  
and Exxon Research and Engineering Co.\*\*, Linden, NJ 07036

INTRODUCTION

Anthracene oil was hydrotreated using flow-through trickle-bed reactors containing Co-Mo-alumina catalysts (3). The conditions are specified in Table I. Samples of the feedstock and four reaction mixtures were separated using cation, anion, and complexation chromatography (4). The compound types and the weight percents of the individual homologs present in the acid, base, neutral nitrogen, and hydrocarbon + ether (neutral) fractions were determined from high- and low-resolutions FI/MS and high-resolution 70-eV EI/MS. The basic and neutral fractions were subjected to GC/MS analysis.

RESULTS AND DISCUSSION

The salient results are summarized. Hydrocarbons containing three aromatic rings account for ca. 40% of the feedstock. The parent member of the -18(H)Z series ( $C_{14}H_{10}$ ) was preparatively isolated using GC and identified as  $\geq 98\%$  phenanthrene. The dominance of phenanthrene over anthracene in both high- and low-temperature coal tars has been previously noted (5-10). Thus, phenanthrene and assumably its alkylated homologs comprise the -18(H)Z series and account for 15.6% of the feedstock.

The data in Table II demonstrate the occurrence of extensive phenol deoxygenation. The reactivity of -18(O) through -22(O) and -18(O<sub>2</sub>) and -22(O<sub>2</sub>) compounds is indicated to be independent of the experimental conditions. However, the weight percents for the lower -Z(O) and -Z(O<sub>2</sub>) series reveal that the increased reaction time did not overcome the effect of a decrease in temperature upon reactivity. Comparison of the data in columns 6 and 7 with those in columns 3 and 4 indicates a very small net effect of decreases in both H<sub>2</sub> pressure and space time and catalyst change on deoxygenation.

The acid fraction contains significant amounts of -Z(N) compound types. These compounds and also the ones present in the neutral-nitrogen-containing fraction are indicated to contain the pyrrole nucleus based upon the chemistry associated with the separation and both the molecular weights and formulas for the first homolog observed

for each compound type. For example, as seen in Table III, the carbon number for the first homolog in the -9(N), -15(N), and -21(N) series are those expected for indoles, carbazoles, and benzocarbazoles, respectively. Comparison of the weight percents in columns 4 through 7 with the ones in column 3 of Table III reveal a net nonreactivity for compounds containing the pyrrole nucleus under the specified conditions.

The base fraction from the feed was found to contain -5(N) through -23(N) and -27(N) compound types. These specific -Z series are indicated to be principally composed of compounds possessing the pyridine nucleus based upon the chemistry associated with the separation, the formulas for the first homolog observed in each series, and GC/MS analysis. The -17(N) series ranging from  $C_{13}H_9N$  to  $C_{18}H_{19}N$  is the most abundant one, accounting for 28.8% of the base fraction. The principal components are assumably isomeric azaphenanthrenes and variously alkylated homologs possessing up to 5 alkyl carbons.

The -11(N) series ranging from  $C_9H_7N$  to  $C_{16}H_{21}N$  is the second most abundant one, accounting for ca. 23.5% of the base fraction. The first members of this series, quinoline and isoquinoline by GC/MS, account for 0.9 percent of the feedstock. It is interesting to note that isoquinoline accounts for 1/2 to 2/3 of this total.

The feedstock base fraction also contains -11(NO), -19(NO), and -21(NO) compound types. The molecular formulas correspond to compounds containing both furan and pyridine nuclei. It is interesting to note that this fraction contains in excess of 40 heterocyclic compounds containing two nitrogen atoms (11). This appears to be the first report of numerous  $C_NH_{2N+Z(N_2)}N_2$  compounds in coal liquids and only the second instance (12) in which dinitrogen compounds have been observed in these materials.

The mass spectral and the GC/MS data demonstrate that the complexity of the base fractions is significantly increased under all conditions used (see Table I) in hydrotreating the anthracene oil. Table IV presents mole data for the reactant and product bases comprising the 129-139 molecular-weight series. The moles of quinoline (I) and isoquinoline (II) in the feed are ca.  $2.2 \times 10^{-3}$  and  $4.4 \times 10^{-3}$ , respectively, by GC/MS. In addition, GC/MS reveals the absence of II in the reactor bases. In regard to  $C_9H_{11}N$ , GC/MS indicates the presence of 1,2,3,4-tetrahydroquinoline (IIIa) and the absence of both 5,6,7,8-tetrahydroquinoline (IIIb) and tetrahydroisoquinolines (IV). Finally, the GC/MS analyses confirm the presence of minor and significant amounts of 2-propylaniline (V) in the feedstock and reactor-1 bases, respectively. These results are at least qualitatively consistent with those obtained from reaction of I with  $H_2$  a) in a batch reactor

using  $\text{MoS}_2$  as the catalyst (13) and b) in a high-pressure/high-temperature liquid-phase reactor using a variety of metal catalysts (14) and from the  $\text{MoS}_2$  catalyzed reaction of II with  $\text{H}_2$  (13).

As shown in Scheme 1 (14), rapid catalytic addition of  $\text{H}_2$  to I produces IIIa and IIIb. The apparent presence of IIIa and the apparent absence of IIIb in the products is at least qualitatively consistent with the considerably greater reactivity of the latter compared to the former (14). Structure-reactivity relationships provide a preference for hydrogenolysis of the N-C(2) bond rather than the C(8a)-N bond in IIIa producing V rather than 3-phenylpropylamine. Both IIIa and IIIb are converted to decahydroquinoline (VI), mass 139; the rate constant for the latter conversion is significantly greater than the one for the former (14). The absence of significant amounts of VI in the products is consistent with its facile conversion to hydrocarbons and  $\text{NH}_3$  (13,14).

The only nitrogen containing compounds observed from the  $\text{MoS}_2$  catalyzed reaction of  $\text{H}_2$  and II were IV and decahydroisoquinoline (VII) (14). VII is a minor product. As shown in Scheme 2, II reacts with  $\text{H}_2$  producing either IVa or IVb. Hydrogenolysis of either the N-C(3) bond or the N-C(2) bond in IVa produces either 2-ethylbenzylamine (VIII) or 2-(2-methylphenyl)ethylamine (IX), respectively. Since VIII and IX contain a benzylic and aliphatic  $\text{NH}_2$  group, respectively, their denitrogenation should be facile. In contrast, the  $\text{NH}_2$  group in V, see Scheme 1, is aromatic and, hence, as observed would be expected to undergo hydrogenolysis less readily. Alternatively, hydrogenation of IVa and IVb produces VII which in turn suffers hydrogenolysis producing hydrocarbons plus  $\text{NH}_3$ .

Table V lists the furan- and thiophene-compound types present in the neutral fractions from the feed and the products. Dibenzofurans and dibenzothiophenes were identified by GC/MS. Carbon-number distributions for these compound types in the feed and in selected reactor samples are also given in Table V. Table VI presents carbon-number distributions for the hydrocarbons in the feed and reactor sample 1.

The weight percents in Table V indicate that the furans were markedly resistant to both hydrogenation and hydrogenolysis under the experimental conditions. It should be noted that on a 100g basis the moles at C-16 and C-17 in the -22(0) series are  $2.8 \times 10^{-3}$  and  $1.8 \times 10^{-3}$  less in product 1 than in the feed. However, this decrease approximates the increase of  $1.8 \times 10^{-3}$  and  $1 \times 10^{-3}$  moles of C-16 and C-17 homologs in the -18(0) series in product 1. Similar results are observed for reactor-sample 3. This result suggests the hydrogenation of benzonaphthenofurans produces tetrahydroderivatives. The apparent unreactivity of the furans towards at least hydrogenation appears surprising.

The weight presents in Table V demonstrate that the thiophenes were very reactive toward sulfur removal under all experimental conditions. The absence of partially hydrogenated thiophenes in the products is consistent with the mechanism of dibenzothiophene desulfurization(15).

Comparison of the carbon-number distributions for the feedstock and reactor-sample 1 in Table VI reveals that the hydrotreating process significantly a) reduced the amount of aromatic and b) increased the quantity of hydroaromatic hydrocarbons. The occurrence of compound crossover in a number of these series, e.g., -14(H), -18(H), and -20(H), does not negate this conclusion although it complicates data interpretation. However, the following examples illustrate the qualitative information which can be deduced concerning the chemical processes occurring during hydrotreating. Dihydrophenanthrene ( $C_{14}H_{12}$ ), tetrahydrophenanthrene ( $C_{14}H_{14}$ ), and octahydrophenanthrene ( $C_{14}H_{18}$ ) which are produced in chromia-alumina hydrotreating of phenanthrene(16) were identified in the product mixtures. Other C-14 compounds (16) involved in this process are 2-ethylbiphenyl, -14(H), 2-butylnaphthalene, -12(H), and 6-butyltetralin, -8(H). Reactor-sample 1 contains ca. 0.03 more moles of C-14 compounds in the -8(H) through -16(H) series than does the feed on a 100g basis. The former contains 0.018 fewer moles of phenanthrene than does the latter. This result suggests that the mechanism for hydrogenation of phenanthrene over chromia-alumina is at least qualitatively applicable to the conditions specified in Table I and that other compounds must contribute to the C-14 pool. In this regard, phenanthrene is a product in the hydrocracking of pyrene(17).

By GC/MS, acenaphthene and biphenyl account for 94% and 6% and 43% and 17% of the  $C_{12}H_{10}$  hydrocarbons in the feed and reactor-sample 1, respectively. On a 100g basis, these values combined with the weight percents in Table VI result in a decrease of 14 millimoles in acenaphthene and an increase of 16 millimoles in tetrahydroacenaphthene between feed and products. This surprisingly good agreement suggests that the former is hydrogenated to the latter. Furthermore, the product mixture contains ca. 6 millimoles more biphenyl than does the feed. This result is not inconsistent with the expected formation of 4 millimoles from desulfurization(15) of dibenzothiophene.

Finally, the increase in the weight percent of the -8(H) Z-series from 0.4 in the feedstock to 7.0 in reactor-sample 1 and the distributions of weight percents across both the -8(H) and -12(H) series cannot be entirely explained by hydrogenation in the naphthalene family(17). Rather these results point to hydrogenation/hydrogenolysis of higher-molecular-weight hydrocarbons and/or heteroatom-containing compounds.

# REFERENCES

1. Research at Oklahoma State University supported by the Department of Energy, Contract Number EX-76-C-01-2011.
2. Present address: U.S. Department of Energy, Bartlesville Energy Technology Center, Bartlesville, Oklahoma.
3. M. M. Ahmed and B. L. Crynes, PREPRINTS, Div. Petrol. Chem., Am. Chem. Soc., 22(3), 971(1977).
4. D. M. Jewell, J. H. Weber, J. W. Bunger, H. Plancher, and D. R. Latham, Anal. Chem., 44, 1391(1972).
5. E. Proksch, Z. Analyt. Chem., 233, 23(1966).
6. C. Karr, Jr., P. A. Estep, T. C. L. Chang, and J. R. Comberiat, Bull. U.S. Bureau of Mines, No. 637 (1967).
7. H. Pichler, P. Hennenberger, and G. Schwarz, Brennst.-Chem., 49, 175 (1968).
8. H. Pichler, W. Ripperger, and G. Schwarz, Erdoel Kohle, Erdgas, Petrochem, 23, 91 (1970).
9. K. D. Bartle, Rev. Pure Appl. Chem., 22, 79 (1972).
10. Private communication from T. Aczel and A. G. Sharkey, Jr.
11. R. D. Grigsby, L. R. Schronk, Q. Grindstaff, S. E. Scheppele, and T. Aczel, 27th Annual Conference on Mass Spectrometry and Allied Topics, 1979, in press.
12. A. Marzec, D. Bodzek, and T. Krzyzanowska, in "Organic Chemistry of Coal", J. W. Larsen, Ed., ACS Symposium Series 71, American Chemical Society, Washington, 1978.
13. S. Landa, Z. Kafka, V. Galik, and M. Safar, Collect. Czech. Chem. Comm., 34, 3967 (1967).
14. S. S. Shih, J. R. Katzer, H. Kwart, and A. B. Stiles, PREPRINTS, Div. Petrol. Chem., Am. Chem. Soc., 22(3), 919 (1977).
15. M. Houalla, D. Broderick, V. H. J. deBeer, B. C. Gates, and H. Kwart, PREPRINTS, Div. Petrol. Chem., Am. Chem. Soc., 22(3), 941 (1977).
16. W. L. Wu and H. W. Haynes, Jr., in "Hydrocracking and Hydrotreating", J. W. Ward and S. A. Qader, Ed., ACS Symposium Series 71, American Chemical Society, Washington, 1975.
17. S. A. Qader, J. Inst. Petrol., 59, 178 (1973).

TABLE I  
CONDITIONS FOR HYDROTREATING ANTHRACENE OIL

	REACTOR-SAMPLE			
	1	2	3	4
Reactor Temperature (°F)	700	600	700	700
Reactor Pressure (psig)	1000	1000	1020	507
Space time (hrs)	1.48	2.50	0.75	0.75
Catalyst	Nalco Sphericat		Harshaw HT 400	
	474			

TABLE II  
SUMMARY DATA FOR OXYGEN-CONTAINING ACIDS IN  
FEEDSTOCK AND UPGRADED ANTHRACENE OIL

-Z	Parent Formula	Feedstock	Weight Percent in			
			Reactor-Samples			
			1	2	3	4
6(0)	C <sub>6</sub> H <sub>6</sub> O	4.0	0.1	0.9	0.3	0.8
8(0)	C <sub>9</sub> H <sub>10</sub>	0.5	0.2	0.5	0.4	0.2
12(0)	C <sub>10</sub> H <sub>8</sub> O	1.0	< 0.0	< 0.1	0.0	0.0
14(0)	C <sub>12</sub> H <sub>10</sub> O	1.5	< 0.1	0.5	0.3	0.3
16(0)	C <sub>13</sub> H <sub>10</sub> O	1.2	0.1	0.5	0.3	0.3
18(0)	C <sub>14</sub> H <sub>10</sub> O	0.3	0.0	< 0.1	0.0	0.0
20(0)	C <sub>16</sub> H <sub>12</sub> O	0.4	0.0	0.2	0.1	0.2
22(0)	C <sub>16</sub> H <sub>10</sub> O	0.1	0.0	0.1	0.1	< 0.1
16(O <sub>2</sub> )	C <sub>12</sub> H <sub>8</sub> O <sub>2</sub>	2.8	0.0	0.4	0.0	< 0.1
18(O <sub>2</sub> )	C <sub>14</sub> H <sub>10</sub> O <sub>2</sub>	0.1	0.0	0.0	0.0	0.0
22(O <sub>2</sub> )	C <sub>16</sub> H <sub>10</sub> O <sub>2</sub>	0.1	0.0	0.0	0.0	0.0

TABLE III  
SUMMARY DATA FOR  $C_N H_{2N+Z(N)} N$  COMPOUNDS  
IN THE ACID AND NEUTRAL-NITROGEN FRACTIONS FROM  
FEEDSTOCK AND HYDROTREATED ANTHRACENE OIL

-Z(N)	Parent Formula	Range In <sup>a</sup> N	Feedstock	Weight Percent			
				Reactor-Sample <sup>b</sup>			
				1	2	3	4
9	$C_8H_7N$	9-12	0.2	<0.1	0.1	0.1	0.1
15	$C_{11}H_7N$	12-16	1.8	1.6	1.4	1.9	1.6
17	$C_{13}H_9N$	14-17	0.2	0.2	0.2	0.4	0.1
19	$C_{13}H_{11}N$	14-18	0.2	0.2	0.1	0.1	0.1
21	$C_{15}H_9N$	16-17	0.3	0.3	0.2	0.2	0.1

<sup>a</sup>Values for feedstock. <sup>b</sup>Conditions specified in Table I.

TABLE IV  
MOLES OF BASES AT MOLECULAR WEIGHTS 129-135  
IN FEED AND REACTOR-SAMPLE 1

Mass	Formula	Moles <sup>a</sup> $\times 10^3$ In	
		Feedstock	Reactor Sample 1 <sup>b</sup>
129	$C_9H_7N$	6.6	0.4
133	$C_9H_{11}N$	0.2	1.1
135	$C_9H_{13}N$	0.2	1.8
139	$C_9H_{17}N$	-	0.006
TOTAL		7.0	3.3

<sup>a</sup>Calculated per 100g of feed. <sup>b</sup>Conditions specified in Table I.

TABLE V

## CARBON-NUMBER DISTRIBUTIONS FOR ETHERS IN FEEDSTOCK AND UPGRADED ANTHRACENE OIL

-Z Series	Parent Formula	Sample <sup>a</sup>	Weight Percent at Carbon Number											Total
			8	9	10	11	12	13	14	15	16	17	18	
16(O)	C <sub>12</sub> H <sub>8</sub> <sup>O</sup>	F					2.1	1.4	0.9	0.3				4.7
		R1					2.3	1.5	0.7	0.3				4.8
		R3					2.0	1.4	0.8	0.3				4.5
18(O)	C <sub>15</sub> H <sub>12</sub> <sup>O</sup>	F								0.1	0.1			0.2
		R1								0.1	0.5	0.2		0.8
		R3								0.1	0.6	0.2		0.9
22(O)	C <sub>16</sub> H <sub>10</sub> <sup>O</sup>	F								1.3	0.8			2.1
		R1								0.7	0.4	0.2		1.3
		R3								0.5	0.3	0.1		0.9
26(O)	C <sub>18</sub> H <sub>10</sub> <sup>O</sup>	F											0.1	0.1
		R1											0.1	0.1
		R3											0.1	0.1
10(S)	C <sub>8</sub> H <sub>8</sub> <sup>S</sup>	F		0.2	0.1									0.3
		R1		0.0	0.0									0.0
		R2		0.0	0.0									0.0
16(S)	C <sub>12</sub> H <sub>8</sub> <sup>S</sup>	F					0.8	0.2	0.1					1.1
		R1					0.1	0.1	0.0					0.2
		R2					0.4	0.1	0.0					0.5
22(S)	C <sub>16</sub> H <sub>10</sub> <sup>S</sup>	F									0.2			0.2
		R1									0.1			0.1
		R2									0.1			0.1

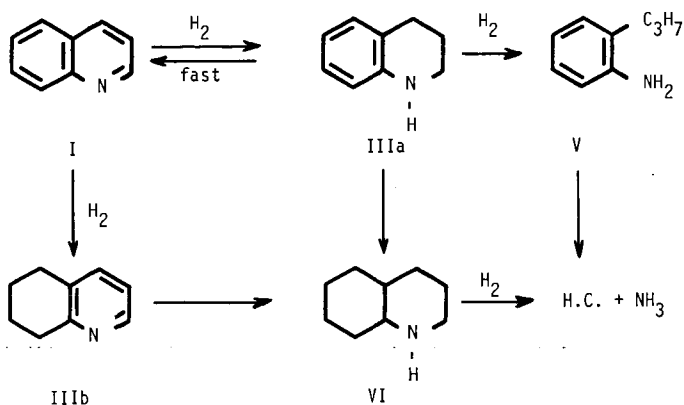
<sup>a</sup>F=Feedstock; R1=Reactor-Sample 1, R2=Reactor-Sample 2, R3=Reactor-Sample 3, Conditions specified in Table I.

TABLE VI  
CARBON-NUMBER DISTRIBUTIONS FOR THE HYDROCARBONS IN THE FEEDS AND IN REACTOR-SAMPLE 1

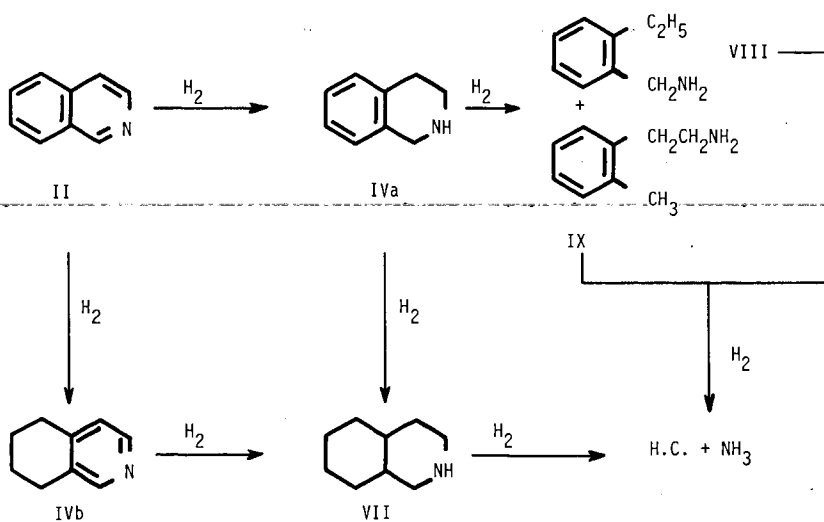
Z(H)	Parent Formula	Sample <sup>a</sup>	Weight Percents at Carbon Number																	Total
			8	9	10	11	12	13	14	15	16	17	18	19	20					
6	C <sub>6</sub> H <sub>6</sub>	F		0.1	0.04															0.1
		R1		0.2	0.2	0.1	0.1													0.6
8	C <sub>9</sub> H <sub>10</sub>	F		0.2	0.1	0.1														0.4
		R1		0.5	3.2	1.4	1.1	0.6	0.2											7.0
10	C <sub>9</sub> H <sub>8</sub>	F	-	-	-	-	-	-	-	-	-	-	-	-	-	-	-	-	-	0.0
		R1					3.0	1.0	1.5	0.5	0.2									6.2
12	C <sub>10</sub> H <sub>8</sub>	F			4.8	2.3	1.3	0.6	0.2	0.03										9.2
		R1			3.9	2.2	1.4	0.7	0.3	0.2	1.2									9.9
14	C <sub>12</sub> H <sub>10</sub>	F					5.3	1.8	1.4	0.4	0.3									9.3
		R1					3.5	1.4	3.3	0.9	0.6	0.3	0.1	0.04						10.1
16	C <sub>12</sub> H <sub>8</sub>	F						2.6	1.8	0.7	0.3	0.1	0.05							5.6
		R1						2.7	3.7	1.2	1.6	0.5	0.3	0.1	0.1	0.1				10.1
18	C <sub>14</sub> H <sub>10</sub>	F							10.4	3.2	1.3	0.4	0.1							15.4
		R1							7.2	2.4	3.9	1.2	0.7	0.2	0.1					15.7
20	C <sub>15</sub> H <sub>10</sub>	F								1.4	2.4	0.9	0.3	0.3						5.3
		R1								0.9	2.7	0.8	1.0	0.2	0.2					5.8
22	C <sub>16</sub> H <sub>10</sub>	F									12.1	2.7	1.6	0.3	0.2					16.9
		R1									6.1	1.3	0.9	0.3	0.3					8.9
24	C <sub>18</sub> H <sub>12</sub>	F											1.6	0.4	0.2					2.2
		R1											0.5	0.2	0.2					0.9
26	C <sub>18</sub> H <sub>10</sub>	F											0.1	0.1	0.2					0.4
		R1											0.2	0.2	0.1					0.5
28	C <sub>20</sub> H <sub>12</sub>	F																		0.3
		R1																		0.1

<sup>a</sup>F=Feedstock; R1=Reactor-Sample 1, Conditions specified in Table I.

SCHEME 1



SCHEME 2



Liquid Sulfur Dioxide - As An Agent  
for Upgrading Coal Liquid

C. V. Philip<sup>†</sup>, Ralph A. Zingaro<sup>\*</sup> and  
Rayford G. Anthony<sup>†</sup>

Departments Chemical Engineering<sup>†</sup> and Chemistry<sup>\*</sup>  
Texas A&M University  
College Station, Texas 77843

INTRODUCTION

An approach to processing coal-derived liquid is to utilize advanced petroleum refining technology. Physical and chemical characteristics of the coal liquid currently produced from the pilot plants is different from that of petroleum crude. Although various coals may appear different, there is a striking similarity in the nature of major chemical species present in the coal liquids from different sources. Analytical data (1 to 7) on various coal liquids and various distillation cuts show that coal liquids are composed of bulk species such as straight chain hydrocarbons, 'asphaltenes', one or two ring alkylated aromatics (such as alkylated benzenes, indans and naphthalenes), phenols (alkylated phenols, indanols and naphthols). Straight chain hydrocarbons include slightly branched hydrocarbons such as pristene and phytane and long chain monoclefin. The concept of using sulfur dioxide for upgrading coal liquid is very attractive due to the fact that sulfur is going to be one of the large byproducts of any coal conversion technology. Liquid sulfur dioxide is a very good solvent for most of the bulk species in any coal liquid except for saturated hydrocarbons. Now the coal liquefaction technology is very costly due to several factors including consumption of large quantities of hydrogen to liquefy coal. The recovery of saturated hydrocarbon, the hydrogen rich fraction, from the coal liquid has great economic interest.

EXPERIMENTAL

Since liquid sulfur dioxide boils at  $-10^{\circ}\text{C}$ , the extraction can be conducted at atmospheric conditions. The liquid sulfur dioxide is obtained by cooling the gas from the cylinder using Dry Ice-acetone mixture. When a coal liquid (usually in a waxy state) is treated with liquid sulfur dioxide, the insolubles remain with the minerals and the coal fragments as a solid residue. The  $\text{SO}_2$ -solubles are separated from the insolubles by filtration. The filtrate is degased<sup>2</sup> to remove  $\text{SO}_2$  from the  $\text{SO}_2$ -solubles. The hydrocarbons in the  $\text{SO}_2$ -insoluble residue are separated from the minerals and coal fragments by soxhlet extraction with tetrahydrofuran (THF-additive free). Both  $\text{SO}_2$ -solubles and the THF extract of  $\text{SO}_2$ -insolubles were separated by GPC. The details of GPC separation technique is published elsewhere<sup>(7)</sup>. The GPC system uses four 100A  $\mu$ Styragel columns (total length: 120 cm.) and THF (dry, additive free) as the liquid mobile phase. Two hundred  $\mu\text{l}$  of 50% THF solutions of the  $\text{SO}_2$ -solubles were separated into four fraction by GPC. Since the preliminary tests revealed that the THF extract of the  $\text{SO}_2$ -insolubles are mostly saturated hydrocarbons and other major bulk species are absent, the GPC did not play a significant role in the separation except to remove the gc-nonvolatiles from the sample, as they belong to larger linear molecular size. The GPC fractions 1 and 2 of  $\text{SO}_2$ -solubles are gc-nonvolatiles and they can not be analyzed by GC-MS. All other fractions were analyzed by GC-MS. Proton nmr and ir gave some qualitative information on the nonvolatiles.

## RESULTS AND DISCUSSION

Liquid sulfur dioxide was used to separate two coal liquids produced from West Virginia subbituminous coal and North Dakota lignite. The samples were obtained from the pilot plant at Pittsburgh Energy Technology Center where SRC I process was used for the liquefaction. Since the liquid sulfur dioxide separation of saturated hydrocarbons from the coal liquid worked equally well for both coal liquids only the separation of SRC from West Virginia subbituminous coal is discussed in detail for the analytical evaluation of the SO<sub>2</sub> separation. Figure 1 is the GPC of SRC from the subbituminous coal. The components of the coal liquid are separated in the order of decreasing linear molecular size<sup>(10)</sup>. For analytical convenience the effluents from the GPC were collected as four fractions. Fraction 1 is composed of high molecular weight species which are nonvolatiles for gc separations. Fraction 2 is composed of saturated hydrocarbons, which could be separated and identified by GC-MS and 'asphaltenes' (9)-a mixture of high molecular weight species which have comparable linear molecular size to straight chain alkanes in the range n C<sub>14</sub>H<sub>30</sub> to n C<sub>44</sub>H<sub>90</sub>. Vacuum distillation separates the nonvolatile asphaltenes from the volatile alkanes. Fraction 3 is composed mostly of phenols which have an 'effective linear molecular size' of normal alkanes ranging from C<sub>7</sub>H<sub>16</sub> to C<sub>13</sub>H<sub>28</sub>. Each molecule of phenol has a tendency to hydrogen bond with one molecule of THF to result in an increase in effective linear molecular size by 3 to 4 linear carbon units (propane to butane size). Fraction 4 is mostly aromatics. In a non hydrogen bonding system such as toluene both phenols and aromatics will have similar molecular size and hence they could not be separated by GPC using toluene as the mobile liquid phase.

Figure 2 is the GPC of SO<sub>2</sub>-solubles of SRC from subbituminous coal. As in the case of the sample in Figure 1, the GPC effluent was collected as four fractions. After SO<sub>2</sub> treatment the GPC areas of fraction 1 and 2 have decreased and the analysis of fraction 2 of SO<sub>2</sub>-solubles does not show any alkanes. Elemental analysis of Fraction 2 after evaporating all the THF shows the following composition

C	H	S	N	O
83.79%	7.39%	3.96%	1.64%	3.22%(by diff.)

The proton nmr spectra of fraction 2 of SO<sub>2</sub>-solubles resembles the nmr of asphaltenes reported by other workers<sup>(1)</sup>. The elemental composition and the GPC size distribution agrees with the published values for coal derived asphaltenes<sup>(1,3)</sup>. Fractions 3 and 4 of SO<sub>2</sub>-solubles were separated and identified by GC-MS (see figure 4 and 5). These fractions contain only a small amount of alkanes. The components are listed in Table I and II.

Figure 3 shows the GPC of the THF extract of the SO<sub>2</sub>-insolubles. The GC-MS of the THF extract is shown in figure 6 and the components are listed in Table III. The THF extract is free of any phenols or aromatics and contains only straight chain hydrocarbons showing the insolubility of straight chain hydrocarbons as well as branched saturated hydrocarbons in liquid SO<sub>2</sub> even after stirring the sample in SO<sub>2</sub> for several hours.

When SRL produced from North Dakota lignite was treated with liquid sulfur dioxide, the bulk of the coal liquid dissolved except the saturated hydrocarbons and the mineral rich residue. The SO<sub>2</sub>-soluble part did not contain any saturated hydrocarbons. The THF extract of the insolubles were mostly alkanes ranging from n-dodecane (C<sub>12</sub>H<sub>26</sub>) to n-tetratetracontane (C<sub>44</sub>H<sub>90</sub>).

Since most of the coal liquids are composed of more or less similar major species, may differ in composition, liquid sulfur dioxide can be used to extract all the aromatic species of the coal liquid, which is free of saturated hydrocarbons and ash precursors. After degasing SO<sub>2</sub>, distillation under reduced pressure can yield all the phenols and aromatics from the SO<sub>2</sub>-solubles of the coal liquid. The residue which is more or less identical to GPC-Fraction 2 of SO<sub>2</sub>-solubles can be called coal asphaltenes. The

average molecular size of coal asphaltenes (linear molecular size is more precise since it is derived from GPC data) is smaller than that of petroleum derived asphaltenes.

#### ACKNOWLEDGMENTS

The financial support of the Texas Engineering Experiment Station, the Texas A&M University Center for Energy and Mineral Resources and Dow Chemical Co., The Alcoa Foundation, Pittsburgh, PA., Department of Chemical Engineering, and the Gulf Oil Company. Mrs. Argentina Vindiola assisted in collecting some of the data.

#### REFERENCES

1. Azel, T., Williams, R. B., Pancirov, R. J., and Karchmer, J. H., "Chemical Properties of Synthoil Products and Feeds," Report prepared for U.S. Energy Research and Development Administration, FE8007, 1976.
2. White, C. M., Shultz, J. L., and Sharkey, Jr. A. C., *Nature* 268, 620 (1977).
3. Bockrath, B. C., Delle Donne, C. L., and Schweighardt, F. K., *Fuel*, 57, (4), 1978.
4. Philip, C. V., and Anthony, R. G., *TEES PUBLICATIONS, TECH BN.*, 78-2, 10 (1978).
5. Philip, C. V., and Anthony, R. G., "Organic Chemistry of Coal," *ACS Symposium Series*, 258, (1978).
6. Philip, C. V., and Anthony, R. G., *Preprints ACE Fuel Div.* 24 No. 4, 196, Miami, (1978).
7. Philip, C. V., and Anthony, R. G., *Preprints ACE Fuel Div.*, 24 No 3, 204, Washington, (1979).
8. Our unpublished GC-MS data on various coal liquids and distillation cuts.
9. The term 'asphaltene' is used for the coal liquid fraction which is nonvolatile but soluble in tetrahydrofuran (THF) and  $\text{SO}_2$  currently.
10. GPC is used for molecular weight determinations as well as for molecular size determinations. Our unpublished GPC data on a number of compounds such as normal alkanes, amines, alcohols, multi-ring aromatics and etc. shows that the retention volume is a function of the length of the molecule rather than molecular volume or any other molecular size parameters. Therefore, authors think that it is quite appropriate to say that GPC separations are on the basis of linear molecular size rather than just molecular size.

Table I Phenolic Fraction (GPC Fraction #3 From SO<sub>2</sub> - Solubles)

Retention Time (min)	Compound	Retention Time (min)	Compound
4.5	Phenol	21.7	C <sub>4</sub> -Alkylphenol
6.7	o-Cresol	22.3	C <sub>4</sub> -Alkylphenol
7.7	p-Cresol + m-Cresol	23.2	C <sub>5</sub> -Alkylphenol + Methyl Indanol
9.9	C <sub>2</sub> -Alkylphenol		C <sub>5</sub> -Alkylphenol + n C <sub>13</sub> H <sub>28</sub> + Methyl Indanol
11.0	C <sub>2</sub> -Alkylphenol	24.3	Methyl Indanol
11.6	C <sub>2</sub> -Alkylphenol		C <sub>5</sub> -Alkylphenol
12.1	C <sub>2</sub> -Alkylphenol	24.8	C <sub>5</sub> -Alkylphenol
13.0	C <sub>3</sub> -Alkylphenol	25.7	C <sub>5</sub> -Alkylphenol
13.5	C <sub>3</sub> -Alkylphenol	26.2	C <sub>5</sub> -Alkylphenol
14.1	C <sub>3</sub> -Alkylphenol	26.6	C <sub>5</sub> -Alkylphenol
14.6	C <sub>3</sub> -Alkylphenol	27.1	C <sub>5</sub> -Alkylphenol
15.5	C <sub>3</sub> -Alkylphenol	27.7	C <sub>2</sub> -Indanol + C <sub>5</sub> Alkylphenol
16.2	C <sub>3</sub> -Alkylphenol	28.3	C <sub>5</sub> -Alkylphenon + Dimethyl Indanol
16.7	C <sub>3</sub> -Alkylphenol	29.1	C <sub>6</sub> -Alkylphenol + n C <sub>14</sub> H <sub>30</sub> (trace)
17.3	C <sub>3</sub> -Alkylphenol	30.2	C <sub>2</sub> -Alkylindanol + C <sub>6</sub> Alkylphenol
18.0	C <sub>3</sub> -Alkylphenol	31.7	C <sub>2</sub> -Alkylindanol + C <sub>6</sub> Alkylphenol
18.5	C <sub>4</sub> -Alkylphenol + n Dodecane (trace)	32.6	C <sub>6</sub> -Alkylphenol + C <sub>2</sub> Alkyl Naphthol
19.3	C <sub>4</sub> -Alkylphenol	33.7	C <sub>6</sub> -Alkylphenol + C <sub>2</sub> Alkyl Naphthol
19.6	C <sub>4</sub> -Alkylphenol	34.4	C <sub>3</sub> -Alkylindanol
20.1	C <sub>4</sub> -Alkylphenol	36.0	C <sub>3</sub> -Alkylindanol
20.5	C <sub>4</sub> -Alkylphenol	36.5	C <sub>3</sub> -Alkylindanol
		37.2	C <sub>3</sub> -Alkylindanol
		38.2	C <sub>1</sub> -Alkyl naphthol + C <sub>3</sub> Alkylindanol

Table II Aromatic Fraction (GPC fraction #4 From SO<sub>2</sub> - Solubles)

Retention Time (min.)	Compound	Retention Time (min.)	Compound
3.6	Phenol	18.9	C <sub>1</sub> -Alkyl naphthalene + C <sub>3</sub> Alkylindan
4.6	C <sub>3</sub> -Alkylbenzene		C <sub>3</sub> -Alkylindan
5.4	o-Cresol	19.5	C <sub>3</sub> -Alkylindan
6.2	p-Cresol	20.2	C <sub>3</sub> -Alkylindan
7.3	m-Cresol	21.5	C <sub>4</sub> -Alkylindan
8.0	C <sub>2</sub> -Alkylphenol	22.6	C <sub>4</sub> -Alkylindan
8.8	C <sub>2</sub> -Alkylphenol	23.4	C <sub>4</sub> -Alkylindan
9.4	C <sub>2</sub> -Alkylphenol	24.2	C <sub>2</sub> -Alkyl naphthalene + C <sub>4</sub> -Alkylindane
9.9	C <sub>2</sub> -Alkylphenol + Methyl Indan +	24.6	C <sub>4</sub> -Alkylindane + C <sub>2</sub> -Alkyl naphthalene
10.3	Methyl Indan		C <sub>4</sub> -Alkylindane + C <sub>2</sub> -Alkyl naphthalene
11.2	C <sub>1</sub> -Alkylindan	25.0	C <sub>4</sub> -Alkylindane + C <sub>2</sub> -Alkyl naphthalene
12.1	Naphthalene		C <sub>4</sub> -Alkylindane + C <sub>2</sub> -Alkyl naphthalene
12.8	C <sub>2</sub> -Alkyl Indan	25.5	C <sub>4</sub> -Alkylindane + C <sub>2</sub> -Alkyl naphthalene
13.4	C <sub>2</sub> -Alkylindan		C <sub>2</sub> -Alkyl naphthalene
14.5	C <sub>2</sub> -Alkylindan	26.7	C <sub>2</sub> -Alkyl naphthalene
15.5	C <sub>2</sub> -Alkylindan	27.5	C <sub>2</sub> -Alkyl naphthalene
16.3	C <sub>2</sub> -Alkylindan	28.1	C <sub>2</sub> -Alkylindan
17.0	C <sub>2</sub> -Alkylindan	28.7	C <sub>3</sub> -Alkyl naphthalene
17.1	C <sub>1</sub> -Alkyl naphthalene	30.0	C <sub>3</sub> -Alkyl naphthalene
18.2	C <sub>3</sub> -Alkylindan + C <sub>1</sub> -Alkyl naphthalene	31.7	C <sub>3</sub> -Alkyl naphthalene

Table III Hydrocarbon Chains Separated from THF Extract  
of  $\text{SO}_2$  - Insolubles

Retention Time (min.)	Compound	Retention Time (min.)	Compound
12.9	Tridecane	31.0	Eicosane
13.6	Tetradecane	33.4	Heneicosane
15.4	$\text{C}_{14}\text{H}_{30}$	35.9	Docosane
16.7	Pentadecane	38.2	Tricosane
19.7	Hexadecane	40.4	Tetracosane
21.0	$\text{C}_{16}\text{H}_{34}$	42.6	Pentacosane
22.7	Heptadecane + Pristine	44.7	Hexacosane
25.6	Octadecane	46.7	Heptacosane
28.4	Nonadecane		

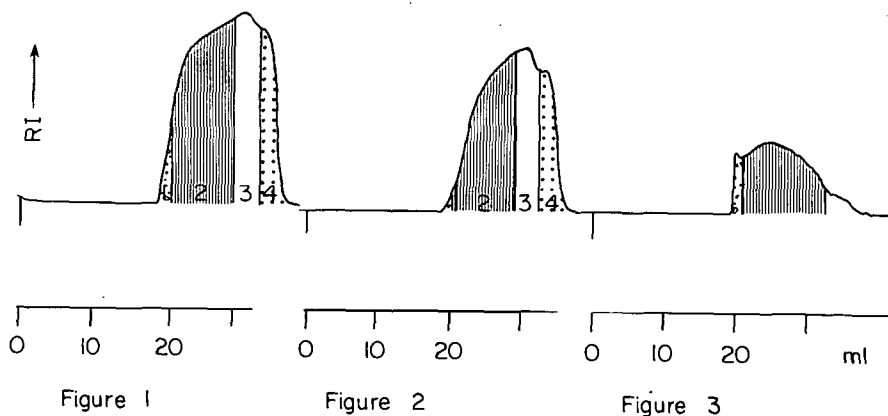


Figure 1. GPC separation of SRC from West Virginia subbituminous coal. The GPC system consisted of four 100 Å Styragel columns and the THF flow rate of 1 ml/min.

Figure 2. GPC separation of  $\text{SO}_2$ -solubles of SRC from West Virginia subbituminous coal. Fraction 3 and 4 are identified by GC-MS (see figures 4 and 5 as well as Table I and II).

Figure 3. GPC of the THF extract of  $\text{SO}_2$ -insolubles of SRC from West Virginia subbituminous coal. See figure 6 for the GC-MS of the extract and Table III for the identification of the components.

Figure 4

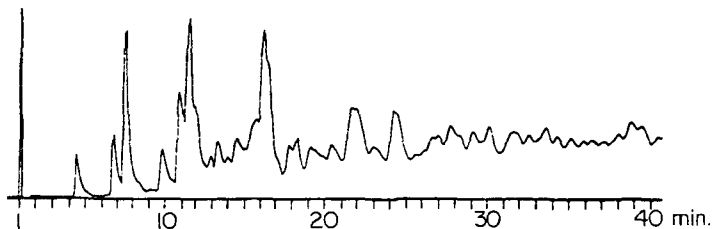


Figure 5

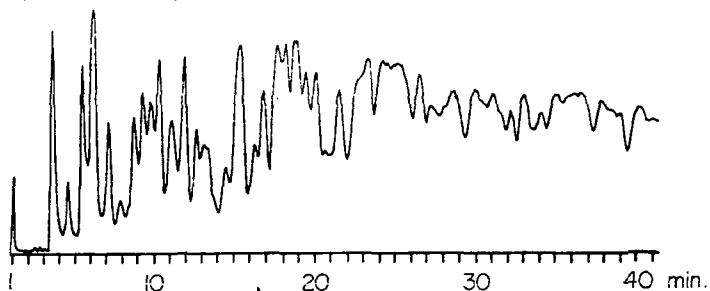


Figure 6

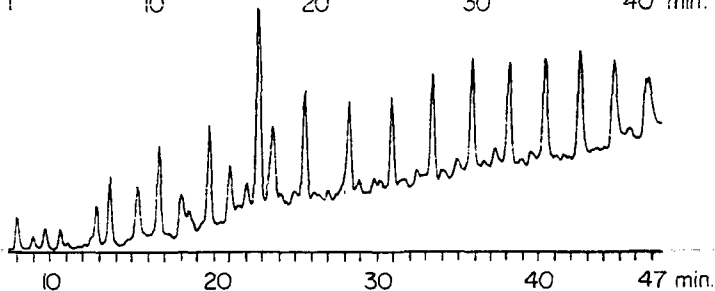


Figure 4. Total ion gas chromatogram of GPC fraction 3 of  $\text{SO}_2$ -solubles (Figure 2). Column: 5% Dexsil 300 on 100/120 Chromosorb H-WP, 1/8 in. od  $\times$  8 ft., Carrier gas: 20 ml helium/min., temperature program: 80-270°C at 2°C/min. for 40 min. followed by 4°C/min. See Table I for peak identification.

Figure 5. Total ion gas chromatogram of GPC fraction 4 of  $\text{SO}_2$ -solubles (figure 2). Same GC condition as in figure 4. See Table III for peak identification.

Figure 6. Total ion gas chromatogram of the THF extract of  $\text{SO}_2$ -insoluble of SRC from West Virginia subbituminous coal. GC conditions were same as in figure 4 except the temperature program of 80 to 270°C at 4°C/min. see Table III for peak identification.

HYDRODESULFURIZATION OF DIBENZOTHIOPHENE CATALYZED BY  
SULFIDED  $\text{CoO-MoO}_3/\gamma\text{-Al}_2\text{O}_3$ : THE REACTION KINETICS

D. H. Broderick and B. C. Gates

Center for Catalytic Science and Technology  
Department of Chemical Engineering  
University of Delaware  
Newark, Delaware 19711

INTRODUCTION

A renewed interest in hydrodesulfurization has come about largely as a result of the need to process more and heavier feedstocks, including synfuels. It has been recognized that model compounds like thiophene are not representative of the least reactive sulfur-containing constituents of these feedstocks. More representative compounds are dibenzothiophenes and benzonaphthothiophenes, which are present in high concentrations in heavy oils (and especially in coal-derived liquids) and are one to two orders of magnitude less reactive than thiophene (1,2).

There is a need for quantitative kinetics characterizing hydroprocessing of these relatively unreactive compounds at temperatures and pressures representative of commercial operation. The goal of this research was to determine detailed kinetics of dibenzothiophene hydrodesulfurization using a high-pressure flow microreactor (3). Earlier work had established the reaction network in dibenzothiophene hydrodesulfurization catalyzed by a commercial presulfided  $\text{CoO-MoO}_3/\gamma\text{-Al}_2\text{O}_3$  (4). Early kinetics studies of dibenzothiophene hydrodesulfurization (5,6) fail to account for the complete reaction network and are lacking in experimental detail. Recent kinetics studies (7,8) of dibenzothiophene hydrodesulfurization also fail to provide sufficient detail of the reaction network, and the range of hydrogen partial pressures applied was so low and not all the parameters in the rate equations could be determined from the data.

In the present study rates of the two primary reactions of dibenzothiophene with hydrogen were measured independently, and the full set of data was analyzed and summarized in the form of Langmuir-Hinshelwood rate equations. The data allowed precise estimation of all the kinetics parameters at three temperatures.

EXPERIMENTAL

Materials

The catalyst was a commercial  $\text{CoO-MoO}_3/\gamma\text{-Al}_2\text{O}_3$  (American Cyanamid HDS 16A) which was crushed and sieved to 149-178  $\mu\text{m}$  (80-100 mesh) particle size and sulfided in situ. Catalyst compositions are given elsewhere (4). Dibenzothiophene (Eastman, reagent grade) was dissolved in n-hexadecane (Humphrey Chemical Co., specially distilled Lots No. 2270375 and 4090577), and the solution was filtered through a 0.5  $\mu\text{m}$  filter element (Milipore). Biphenyl (Eastman, reagent grade) was used as supplied. Hydrogen was obtained from Linde as 3500 psi grade and treated as described below to remove traces of moisture and oxygen.  $\text{H}_2\text{S}$  was supplied by Linde in custom mixtures with hydrogen in concentrations of 0.5 to 10 mole%  $\text{H}_2\text{S}$ . Alundum "RR" (Fisher

Scientific, Blue Label) was sieved to 90 mesh and used as an inert reactor packing.

A high-pressure flow microreactor, described in detail by Eliezer et al. (3), was modified to allow for saturation of the feed mixture with a predetermined  $H_2S$  partial pressure (9). The catalyst ( $6.5 \times 10^{-5}$  to  $1.2 \times 10^{-4}$  kg) was mixed with alundum ( $2.31 \times 10^{-4}$  to  $4.25 \times 10^{-4}$  kg) to give the range of bed volumes [ $(2.0-3.6) \times 10^{-7}$  m<sup>3</sup>] and bed heights [ $(2.5-4.5) \times 10^{-2}$  m]. The catalyst was presulfided in the reactor for two hours in a  $5.0 \times 10^{-7}$  to  $8 \times 10^{-7}$  m<sup>3</sup>/s flow of 10 vol% hydrogen sulfide in hydrogen at atmospheric pressure and 673°K.

Reactant solutions containing 0.3-4.9 mole% dibenzothiophene in n-hexadecane or 1.24 mole% dibenzothiophene and 0.6 or 2.9 mole% biphenyl in n-hexadecane were prepared. After the solution ( $5 \times 10^{-4}$  to  $7 \times 10^{-4}$  m<sup>3</sup>) had been loaded into a stirred autoclave, it was saturated with hydrogen or hydrogen plus  $H_2S$  at predetermined partial pressures after the mixture had been purged for 2 hr with the gas mixture.  $H_2S$  partial pressures were varied from 0 to 1 atm, and hydrogen partial pressures were varied between 34 and 150 atm. Low-pressure gas solubility data served as a basis for extrapolation to high saturation pressures, as described elsewhere (9), for calculating hydrogen and  $H_2S$  concentrations in the reactor. Reactant concentrations used to correlate the reaction rate data were calculated for the liquid density at the temperature and pressure of the reactor.

Immediately after sulfiding of the catalyst, the reactor was cooled to 573°K, and flow of reactant mixture was initiated. The pressure in the reactor was maintained at  $178 \pm 7$  atm to ensure against formation of a gas phase inside the reactor. A catalyst break-in period of 50 to 72 hr was allowed, after which the reactor was run with differential conversion of dibenzothiophene to obtain reaction rate data. Over an extended period, hydrogen and  $H_2S$  partial pressures were varied, and solutions with the above-mentioned dibenzothiophene concentrations were each investigated at 548, 573 and 598°K. Throughout each run, the rate of reaction was repeatedly measured at the standard condition of 573°K, 96 atm hydrogen partial pressure, 1.24 mole% dibenzothiophene, and 0 or 0.16 atm  $H_2S$  partial pressure; these data demonstrated the lack of significant catalyst deactivation.

At each run condition, four to eight liquid product samples were collected and analyzed by glc. An Antek 462 gas chromatograph equipped with a flame ionization detector and an electronic integrator was used. The column was a 3.4 m stainless steel column having a  $2.3 \times 10^{-3}$  m ID and packed with 3% SP-2100 DB (methyl silicone fluid--the basic sites were deactivated) on 100-200 mesh Supelcoport (Supelco) at 423°K with a helium carrier-gas flow rate of about  $5 \times 10^{-7}$  m<sup>3</sup>/s. Gaseous products, such as  $H_2S$  and any light cracking products, were not collected. In the routine analysis, dibenzothiophene, biphenyl, cyclohexylbenzene, and 1,2,3,4-tetrahydrodibenzothiophene were determined quantitatively. Another product formed in equilibrium with 1,2,3,4-tetrahydrodibenzothiophene, i.e., 1,2,3,4,10,11-hexahydrodibenzothiophene (4), was masked by the solvent.

Using a wall-coated open tubular column (Perkin-Elmer OV-101) in a Perkin-Elmer 3920 B gas chromatograph, a sufficient number of samples were reanalyzed to establish the equilibrium constant for the reaction  $1,2,3,4\text{-tetrahydrodibenzothiophene} + H_2 \rightleftharpoons 1,2,3,4,10,11\text{-}$

hexahydrodibenzothiophene] at the three temperatures studied. Equilibrium constants are given in Table 1. The concentration of 1,2,3,4,10,11-hexahydrodibenzothiophene was then calculated for each sample from the equilibrium constant and the known concentration of hydrogen and 1,2,3,4-tetrahydrodibenzothiophene. Total aromatic carbon in the product stream was typically 98 to 99% of the amount of dibenzothiophene in the feed mixture.

## RESULTS

Preliminary experiments reported earlier (4) showed that the reactor filled with alundum alone had negligible activity for dibenzothiophene hydrodesulfurization, and intraparticle and extraparticle mass transfer resistances were negligible.

Addition of 0.02 mole of  $H_2S$ /liter of reactant solution was necessary to stabilize the catalyst (10). With constant catalytic activity, rates were determined from differential conversions for a wide range of reactant and product concentrations at 548, 573, and 578°K; detailed data are given elsewhere (9). Concentrations and temperatures were changed randomly throughout, with periodic activity checks at the standard conditions.

Data were plotted as fractional conversion to cyclohexylbenzene, to biphenyl, and to cyclohexylbenzene plus 1,2,3,4-tetrahydrodibenzothiophene plus 1,2,3,4,10,11-hexahydrodibenzothiophene (9). The plots show a linear dependence of conversion on WHSV, and the first set of data falls near a curve that approaches the origin with near-zero slope. These results are consistent with the reaction network proposed for dibenzothiophene hydrodesulfurization by Houalla *et al.* (4). This network indicates two primary reactions: Hydrogenation of one aromatic ring gives an equilibrium mixture of 1,2,3,4-tetrahydrodibenzothiophene and 1,2,3,4,10,11-hexahydrodibenzothiophene; hydrodesulfurization of these two intermediates occurs rapidly to give cyclohexylbenzene. This combination of reactions is referred to as the hydrogenation route, and this combination of products determined rates of hydrogenation of dibenzothiophene. The second reaction was direct hydrodesulfurization of dibenzothiophene to give biphenyl, which is referred to as the hydrogenolysis reaction. Biphenyl also reacted with hydrogen to give cyclohexylbenzene, but this reaction was typically two orders of magnitude slower than the rate of dibenzothiophene hydrogenolysis (11).

In summary, the reactant and product concentration data give the overall rate of dibenzothiophene disappearance and also the rates of the two primary reactions of dibenzothiophene, one aromatic ring hydrogenation, and the other hydrogenolysis.

There was a consistent discrepancy in the results indicated by lack of closure of the mass balance on carbon. The sum of the hydrogenation and hydrogenolysis rates was on the average 80-85% of the rate of dibenzothiophene disappearance. The cause of this imbalance could not be determined, but it appears most likely to have been the result of some cracking to volatiles lost in sample collection; it is possible that some heavier products were formed, but the lack of catalyst deactivation suggests that the former possibility is more likely. The rate of unobserved product formation was virtually independent of reaction conditions, and the lack of closure of the

mass balance therefore did not prevent meaningful measurement of the reaction rates.

Representative plots of some of the rate data are given in Figures 1-3. A Langmuir dependence of rate on dibenzothiophene concentration is suggested for each reaction. The rate of hydrogenation is linearly dependent on hydrogen concentration, and the rate of hydrogenolysis shows a Langmuir dependence on hydrogen concentration. Inhibition by hydrogen sulfide was observed for dibenzothiophene hydrogenolysis, but a striking and surprising absence of hydrogen sulfide inhibition is noted for hydrogenation. The effect of biphenyl concentration on the overall rate of dibenzothiophene conversion was negligible at the lower temperatures; a small inhibition effect was observed at 598°K.

#### DISCUSSION

A number of rate equations, both purely empirical equations and equations corresponding to Langmuir-Hinshelwood models, were evaluated in terms of their ability to represent the data for dibenzothiophene hydrogenation and hydrogenolysis. An independent set of equations was considered for each of the two reactions. The full set of equations is considered elsewhere (9), and here we consider only the equations giving the best fits to the data.

A non-linear least-squares regression analysis was used with each equation in Tables 2 and 3 to determine the best equations for representing the data. A library program, NLLS (1977), from the University of Delaware Computing Center (based on the Marquardt regression technique) was used. The output of the program includes the parameter values giving the best fit as determined by the routine and several statistical measures of the goodness of fit. These are (1)  $\phi_{\min}$ , the minimized sum of the squares of the differences between the observed and predicted rates for each condition, (2) a correlation matrix representing the degree of independence of each of the equation parameters from the other parameters, and (3) non-linear 95% confidence limits given as an upper and lower bound on the value of each of the parameters. Summarized in Tables 2 and 3 are the parameter values, the largest difference between the parameter value and the upper or lower bound, and the calculated  $\phi_{\min}$  values. The full sets of equations evaluated for each reaction are given in Broderick's thesis (9).

In addition to the statistical criteria of goodness of fit, there are several criteria determining whether an equation has physical meaning: (1) The estimated rate constant and adsorption constants should be positive or include positive values within their error bounds; (2) a plot of the logarithm of the rate constant versus reciprocal absolute temperature (Arrhenius plot) should be linear with a negative slope; (3) a plot of the logarithm of each adsorption equilibrium constant versus reciprocal absolute temperature (van't Hoff plot) should be linear with a positive slope except when chemisorption is endothermic; and (4) a visual comparison between experimentally measured trends and predicted curves should show satisfactory agreement.

The six best equations for the hydrogenolysis reaction data are given in Table 2. Of these, the first four can be derived from the Langmuir-Hinshelwood model assuming various forms of competitive and noncompetitive adsorption, dissociative or undissociative. The last

two equations are similar in form but do not correspond to any simple Langmuir-Hinshelwood model.

Equations (HS-3), (HS-5), and (HS-6) were found to satisfy all the physical and statistical criteria enumerated above. If, in addition, an equation of Langmuir-Hinshelwood formulation is preferred, Eq. (HS-3) is the only acceptable choice. Eq. (HS-1) gives a poorer fit, judging by the magnitude of  $\phi_{\min}$ . Eqs. (HS-2) and (HS-4) showed strong parameter correlation and relatively large deviations from linearity of the Arrhenius plot.

Eq. (HS-5) differs from Eq. (HS-3) only in the half power on the term  $K_S C_S$  in the denominator. That same power on  $K_S C_S$  in Eq. (HS-6) is largely responsible for the good fit observed for this equation as well. The half power on  $K_S C_S$  in Eq. (HS-5) might be interpreted as a suggestion that adsorption of  $H_2S$  may occur dissociatively. This suggestion is not unprecedented (12), but it is considered speculative if based only on kinetics data.

Eq. (HS-3) is recommended as the best equation resting on a Langmuir-Hinshelwood model for representing the data for hydrogenolysis at all conditions studied. From the Arrhenius plot for this equation, the activation energy, determined from the temperature dependence of  $k/K_p$ , is 30 kcal/gmole. Following the Langmuir-Hinshelwood model, the heats of adsorption for dibenzothiophene,  $H_2S$ , and hydrogen were calculated to be -4.5, -5.3, and 8.4 kcal/gmole, respectively. The positive value for the heat of adsorption of hydrogen was observed for all of the equations tested and is perhaps an anomaly associated with the imprecision in the data; the 90% confidence limits on the heat of adsorption are large and include negative values.

Data for the rate of dibenzothiophene hydrogenation were best represented by the equations in Table 3; other equations are considered in Broderick's thesis (9). Differences in goodness of fit among these four equations are relatively small. Eq. (HN-1) is recommended for its goodness of fit, its simple form, and its low parameter correlation and error bounds relative to the other equations. Eqs. (HN-2) and (HN-3) have high error bounds on  $K_H$ , and Eqs. (HN-2) and (HN-4) show large deviations from linear Arrhenius plots. Differences in  $\phi_{\min}$  are not significant when compared with the standard deviations of the data. The temperature dependence of  $k'$  (defined as  $k/K_p$ ) and  $K_p$  were calculated from Arrhenius and van't Hoff plots. An activation energy of 27.6 kcal/gmole and a heat of adsorption for dibenzothiophene of -1.4 kcal/gmole resulted.

The literature on hydrogenolysis reaction kinetics in hydrodesulfurization of thiophenic compounds catalyzed by Co-Mo/ $\gamma$ - $Al_2O_3$  is in general agreement with the results for dibenzothiophene. Much of the work has concerned thiophene (13-16) and benzothiophene (17) at pressures near atmospheric and for narrow ranges of hydrogen partial pressure. There is much evidence that the principal reaction for both compounds is hydrogenolysis. There is strong agreement that the dependence of rate on the concentrations of thiophenic reactant and of  $H_2S$  is the same as shown in Eq. (HS-3). The dependence of rate on hydrogen partial pressure has typically been represented as first order at low partial pressures (13-14,16), although data have been meager. One of the contributions of the present kinetics study was

therefore the clear determination of the dependence of rate on hydrogen concentration under conditions more typical of commercial processes.

The results of previous kinetics studies of dibenzothiophene differ somewhat from the kinetics for hydrogenolysis reported here. For conditions similar to those applied here but for a maximum hydrogen partial pressure of 31 atm, Espino et al. (7) and Mahoney et al. (8) reported a rate equation with a power of 1 on the denominator term for adsorption of  $H_2S$  and dibenzothiophene. Mahoney et al. observed a first order dependence of rate on hydrogen partial pressure. In neither study was the rate of hydrogenation distinguished from the rate of hydrogenolysis, and we infer that under the reported reaction conditions, both reactions contributed to the measured rates of dibenzothiophene conversion. Thus the reported kinetics do not represent hydrogenolysis alone, but correlate all reaction rates. They are in good agreement with the sum of the equations for hydrogenolysis and hydrogenation determined in this work (9).

Reported activation energies for hydrogenolysis of thiophene and benzothiophene range from 4 to 20 kcal/gmole (9) compared with approximately 30 kcal/gmole for hydrogenolysis of the less reactive dibenzothiophene. If we interpret the Langmuir-Hinshelwood rate equation literally (which is surely an oversimplification), we can infer values of the heats of adsorption from the slopes of the van't Hoff plots. The heat of adsorption calculated for  $H_2S$  implied by the hydrogenolysis rate equation falls within the range reported in the literature (5-20 kcal/gmole), and the value for dibenzothiophene (4.5 kcal/gmole) is lower than those for thiophene and benzothiophene (12-24 kcal/gmole).

Literature on the hydrogenation reaction of dibenzothiophene consists of the work by Houalla et al. (4) and Bhide (18), who used large excesses of hydrogen and accurately approximated the rate of dibenzothiophene disappearance by hydrogenation as a pseudo first-order reaction. Hydrogenations of other heteroaromatics, such as quinoline and pyridine, and of aromatics such as biphenyl, naphthalene, and benzene catalyzed by presulfided Co-Mo/ $\gamma-Al_2O_3$  have been studied, and limited kinetics data have been reported. For biphenyl, Espino et al. (7) represented rate data with a Langmuir-Hinshelwood equation indicating competitive adsorption of biphenyl and cyclohexylbenzene on one kind of site and of hydrogen on another. No measure of inhibition by  $H_2S$  was determined. Few details were given concerning the data and the criteria for selection of the rate equation. For pyridine (19) and quinoline (18,20) the rate of hydrogenation of the aromatic ring (or rings) was approximated as first order in heteroaromatic, but the rate constant decreased with increasing reactant concentration, suggesting self inhibition of reaction. The order of reaction in hydrogen partial pressure ranged from 1 to 1.5 for pyridine, and from 0.5 to 1 for quinoline. The effect of  $H_2S$  on the rate of hydrogenation of quinoline was negligible, and for pyridine,  $H_2S$  was an inhibitor when  $<2$  mole%  $H_2S$  was present, and otherwise the rate was independent of  $H_2S$  concentration. For the most part, these kinetics results for hydrogenation reactions of nitrogen-containing aromatics are in agreement with the dibenzothiophene hydrogenation kinetics represented by Eq. (HN-1). These results suggest a rather wide application of Eq. (HN-1) for hydrogenation of aromatics and heteroaromatics.

Studying the hydrodesulfurization kinetics of dibenzothiophene has provided a unique opportunity to examine carbon-sulfur bond hydrogenolysis reactions and aromatic ring hydrogenation under identical conditions. Both reactions are of major importance in hydroprocessing. The kinetics results provide some insight into the mechanisms of the catalytic mechanisms, on one hand, and suggestions for tailoring the catalyst and process conditions to the desired product selectivity, on the other.

Comparison of Figures 1 and 2 and Eqs. (HS-3) and (HN-1) suggests that for sulfided  $\text{CoO-Mo}/\gamma\text{-Al}_2\text{O}_3$  catalyst, the reaction mechanism and catalytic sites differ for hydrogenation and hydrogenolysis. The literature supports the proposal of two different kinds of sites for hydrogenation and hydrogenolysis. The evidence is provided by results of poisoning (14,21,22) and kinetics (13,14,17,18) studies. One kind of site is strongly poisoned by bases such as pyridine and quinoline, and the other is less acidic and less sensitive to such poisons. The former sites are associated with hydrogenation activity and the latter with C-S bond scission activity, although some overlap is expected. From Equation (HN-1), it is inferred that the hydrogenation sites do not bond strongly to hydrogen or  $\text{H}_2\text{S}$ , but they do bond strongly to dibenzothiophene. In contrast,  $\text{H}_2\text{S}$  does compete strongly with dibenzothiophene for hydrogenolysis sites, as follows from Eq. (HS-3). The form of this equation suggests the hydrogen adsorbs on still another type of site, as is expected from the known formation of -SH groups on the surface.

The structure of dibenzothiophene adsorbed on the catalyst surface is unknown, but the extensive hydrogenation of the benzenoid rings suggests considerable ring interaction with the surface. Dibenzothiophene, being a planar molecule, is believed to adsorb in a plane parallel to the catalyst surface favorable to metal-ring interactions at anion vacancies on the surface. Proposals for adsorption via  $\pi$ -complex formation (23,24) or multi-point bonding (25) are strengthened by these results.

A well-recognized concern in hydroprocessing is the consumption of expensive hydrogen. Considering quantitatively the marked differences in the kinetics reported here for hydrogenation and hydrogenolysis of dibenzothiophene, we recognize two important processing variables for minimizing the hydrogen consumption in hydrodesulfurization. Decreased  $\text{H}_2\text{S}$  concentrations (obtainable by recycle gas scrubbing) favor hydrogenolysis. The change in selectivity is dramatic for  $\text{H}_2\text{S}$  concentrations between about zero and 0.1 gmole/liter. Temperature also strongly influences the relative rates of hydrogenation and hydrogenolysis. As the temperature is raised, the relative rate of hydrogenolysis increases sharply. The selectivity for dibenzothiophene hydrogenolysis also increases with increasing concentration of quinoline, an inhibitor of both hydrogenation and hydrogenolysis reactions (18). It is important to remember that, in general, competition between the sulfur-containing reactant and other feed components may alter the kinetics and selectivity. Recognizing this limitation, we recommend the kinetics presented here for qualitative guidance in process design and suggest that the form of the rate equation (modified to account for the presence of various inhibitors) could be of use in reaction engineering models for process simulation.

#### ACKNOWLEDGMENT

This research was supported by the Department of Energy.

# REFERENCES

- (1) Houalla, M., D. Broderick, V. H. J. de Beer, B. C. Gates, and H. Kwart, Preprints, ACS Div. Petrol. Chem., **22**, 941 (1977).
- (2) Nag, N. K., A. V. Sapre, D. H. Broderick, and B. C. Gates, J. Catal., **57**, 509 (1979).
- (3) Eliezer, K. F., M. Bhinde, M. Houalla, D. H. Broderick, B. C. Gates, J. R. Katzer, and J. H. Olson, Ind. Eng. Chem. Fundamentals, **16**, 380 (1977).
- (4) Houalla, M., N. K. Nag, A. V. Sapre, D. H. Broderick, and B. C. Gates, AIChE J., **24**, 1015 (1978).
- (5) Obolentsev, R. D., and A. V. Mashkina, Doklady Akad. Nauk SSSR, **119**, 1187 (1958).
- (6) Obolentsev, R. D., and A. V. Mashkina, Khim. Seraorganicheskikh Soedinenii Soderzh v Neftyakh i Nefteprod Akad. Nauk SSSR, **2**, 228 (1959).
- (7) Espino, R. L., J. E. Sobel, G. H. Singhal, and G. A. Huff, Jr., Preprints, ACS Div. Petrol. Chem., **23** (1), 46 (1978).
- (8) Mahoney, J. A., K. K. Robinson, and E. C. Myers, Chemtech, **8**, 758 (1978).
- (9) Broderick, D. H., Ph.D. Thesis, University of Delaware, 1980.
- (10) Broderick, D. H., Schuit, G. C. A., and Gates, B. C., J. Catal., **54**, 94 (1978).
- (11) Sapre, A. V., and B. C. Gates, Preprints, ACS Div. Fuel Chem., in press.
- (12) Massoth, F. E., J. Catal., **36**, 164 (1975).
- (13) Satterfield, C. N., and G. W. Roberts, AIChE J., **14** (1), 159 (1968).
- (14) Lee, H. C., and J. B. Butt, J. Catal., **49**, 320 (1977).
- (15) Phillipson, J. J., AIChE Meeting, Houston, 1971.
- (16) Morooka, S., and C. E. Hamrin, Chem. Eng. Sci., **32**, 125 (1977).
- (17) Kilanowski, D. R., and B. C. Gates, J. Catal., in press.
- (18) Bhinde, M. V., Ph.D. Thesis, University of Delaware (1979).
- (19) Goudriaan, F., Ph.D. Thesis, Twente Institute of Technology, The Netherlands (1974).
- (20) Shih, S. S., J. R. Katzer, H. Kwart, and A. B. Stiles, Preprints, ACS Div. Petrol. Chem., **22**, 919 (1977).
- (21) Desikan, P., and C. H. Amberg, Can. J. Chem., **42**, 843 (1964).

- (22) Urimoto, H., and N. Sakikawa, Sekiyu Gakkaishi, 15 (11), 926 (1972).
- (23) Cowley, S. W., Ph.D. Thesis, Southern Illinois University, Carbondale (1975).
- (24) Singhal, G. H., and R. L. Espino, Preprints, ACS Div. Petrol. Chem., 23 (1), 36 (1978).
- (25) Kwart, H., G. C. A. Schuit, and B. C. Gates, J. Catal., in press.

#### NOMENCLATURE

$C_i$	Concentration of Species "i"	$k'$	Intrinsic Rate Constant ( $= k/K_0/K_H$ )
D	Dibenzothiophene	$K_i$	Adsorption Equilibrium Constant of Species i
H	Hydrogen ( $H_2$ )	S	Hydrogen Sulfide ( $H_2S$ )
HHD	Hexadhydrodibenzothiophene	THD	Tetrahydrodibenzothiophene
k	Observed Rate Constant		

TABLE 1

Temperature Dependence of the  
Equilibrium Constant  $K_X$

Temp., $^{\circ}K$	$K_X^a$
548	$5.76 \pm 0.29^b$
573	$3.45 \pm 0.33$
598	$2.05 \pm 0.17$

$$K_X \approx \text{EXP } (-\Delta G^{\circ}/RT),$$

$$\Delta G^{\circ} = 13,400 - T(^{\circ}K) \times 10.55 \text{ cal/gmole}$$

<sup>a</sup> $K_X$  is defined as  $X_{HHD}/X_H X_{THD}$  where  $X_i$  is the mole fraction of species i.

<sup>b</sup> $K_X$  was calculated for various  $X_H$  and averaged. Error bound is standard deviation.

TABLE 2

## Rate Equations Best Fitting Dibenzothiophene Hydrogenolysis Kinetic Data

Rate Equation	Temp., °C	$10^6 \times k, \text{ hr}^{-1}$ mole-% of catalyst: sec	$k_D$ , liter/mole	$k_H$ , liter/mole	$k_S$ , liter/mole	$10^6 \times t_{\text{min}}$ , ( $\frac{\text{mole}}{\text{mole}} \cdot \text{sec}$ ) <sup>2</sup> % of catalyst: sec
(HS-1) $\frac{k C_D C_H}{(1 + K_D C_D + K_S C_S)^2}$	275 300 325	11.4 ± 1.3 39.9 ± 4.3 130 ± 15	10.3 ± 3.0 7.2 ± 2.5 6.6 ± 2.6	-- -- --	86 ± 16 74 ± 12 59 ± 11	0.366 6.81 82.3
(HS-2) $\frac{k C_D C_H}{(1 + K_D C_D + K_S C_S + K_H C_H)^2}$	275 300 325	30.1 ± 3.9 200 ± 22 439 ± 53	18.1 ± 5.8 18.5 ± 6.1 14.5 ± 5.0	2.9 ± 1.3 6.0 ± 1.4 4.1 ± 1.2	137 ± 31 161 ± 27 103 ± 21	0.342 5.39 63.3
(HS-3) $\frac{k C_D C_H}{(1 + K_D C_D + K_S C_S)^2 (1 + K_H C_H)}$	275 300 325	15.7 ± 2.0 69.3 ± 7.5 215 ± 26	11.5 ± 3.5 8.7 ± 2.7 8.2 ± 2.8	1.6 ± 1.0 3.2 ± 1.1 2.9 ± 1.2	86 ± 19 75 ± 12 58 ± 12	0.341 5.36 63.4
(HS-4) $\frac{k C_D C_H}{(1 + K_D C_D + K_S C_S)^2 [1 + (K_H C_H)^{1/2}]^2}$	275 300 325	20.3 106.3 315	11.4 8.5 8.1	0.46 1.72 1.40	86.5 74.9 58.1	0.341 5.41 64.6
(HS-5) $\frac{k C_D C_H}{[1 + K_D C_D + (K_S C_S)^{1/2}]^2 (1 + K_H C_H)}$	275 300 325	59.9 ± 4.7 205 ± 14 503 ± 33	23.9 ± 3.8 16.4 ± 2.7 13.3 ± 2.2	1.77 ± 0.59 3.20 ± 0.61 2.96 ± 0.60	868 ± 144 518 ± 72 256 ± 38	0.122 1.99 18.7
(HS-6) $\frac{k C_D C_H}{(1 + K_D C_D + K_H C_H)^2 [1 + (K_S C_S)^{1/2}]^2}$	275 300 325	25.1 ± 1.9 111.0 ± 7.4 323 ± 21	5.2 ± 1.2 4.7 ± 1.0 5.0 ± 0.9	0.89 ± 0.28 1.44 ± 0.27 1.38 ± 0.27	270 ± 42 221 ± 29 127 ± 17	0.122 1.98 18.3

TABLE 3  
Rate Equations Best Fitting Dibenzothiophene Hydrogenation Kinetics Data

Rate Equation	Temp., °C	$10^6 \times k$ , $\frac{\text{liter}^2}{\text{gmole} \cdot \text{g of catalyst} \cdot \text{sec}}$	$K_D$ , $\frac{\text{liter}}{\text{gmole}}$	$K_H$ , $\frac{\text{liter}}{\text{gmole}}$	$K_S$ , $\frac{\text{liter}}{\text{gmole}}$	$10^{17} \times \phi_{\min}$ , $\left(\frac{\text{gmole}}{\text{g of catalyst} \cdot \text{sec}}\right)^2$
(HN-1) $k \frac{C_D C_H}{(1+K_D C_D)}$	275 300 325	2.78 ± 0.11 8.11 ± 0.24 20.9 ± 0.57	7.39 ± 0.89 7.70 ± 0.72 6.61 ± 0.55	-- -- --	--	1.30 7.14 24.3
(HN-2) $k \frac{C_D C_H}{(1+K_D C_D)(1+K_H C_H)}$	275 300 325	2.95 ± 0.14 8.60 ± 0.30 21.6 ± 0.7	7.6 ± 1.07 7.92 ± 0.85 6.73 ± 0.67	0.25 ± 0.25 0.26 ± 0.19 0.14 ± 0.16	-- -- --	1.26 6.78 23.7
(HN-3) $k \frac{C_D C_H}{(1+K_D C_D + K_H C_H)}$	275 300 325	2.98 ± 0.14 8.69 ± 0.30 21.7 ± 0.66	8.0 ± 1.1 8.4 ± 0.9 6.9 ± 0.7	0.31 ± 0.35 0.32 ± 0.26 0.16 ± 0.22	-- -- --	1.26 6.80 23.7
(HN-4) $k \frac{C_D C_H}{[1+(K_D C_D)^{\frac{1}{2}}]^2 (1+K_H C_H)}$	275 300 325	4.34 ± 0.18 12.6 ± 0.4 30.2 ± 0.74	3.78 ± 0.50 3.91 ± 0.41 2.81 ± 0.25	0.27 ± 0.22 0.27 ± 0.17 0.16 ± 0.13	-- -- --	0.987 5.73 16.0

FIGURE 1

REACTION RATES IN DIBENZOTHIOPHENE  
HYDRODESULFURIZATION AS A FUNCTION OF  
HYDROGEN CONCENTRATION AT 300°C

Curves are Predicted by Fitted Rate  
Equations Described in the Text

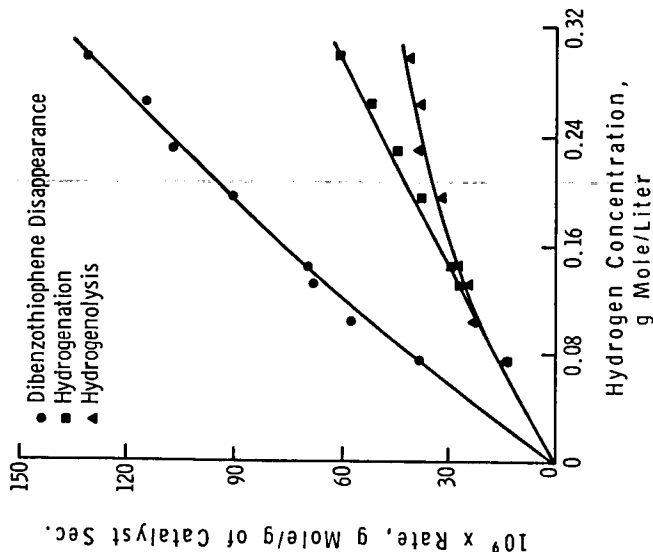


FIGURE 2

REACTION RATES IN DIBENZOTHIOPHENE  
HYDRODESULFURIZATION AS A FUNCTION OF  
DIBENZOTHIOPHENE CONCENTRATION AT 300°C

Curves are Predicted by Fitted Rate  
Equations Described in the Text

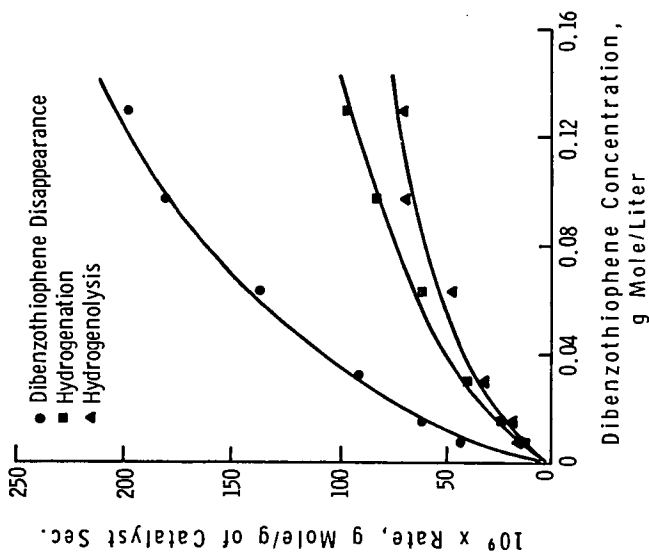
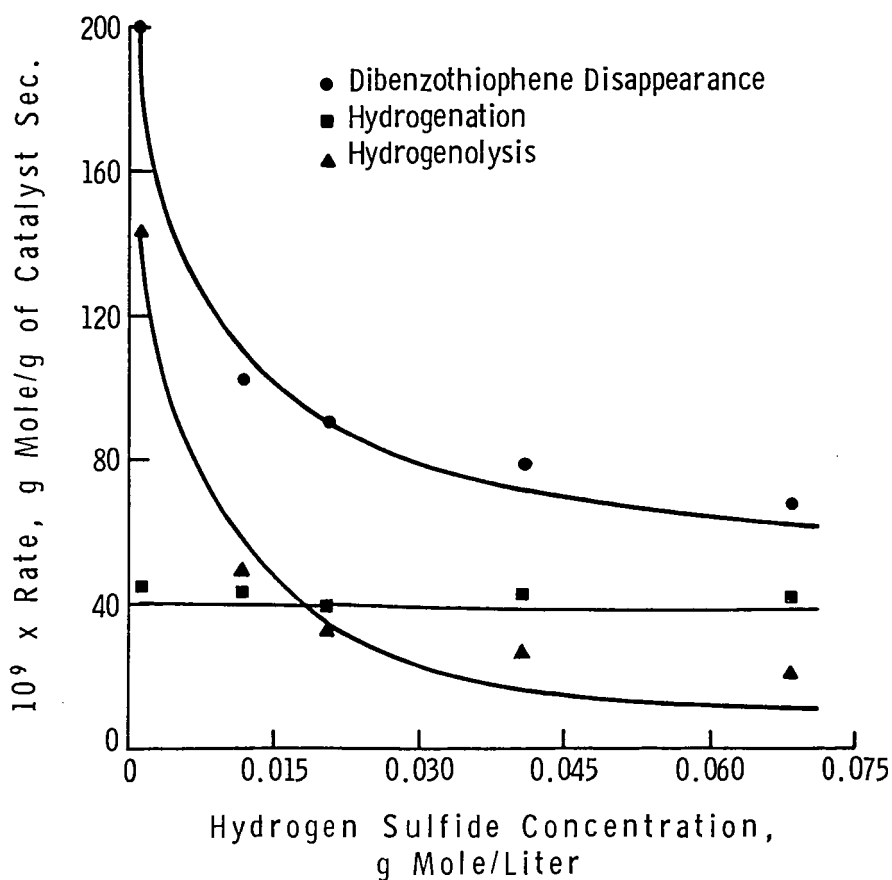


FIGURE 3

REACTION RATES IN DIBENZOTHIOPHENE  
HYDRODESULFURIZATION AS A FUNCTION OF  
HYDROGEN SULFIDE CONCENTRATION AT 300°C

Curves are Predicted by the Fitted Rate  
Equations Described in the Text



Hydrogenation of Aromatic Hydrocarbons  
Catalyzed by Sulfided  $\text{CoO-MoO}_3/\gamma\text{-Al}_2\text{O}_3$ :  
Reactivities, Reaction Networks, and Kinetics

A. V. Sapre and B. C. Gates

Center for Catalytic Science and Technology  
Department of Chemical Engineering  
University of Delaware  
Newark, Delaware 19711

INTRODUCTION

Accompanying the recent emphasis on new energy sources, there has been a surge of development work on processes for upgrading heavy fossil fuels, including coal liquids, shale oil, tar sands, and petroleum residua. Upgrading is normally effected by hydrotreating in the presence of catalysts like "cobalt molybdate" or "nickel molybdate" at 50-250 atm and 300-450°C (1). In these applications, the principal catalytic reactions are hydrodesulfurization, hydrodenitrogenation, hydrodeoxygenation, hydrocracking, and hydrogenation of aromatics. Among the slowest of these reactions are the aromatic hydrogenations, which take on great importance because hydrodenitrogenation of polycyclic aromatics does not take place until ring saturation has occurred (2). It therefore appears that with the best available catalysts, hydrogenation of aromatics is the class of hydroprocessing reactions most deserving of careful study.

Hydrogenation of aromatics is also important in developing coal liquefaction technology exemplified by the donor solvent process and some forms of the solvent refined coal process (3); in these processes the product liquid undergoes catalytic hydrogenation and is then recycled to the liquefaction reactor, where it transfers hydrogen to the liquefying coal (4).

The literature of catalytic hydroprocessing provides only fragmentary information about the reaction networks, reactivities, and kinetics in aromatic hydrogenation, most of the work having been done with unpromoted catalysts at conditions far removed from those of industrial interest (5). The reported kinetics data for hydrogenation of aromatics in the presence of promoted sulfided catalyst like "cobalt molybdate" are limited to benzene, cyclohexene, toluene, phenanthrene, and naphthalene (6-11).

The experiments reported here were carried out to establish the reactivities and reaction networks for hydrogenation of benzene, biphenyl, naphthalene, and 2-phenylnaphthalene as well as detailed kinetics of biphenyl hydrogenation in the presence of a commercial catalyst (sulfided "cobalt molybdate,"  $\text{CoO-MoO}_3/\gamma\text{-Al}_2\text{O}_3$ ). The relative reactivities and reaction networks were determined at a pressure (75 atm), and temperature (325°C) representative of industrial conditions. The biphenyl kinetics experiments were done over a pressure range of 64-200 atm and a temperature range of 300-375°C.

Biphenyl and 2-phenylnaphthalene were chosen as model reactants in part because they are the principal aromatic products formed in the hydrodesulfurization of dibenzothiophene and of benzo[b]naphtho[2,3-d]-

thiophene, respectively (12,13). The latter two compounds are typical of the least reactive sulfur-containing compounds found in the heavier petroleum residua and coal-derived liquids. Naphthalene was chosen because upon hydrogenation it forms tetralin, the most widely used model compound used as a hydrogen donor in coal liquefaction experiments.

#### EXPERIMENTAL

The experiments designed to determine relative reactivities were carried out in a commercial one-liter batch reactor (Autoclave Engineers). The design of the autoclave allowed charging of the catalyst after the reactants had been brought to reaction temperature, thereby virtually eliminating any heat-up period which would prevent elucidation of isothermal kinetics from the conversion data (14). The catalyst was particles ( $\sim 150\mu\text{m}$ ) of  $\text{CoO-MoO}_3/\gamma\text{-Al}_2\text{O}_3$  (American Cyanamid HDS 16A), 2g of which were externally sulfided at  $400^\circ\text{C}$  with 10 vol%  $\text{H}_2\text{S}$  in  $\text{H}_2$  at atmospheric pressure for two hours prior to being charged to the reactor. The reactant solution (375 ml) contained roughly 0.75 mole% of the hydrocarbon reactant in *n*-hexadecane (Humphrey Chemical Co., redistilled). The solution was saturated with hydrogen at the reaction temperature, providing a large stoichiometric excess of this reactant. The reactor was operated at  $75 \pm 2$  atm and  $325 \pm 1^\circ\text{C}$  in all the experiments. Carbon disulfide, 0.1 mole%, was added to the reaction mixture. It was found that this source of sulfur in the reactant was essential to maintain the activity of the catalyst by maintaining it in the sulfided form (15). The  $\text{CS}_2$  was almost instantaneously converted into  $\text{H}_2\text{S}$  under the reaction conditions, the rate of the hydrogenolysis reaction



being at least 8000 times greater than that of the aromatic hydrogenation reactions.

The biphenyl kinetics studies were carried out using a high-pressure flow microreactor, the design and operation of which are described elsewhere (16). The reactor operated with solid particles of catalyst and a liquid reactant phase saturated with hydrogen.

The operating conditions of the flow reactor used for the kinetics experiments are summarized in Table 1.

TABLE 1. Operating conditions for the flow reactor

Catalyst: commercial  $\text{CoO-MoO}_3/\gamma\text{-Al}_2\text{O}_3$  (American Cyanamid HDS 16A)  
 mass: 0.025-0.050g diluted with particles of alundum  
 particle size:  $150\mu\text{m}$   
 volume of catalyst bed:  $0.325\text{ cm}^3$   
 length of bed: 4.0 cm  
 Catalyst pretreatment: sulfided in situ with 10%  $\text{H}_2\text{S}$  in  $\text{H}_2$  for two hours at  $400^\circ\text{C}$   
 Reactor pressure: 64-200 atm  
 Temperature:  $300\text{-}375^\circ\text{C}$   
 Biphenyl concentration:  $5\text{-}25 \times 10^{-3}$  gmoles/liter  
 Cyclohexylbenzene concentration:  $0\text{-}13 \times 10^{-3}$  gmoles/liter  
 Carbon disulfide concentration:  $4\text{-}18 \times 10^{-3}$  gmoles/liter  
 Hydrogen concentration:  $100\text{-}450 \times 10^{-3}$  gmoles/liter  
 Liquid flow rate:  $0.2\text{-}60\text{ cm}^3/\text{hr}$ .  
 Solvent (carrier oil): *n*-hexadecane.

### Materials:

The reagents naphthalene (>99%) and benzene (>99%) were supplied by Fisher; bicyclohexyl (>98%), cyclohexylbenzene (>98%), and tetralin (>99%) by Aldrich; biphenyl (>98%) by Eastman; and 2-phenylnaphthalene (>98%) by ICN Pharmaceuticals. All these reagents were used without further purification.

### Product analysis:

The product samples from the flow reactor were analyzed with an Antek 440L gas chromatograph equipped with a flame ionization detector. The column was packed with methylsilicone on 100-200 mesh Supelcoport (GP 3% SP-2100 DB) operated at 140°C.

The product samples drawn periodically from the batch reactor were analyzed with a Perkin-Elmer 3920 B gas chromatograph equipped with a flame ionization detector and a 0.8 mm-O.D. X 0.025 mm-I.D. X 100-m-long wall-coated open tubular column (the liquid phase was OV-101, Perkin Elmer) with an all-glass splitter injector. The column temperature was varied depending on the reactant compound, and temperature programming was used to improve peak resolution.

Principal reaction products formed from benzene, biphenyl, and naphthalene were identified by comparing glc retention times of the known compounds with retention times of components of the product mixtures. For identification of the primary products of 2-phenylnaphthalene hydrogenation, tricarbonylchromium complexes of the products were synthesized using chromium hexacarbonyl (17). The tricarbonyl chromium complexes which were formed were separated by the column chromatography technique on an alumina (4% water) column. The hydrocarbon solvent and uncomplexed material were eluted with n-pentane. The separation of the complexes on the column was achieved by using different proportions of n-pentane and methylene chloride. The structures of the recrystallized complexes were determined by proton NMR spectroscopy; details of this technique are given elsewhere (13).

From these product analyses, conversion-time data were obtained for each set of reactants and products in the batch reactor experiments. In the flow reactor, differential conversions were measured to determine rate data directly. The rate data were obtained over a wide range of independent variables; mixed feeds were used, including the reaction products in widely varied concentrations.

### RESULTS AND DISCUSSION

Figure 1 shows the principal products and the reaction networks for the aromatic compounds studied in the batch reactor. In all these experiments, mass balances obtained from the unconverted reactant and the products were good. Naphthalene analysis was extremely good, and mass balance of more than 98% was observed for all the samples.

In the flow-reactor experiments a linear relation between conversion and inverse space velocity was observed up to about 15% biphenyl conversion, demonstrating that all the data reported here represented differential conversions. These low-conversion data always showed more than 99% mass balance.

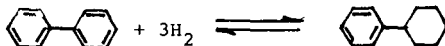
Blank experiments performed in the batch reactor with hydrogen and biphenyl and with hydrogen and cyclohexylbenzene confirmed that there was no observable conversion of these reactants even under more severe conditions (400°C and 100 atm), indicating that all the observed reactions were catalytic. These results are consistent with the thermochemical calculations reported by Ross et al. (20), showing the extreme stability of the C-C bond towards homolysis and free radical formation in the molecules like biphenyl and naphthalene.

In batch experiments with benzene, cyclohexane was observed as the only primary product. The concentration-time profiles for the benzene reaction are shown in Fig. 2. The unidentified hydrocarbon indicated in the benzene reaction network (Fig. 1) was not separated in the glc analysis. The benzene-cyclohexane reaction is reversible and is well documented in the literature (5), and so experiments with cyclohexane as a reactant were not done.

The most thorough set of experiments was carried out with biphenyl, which reacted with hydrogen to give cyclohexylbenzene as a primary product. Cyclohexylbenzene was subsequently converted into bicyclohexyl. The concentration-time plots for the biphenyl reaction network are shown in Fig. 3; the data clearly show that bicyclohexyl is a secondary product, since the slope of the curve at zero time is zero.

Three unidentified hydrocarbon products having very nearly equal retention times on the glc column were also observed in small quantity (in total, about 10% at the maximum conversion). Hydrogenation experiments carried out with cyclohexylbenzene and with bicyclohexyl as the reactants showed that these hydrocarbons were formed as primary products from cyclohexylbenzene, but not from bicyclohexyl. The comparison of the glc retention times of these products with those of several possible products obtained from ring opening (substituted benzene or cyclohexane) and substituted indane and tetralin suggest that these products were not obtained by cracking of biphenyl or by C-C bond cleavage followed by ring closure. Urimoto et al. (18) performed dibenzothiophene hydrodesulfurization experiments and observed 3-methylcyclopentylcyclohexane and 3-3'-dimethyldicyclopentyl products using a catalyst and reaction conditions similar to those used in this work, which indicates the occurrence of isomerization reactions. During hydroprocessing reactions, isomerization of cyclohexane to methylcyclopentane and of tetralin to methyl indane is reported in the literature (5,19). This information suggests that the three unidentified products could be isomerized products formed from cyclohexylbenzene--for example, methylcyclopentylbenzene.

These three products together are represented as hydrocarbons in the reaction network shown in Fig. 1. In experiments with hydrogen and cyclohexylbenzene as reactants, biphenyl was formed, indicating that the primary hydrogenation reaction,



is reversible. The experiments in the flow reactor were designed to determine the nonlinear rate expression for this primary hydrogenation-dehydrogenation reaction. Fig. 4 shows a typical set of data obtained at 350°C. The differential conversion experiments were done at 300, 325, 350 and 375°C; the full set of rate data was fitted with a non-

linear least squares technique (21). The following rate expression represents the data with a high degree of accuracy, but several other equations (similar in form) provide comparable fits. Work on discrimination of the equations is continuing; this rate expression should be considered tentative:

$$r = \frac{k K_{\text{BPH}} K_{\text{H}_2}^3 (C_{\text{BPH}}^3 C_{\text{H}_2}^3 - \frac{1}{K_E} C_{\text{CHB}})}{(1.0 + K_{\text{BPH}} C_{\text{BPH}} + K_{\text{H}_2} S C_{\text{H}_2} S)^2 (1.0 + K_{\text{H}_2} C_{\text{H}_2})^2} \quad (2)$$

$$k = 8 \times 10^7 \exp\left(-\frac{32,000}{RT}\right)$$

$$K_{\text{BPH}} = 4.5 \times 10^{-5} \exp\left(\frac{14,000}{RT}\right)$$

$$K_{\text{H}_2} S = 1.6 \times 10^{-4} \exp\left(\frac{13,000}{RT}\right)$$

$$K_{\text{H}_2} = 4.25 \exp\left(\frac{4,000}{RT}\right)$$

$$K_E = 2.2 \times 10^{-3} \exp\left(\frac{16,500}{RT}\right)$$

BPH = biphenyl, H<sub>2</sub> = hydrogen, CHB = cyclohexylbenzene

The smooth lines in Fig. 4 are the predictions based on the above equation. It is clear that this equation fits the data well.

In batch experiments, naphthalene was hydrogenated to give 1,2,3,4-tetrahydronaphthalene (tetralin) as a primary product. Tetralin was further hydrogenated to give cis- and trans-decahydronaphthalene (decalin). Time-concentration profiles for naphthalene and its reaction products are presented in Fig. 5. From these data, it is evident that equilibrium is approached between tetralin and naphthalene.

In experiments with hydrogen and tetralin as reactants, naphthalene was formed, indicating that the primary hydrogenation reaction is reversible. Trans-decalin was the predominant isomer of decalin. No other hydrocarbon products were detected.

Hydrogenation of 2-phenylnaphthalene gave two primary products, 2-phenyltetralin and 6-phenyltetralin, each of which experienced further hydrogenation. The concentration-time profiles are presented in Fig. 6. The secondary products are represented together as hydrocarbons in this analysis, consisting chiefly of phenyl-substituted decalins. 2-Phenyltetralin or 6-phenyltetralin are not commercially available, and experiments were not performed with these as reactants to demonstrate whether the primary hydrogenation reactions were reversible. But on the basis of the experience with biphenyl and naphthalene, it was assumed that the primary hydrogenation reactions are reversible. It can be seen from the data presented in Fig. 6 that equilibrium is approached between 2-phenylnaphthalene and its two primary products, 2-phenyltetralin and 6-phenyltetralin.

In contrast to these hydrogenation reactions, hydrodesulfurization reactions are practically irreversible, and the conversion data for the individual sulfur-containing compounds follow pseudo-first order behavior (23). As the primary hydrogenation reactions studied here are reversible, a deviation from the pseudo-first order behavior was observed as equilibrium was approached. The pseudo-first order rate constants for the overall disappearance of the component, determined from the low conversion data, are summarized in Table 2. For the determination of rate constants to represent the reaction networks from the high conversion data, it was assumed that each reaction in the network was pseudo-first order in the organic reactant. All the reversibilities were taken into account in representing quantitative kinetics for the complete reaction networks. The pseudo-first order rate constants were estimated from the full set of data determined in the experiments with each organic reactant, as follows: (1) In the case of benzene and biphenyl, raw concentration versus time data were smoothed by fitting spline functions using the IMSL subroutine ICSMOU (24); this program performs one dimensional data smoothing by error detection and is highly effective in smoothing a data set only mildly contaminated with isolated errors; (2) the smoothed data were used with equal weighting in the Carlton 2 program (25) to determine best values of the individual rate constants. The values of the rate constants for the individual reactions in the networks are shown in Fig. 1. The lines in Figs. 2,3,5,6 represent the model predictions from the estimated pseudo first-order rate constants based on the individual reaction networks shown in Fig. 1.

TABLE 2. Pseudo-first order rate constants for hydrogenation catalyzed by sulfided  $\text{CoO-MoO}_3/\gamma\text{-Al}_2\text{O}_3$  at 325°C and 75 atm.

Reactant	Concentration, mole%	$10^6 \times$ Pseudo-first order rate constant $\text{m}^3/\text{kg of catalyst} \cdot \text{sec}^a$
Benzene	0.65	$2.8 \pm 0.1$
Biphenyl	0.80	$3.0 \pm 0.2$
Naphthalene	0.85	$58.9 \pm 3.6$
2-Phenylnaphthalene	0.75	$61.4 \pm 5.3$

<sup>a</sup>Data are reported with 95% confidence limits.

The final conversion levels for naphthalene and 2-phenylnaphthalene were of the order of 99%, whereas biphenyl and benzene were only about 75% converted after completion of the experiments. Experiments were carried out for long periods so that good estimates of the equilibrium constants could be obtained from the conversion data. The equilibrium constant for the biphenyl hydrogenation,  $K_E = [\text{CCHB}/\text{CBPH} \cdot \text{CH}_2^3]_{\text{equil.}} = 365$ , obtained from the above analysis of the kinetics, agrees fairly well with Frye's (26) gas-phase equilibrium experiments. At 325°C his data indicate  $K_E$  to be equal to 485.

From these networks, it can be seen that primary products obtained by aromatic hydrogenation are hydroaromatics, potential hydrogen donors which can readily be dehydrogenated in the presence of liquefying coal. The relative hydrogen-donor capacity of several

hydroaromatics was determined by Doyle (22), his results showing that tetralin or substituted tetralins are much better hydrogen donors than cyclohexylbenzene.

Liquefaction of coal has been shown to occur almost instantaneously upon reaching a high temperature in the presence of a hydrogen-donor solvent (27). Thus the slow steps in the hydrogenation/liquefaction process may be the hydrogenation of the recycle solvent to replenish hydrogen donor species (28). One of the objectives in the solvent hydrogenation is to maximize the yield of hydroaromatics. The reactions leading to consumption of hydroaromatic (for example, further hydrogenation of tetralin to decalins or isomerization of hydroaromatics) are undesirable, as they result in a solvent of reduced hydrogen-donor capacity. From Fig. 1 it is evident that these undesirable side reactions are relatively slow compared with the primary hydrogenation reactions. Under the experimental conditions of this study, the hydrogenation-dehydrogenation equilibrium was favorable towards higher yields of hydroaromatics. The biphenyl kinetics indicates that at higher temperatures dehydrogenation reactions are more significant, which suggests a strategy of maximizing yields of hydroaromatics by applying lower temperatures and high hydrogen partial pressures. The catalyst would also play an important role; the ideal catalyst would have moderate hydrogenation activity to hydrogenate the solvent to constituents like tetralin. But it should not have excessive activity to over-hydrogenate and form poor hydrogen donors like decalin, the formation of which would also represent excessive consumption of the costly hydrogen.

Ahuja et al. (7) ascribed the isomerization of cyclohexane to methylcyclopentane to the acidity of the support, and it follows from their suggestion that the isomerization of hydroaromatics would be less if less acidic catalyst supports (like  $\text{SiO}_2$ ) were used. The isomerization reactions are significantly inhibited by nitrogen-containing compounds (7), hence the feeds with higher concentrations of nitrogen-containing compounds might seem to be favorable--except that nitrogen-containing compounds also strongly inhibit the hydrogenation reactions (2).

The results of Table 1 show that benzene and biphenyl have nearly the same reactivity; naphthalene and 2-phenylnaphthalene have nearly equal reactivities, one order of magnitude less than that of benzene. The high-pressure, high-temperature hydrogenation of benzene and naphthalene reported to occur in the presence of unsupported  $\text{MoS}_2$  and  $\text{WS}_2$  catalysts, indicates a 17-fold higher reactivity of naphthalene in comparison with benzene (5), which agrees well with the results reported in Table 1.

Naphthalene has a resonance energy of 75 kcal/mole, which is less than twice that of benzene's 42 kcal/mole (29), i.e., the rings in naphthalene are less aromatic in character than that of benzene and so more easily reduced, which explains the higher reactivity of naphthalene.

# REFERENCES

- (1) Gates, B. C., Katzer, J. R., and Schuit, G. C. A., "Chemistry of Catalytic Processes," Chap. 5, McGraw-Hill, New York (1979).
- (2) Bhinde, M. V., Ph.D. thesis, University of Delaware (1979).
- (3) National Academy of Sciences, Assessment of Technology for Liquefaction of Coal, Washington, D.C., 1977.
- (4) Furlong, L. E., Effron, E., Vernon, L. W., and Wilson, E. L., Chem. Eng. Progr., **72** (8), 69 (1976).
- (5) Weisser, O., and Landa, S., "Sulphide Catalysts, Their Properties and Applications," Pergamon, New York, 1973.
- (6) Voorhoeve, R. J. H., and Stuiver, J. C. M., J. Catal., **23**, 228 (1971).
- (7) Ahuja, S. P., Derrien, M. L., and LePage, J. F., Ind. Eng. Chem. Prod. Res. Develop., **9**, 272 (1970).
- (8) Huang, C. S., M.S. thesis, University of Mississippi (1976).
- (9) Rollmann, L. D., J. Catal., **46**, 243 (1977).
- (10) de Beer, V. H. J., Dahlmans, J. G. S., and Smeets, J. G. M., J. Catal., **42**, 467 (1976).
- (11) Hagenbach, G., Courty, Ph., and Delmon, B., J. Catal., **23**, 295 (1971).
- (12) Houalla, M., Nag, N. K., Sapre, A. V., Broderick, D. H., and Gates, B. C., AIChE J., **24**, 1015 (1978).
- (13) Sapre, A. V., Broderick, D. H., Fraenkel, D., Gates, B. C., and Nag, N. K., AIChE J., in press.
- (14) Shih, S. S., Katzer, J. R., Kwart, H., and Stiles, A. B., Preprints, ACS Div. Petrol. Chem., **22**, 919 (1977).
- (15) Sapre, A. V., Ph.D. Thesis, University of Delaware, in preparation.
- (16) Eliezer, K. F., Bhinde, M., Houalla, M., Broderick, D. H., Gates, B. C., Katzer, J. R., and Olson, J. H., Ind. Eng. Chem. Fundam., **16**, 380 (1977).
- (17) Nicholls, B., and Whiting, M., J. Chem. Soc. (London), 551 (1959).
- (18) Urimoto, H., and Sakikawa, N., Sekiyu Gakkaishi, **15**, 926 (1972).
- (19) Cronauer, D. C., Jewell, D. M., Shah, Y. T., and Kueser, K. A., Ind. Eng. Chem. Fundam., **17** (4), 291 (1978).

- (20) Ross, D. S. and Blessing, J. E., Prepr. ACS Div. Fuel Chem. 24, 129 (1979).
- (21) NLLS program, University of Delaware Computing Center.
- (22) Doyle, G., Prepr. ACS Div. Petrol. Chem., 21, 165 (1975).
- (23) Nag, N. K., Sapre, A. V., Broderick, D. H., and Gates, B. C., J. Catal., 57, 509 (1979).
- (24) ICSMOU, computer subroutine, International Mathematical and Statistical Library.
- (25) Himmelblau, D. M., Jones, C. R., and Bischoff, K. B., Ind. Eng. Chem. Fundam., 6, 539 (1967).
- (26) Frye, C. G., J. Chem. Eng. Data, 7, 592 (1962).
- (27) Whitehurst, D. D., and Mitchell, T. D., Prepr. ACS Div. of Fuel Chem., 21 (5), 127 (1976).
- (28) Guin, J. A., Tarrer, A. R., Lee, J. M., Lo, L., and Curtis, C. W., Ind. Eng. Chem. Proc. Des. Dev., 18, 371 (1979).
- (29) Pauling, L., "The Nature of The Chemical Bond," Cornell University Press, 1967.

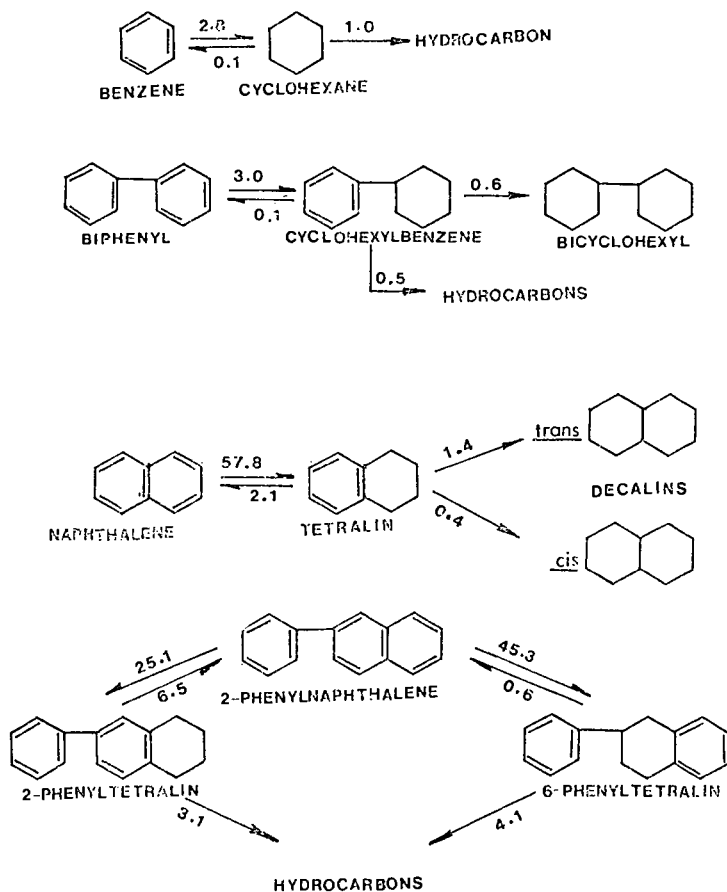


Fig. 1: Reaction networks for hydrogenation of benzene, biphenyl, naphthalene, and 2-phenylnaphthalene in the presence of sulfided  $\text{CoO-MoO}_3/\gamma\text{-Al}_2\text{O}_3$  at  $325^\circ\text{C}$  and 75 atm. Each reaction is approximated as first order in the organic reactant; the numbers next to the arrows are the pseudo first order rate constants in  $10^5 \times$  cubic meters per kilogram of catalyst per second.

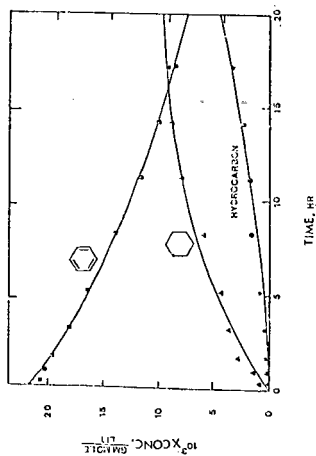


Fig. 2: Conversion of benzene and  $H_2$  in the presence of sulfided  $CoO-MoO_3/\gamma-Al_2O_3$  in a batch reactor at  $325^\circ C$  and 75 atm. The curves are the predictions of the reaction network model of Fig. 1.

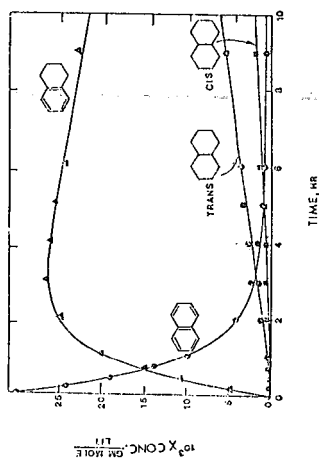


Fig. 5: Conversion of naphthalene and  $H_2$  in the presence of sulfided  $CoO-MoO_3/\gamma-Al_2O_3$  in a batch reactor at  $325^\circ C$  and 75 atm. The curves are the predictions of the reaction network model of Fig. 1.

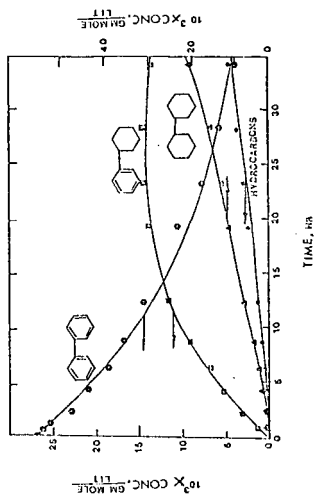


Fig. 3: Conversion of biphenyl and  $H_2$  in the presence of sulfided  $CoO-MoO_3/\gamma-Al_2O_3$  in a batch reactor at  $325^\circ C$  and 75 atm. The curves are the predictions of the reaction network model of Fig. 1.

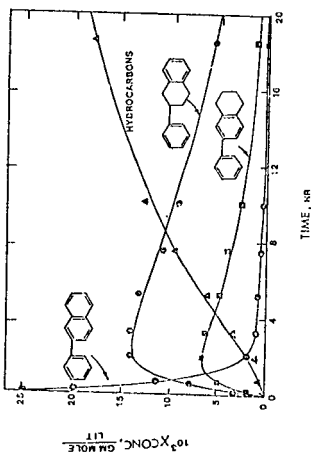


Fig. 6: Conversion of 2-phenylnaphthalene and  $H_2$  in the presence of sulfided  $CoO-MoO_3/\gamma-Al_2O_3$  in a batch reactor at  $325^\circ C$  and 75 atm. The curves are the predictions of the reaction network model of Fig. 1.

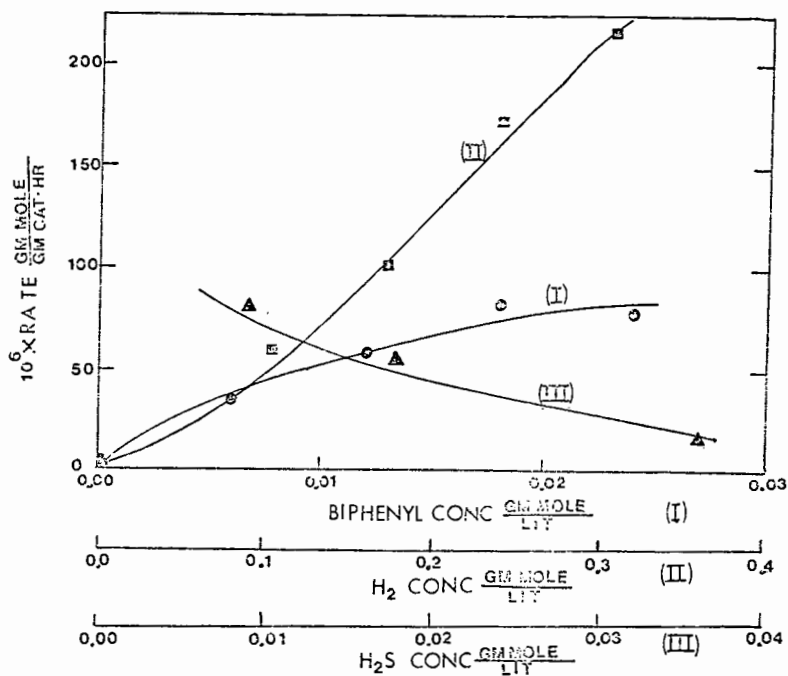


Fig. 4: Rate of biphenyl hydrogenation as a function of hydrogen,  $\text{H}_2\text{S}$ , and biphenyl concentrations at  $350^\circ\text{C}$ . The curves are cubic spline fits through individual points predicted by rate equation given in the text, for the actual concentrations at each point.

CATALYTIC UPGRADING OF H-COAL SYNCRUDES. Dennis J. O'Rear, Richard F. Sullivan, and Bruce E. Stangeland, Chevron Research Company, P.O. Box 1627, Richmond, California 94802.

The net liquid product from the H-Coal liquefaction process was refined to liquid fuels by commercial catalysts in pilot plants which simulate advanced state-of-the-art petroleum hydroprocessing technology. Liquids derived from two different coals were studied: Illinois No. 6 coal (Burning Star Mine) and Wyodak coal. One hydrotreating stage, operated at several severities, upgraded the whole product to either jet, diesel, or heating fuels. In addition, a naphtha was produced which can be used for hydrogen production or as feed to a catalytic reformer. The kerosene jet fuel meets all critical specifications, including smoke point and stability. The maximum yield of jet derived from Illinois coal is almost 90%. The diesel and heating fuels meet most specifications when additives are used. For maximum gasoline production, the hydrotreated H-coal product was converted to naphtha in a single-stage extinction-recycle hydrocracker.

## HYDROTREATMENT AND BIOLOGICAL TEST OF SRC-II COAL LIQUID

Dexter Sutterfield, W. C. Lanning

U.S. Department of Energy, Bartlesville Energy  
Technology Center, P. O. Box 1398, Bartlesville, OK 74003

and R. E. Royer

Inhalation Toxicology Research Institute,  
Lovelace Biomedical and Environmental Research Institute,  
P. O. Box 5890, Albuquerque, New Mexico 87115

### Introduction

Distillate coal liquid from the SRC-II process has been hydrotreated at several levels of severity in a bench-scale continuous flow unit at the Bartlesville Energy Technology Center. The purpose was twofold with the immediate goal to survey process conditions with a commercially available catalyst to provide samples upgraded to varied degrees for detailed characterization analyses and investigation for biological activity. Long-range goals are to contribute to a data base to evaluate raw material sources, liquefaction or other production processes, characterization of feedstocks for further refining to transportation and other end-use fuels, selection of refining processes, and estimation of type and quality of end products expected from combinations of these steps.

The liquid feed and products have been screened for biological activity by the Ames test at Lovelace Biomedical and Environmental Research Institute, Albuquerque, New Mexico.

### Experimental Materials and Procedures

The SRC-II liquid was obtained from the Pittsburg and Midway Coal Mining Co. The liquid was produced from Material Balance Run No. 77 SR-12 on coal from the Pittsburg seam from Consol's Blacksville No. 2 Mine in West Virginia. The middle (177-288° C) and heavy (288-454°C) distillates were blended to the same ratio as produced by the material balance run, e.g., 75.5 percent middle distillate and 24.5 percent heavy distillate. The feed contained 0.23 wt-pct sulfur, 1.06 wt-pct nitrogen and 3.29 wt-pct oxygen and boiled between 185 and 380° C (5-95 percent) by simulated distillation.

The bench-scale hydrogenation unit was designed for operation at up to 3,000 psig and 450° C, with once-through flow of hydrogen, down-flow of gas and liquid over a fixed-bed catalyst. Reactor temperature, pressure, and hydrogen flow and liquid level in the high-pressure product separator were controlled automatically. Liquid product was withdrawn periodically from a low-pressure separator, and the combined high- and low-pressure effluent gas was sampled for analysis.

The catalyst was 100 ml of American Cyanamid HDS-3A, a 1/16-inch diameter extrudate of nickel-molybdenum-alumina. It was diluted with inert, granular alpha-alumina to provide a bed depth of 18 inches in the middle section of a 0.96-inch ID vertical reactor with a 5/16-inch OD internal thermocouple well. The catalyst was progressively more dilute toward the top of the bed to minimize exothermic temperature effects, and end sections were packed with alpha-alumina to provide for preheat and cooling zones.

The catalyst was presulfided and operated for about 100 hours on a petroleum gas oil (200-500° C boiling range, 0.8 wt-pct sulfur) to check controls and provide some catalyst aging before exposure to the coal liquid.

Operating conditions selected as likely to maintain catalyst activity and provide the range of upgrading desired were 2,000 psig pressure, 325 to 400° C, and 0.5 to 1.0 LHSV (volume liquid feed/volume bulk catalyst/hour). Hydrogen flow was held constant at a rate corresponding to 10,000 SCF/bbl to 0.5 LHSV or 5,000 SCF/bbl at 1.0 LHSV. Variation in hydrogen flow rate in once-through operation has little effect at more than 5,000 SCF/bbl. Operation at each condition was for approximately 24 hours to allow 8-12 hours for equilibration plus time to accumulate about 750 ml of liquid product. Table 1 shows the sequence of reactor conditions and essential process results.

TABLE 1. Process conditions and results

Sample Period	Liquid Product					Approx. H <sub>2</sub> Cons., SCF/bbl	Catalyst tempera- ture, °C	Liquid feed rate, LHSV
	Sp. gr., 60°/60°F	Hydrogen, wt-pct	Nitrogen, wt-pct	Sulfur wt-pct	Oxygen wt-pct			
(Feed)	1.003	8.42	1.057	.25	3.29	-	-	-
1	0.921	10.81	0.352	.01	.59	1,930	325	0.50
2	.948	10.06	.631	.02	1.65	1,270	325	1.0
3	.902	11.54	.033	.01	.17	2,670	350	0.50
4	.953	9.80	.700	.02	1.58	970	310	0.50
5	.887	12.24	.001	.01	.09	2,880	375	0.50
6	.877	12.39	.001	.01	.03	3,250	400	0.50
7	.868	12.82	.001	.01	.06	5,010	400	0.35
8	.962	9.68	.742	.01	2.00	980	325	1.0

Period 4 was a test of a very mild condition after a weekend shutdown. Period 7 was a test of the liquid feed pump at a low rate. Period 8 was a brief test for decline in activity from period 2, although the entire operation was too short for significant life testing. Periods in the order of 2,1,3,5, and 6 were intended to cover the desired range of increasing upgrading.

The liquid feed and products were screened for chemical mutagens by use of the Ames assay (1,2).

#### Results and Discussion

The results in table 1 show the expected trends as hydrotreating severity was increased with reaction temperatures in the range of 310 to 400° C. Specific gravity of the product liquid at 375°C decreased from 1.00 for the feed to 0.89 while nitrogen decreased from 1.06 wt-pct to less than .001 wt-pct and oxygen decreased from 3.29 wt-pct to 0.09 wt-pct. Hydrogen content increased from 8.42 wt-pct in the liquid feed to 12.24 wt-pct over this same range of nitrogen removal. Calculated

hydrogen consumptions for this range of conditions varied from 970 to 2,880 SCF/bbl which is within the ranges reported by others (2,3). Precise hydrogen content of the liquid product, used in calculation of hydrogen consumption, was determined by NMR through the courtesy of Phillips Petroleum Company. Analysis of the effluent gas did not include hydrocarbons heavier than ethane. Contributions of the heavier hydrocarbons to hydrogen consumption are small for hydrotreating at conditions which cause very little cracking of hydrocarbons since most of the consumed hydrogen goes into the liquid product.

The distillation range of the liquid products was shifted downward as hydro-treating severity was increased (table 2). The magnitude of the shift of the simulated distillation is shown in the last column which indicates 8 to 22 percent of the feed is converted to material boiling below the five percent point of the feed.

TABLE 2. - Simulated distillation of liquid feed and products

Sample Period	Temp., °C., at wt-percent distilled			wt-percent converted to below 185° C
	5	50	95	
(Feed)	185	255	379	-
4	112	239	361	15
2	131	247	369	9
3	101	235	344	18
4	133	248	375	8
5	96	229	331	21
6	98	225	329	22
7	94	221	326	21
8	156	252	379	7

The increase in product material boiling below 185° C results largely from saturation of aromatic rings and olefins and from removal of heteroatoms. Some hydrocarbons boiling lower than the feed would be formed by cleaving of heteroatom linkages, with very little cracking of hydrocarbons expected. For example, all product liquids had initial boiling points close to that of benzene/cyclohexane.

The results of the Salmonella/Typhimurium Mutagenicity (Ames) assay for the feed and liquid products are given in table 3. The assay was run essentially as described by Ames(1). The assay employs specially constructed strains of Salmonella Typhimurium which are reverted by a wide variety of mutagens from requiring histidine in their growth media back to bacteria capable of synthesizing histidine.

TABLE 3. - Results of the Ames assay

Sample	Concentration, ug/plate	Number of Revertants	
		Without/With Metabolic Activation TA 98	TA 100
Feed	250	30/ <u>1822</u>	144/ <u>322</u>
Feed	100	34/ <u>1122</u>	163/ <u>348</u>
Feed	50	27/ <u>547</u>	150/ <u>306</u>
Feed	25	21/ <u>316</u>	150/204
Feed	5	31/113	134/178
Background	0	21/60	144/142
8	100	15/ <u>131</u>	134/257
4	100	19/111	176/232
2	100	23/ <u>178</u>	151/226
1	100	16/64	158/218
3	100	10/40	161/194
5	100	22/64	162/194
6	100	19/70	128/186
7	100	17/65	153/218
Background	0	25/66	169/220

Some chemicals require metabolic activation (addition of microsomal enzymes) prior to showing mutagenic activity; thus, data are given as number of revertants without/with metabolic activation. The Ames test has thus far demonstrated a strong correlation between positive carcinogenesis in animal tests and mutagenicity in the Ames test (1,4). However, positive results from the Ames test do not conclusively show human risk.

The untreated SRC-II was tested at five concentrations with Salmonella strains TA 98 and TA 100, generally considered the most sensitive strains. In the results indicated in Table 3, an increase in the number of revertants greater than two times the background (no SRC-II feed or product) is sometimes considered to indicate a definite positive (mutagenic) response. The plates which showed a positive response by this criteria are underlined.

Activity decreased with decreasing concentration for the untreated feed but was still nearly double the activity of the background at a concentration of 5 ug per plate. A product dose of one hundred micrograms was selected as a satisfactory screening test since a strong response was observed for the untreated SRC-II at this concentration and since no appreciable cytotoxicity was noted. The hydrogenation periods are listed in order of increasing severity of processing. Activity was decreased essentially to the background level when nitrogen content was decreased to

0.35 wt-pct, oxygen content was decreased to 0.59 wt-pct and hydrogen content was increased from 8.4 to 10.8 wt-pct. This occurred at process conditions of 325° C and 0.5 LHSV feed rate, which had been planned as the lowest reaction temperature expected to give substantial upgrading.

A more complete investigation will require testing of fractions of the coal liquid to identify more active components. Nitrogen and oxygen compounds and aromatic ring structures are important in this respect, with mutagenically active components likely to be in higher-boiling fractions. Tests on mammalian systems are also needed before making assessments concerning potential human risk.

### Summary

Distillate coal liquid from the SRC-II process was hydrotreated in a bench-scale process unit to provide a range of mildly upgraded products for compositional characterization and screening for mutagenicity. Hydrogen content of the liquid was increased from 8.4 to 12.24 wt-pct over the range of process conditions which removed essentially 100 percent of the nitrogen and 95 percent of the oxygen. Results of the Ames assay indicated mutagenic activity of the liquid product decreased by an order of magnitude for 35 percent removal of nitrogen and 52 percent removal of oxygen. Liquid product with 67 percent nitrogen removal and 82 percent oxygen removal showed no mutagenic activity distinguishable from that of the background samples. The full range of effect in decreasing mutagenic activity by the Ames assay was covered by relatively mild hydrotreatment, but assessment of potential human risk must be confirmed using additional mammalian tests.

### References

1. Ames, Bruce N., Joyce McCann, and Edith Yamosaki. Methods for Detecting Carcinogens and Mutagens with Salmonella/Mammalian-Microsome Mutagenicity Test. *Mutation Research*, v. 31, 1975, pp. 347-363.
2. Frumkin, Harry A., Richard F. Sullivan, and Bruce E. Strangeland. Converting SRC-II Process Product to Transportation Fuels. Presented at the 87th National Meeting of AIChE, Boston, MA, August 20, 1979.
3. Lanning, W. C. The Refining of Synthetic Crude Oils. *BETC/IC-76/2*. July 1976, 11 pp.
4. McCann, Joyce, Edmund Choi, Edith Yamosaki, and Bruce N. Ames. Detection of Carcinogens as Mutagens in the Salmonella/Microsome Test: Assay of 300 Chemicals. *Proc. Nat. Acad. Sci. USA*, v. 72, No. 12, 1975, p. 5135.

SYMPOSIUM ON COAL LIQUIDS UPGRADING

PRESENTED BEFORE  
THE DIVISION OF FUEL CHEMISTRY, INC.  
AMERICAN CHEMICAL SOCIETY  
HOUSTON MEETING  
MARCH 25-28, 1980

CATALYST DEACTIVATION IN HYDROTREATING  
COAL-DERIVED LIQUIDS

R. Sivasubramanian,<sup>1</sup> J. H. Olson and J. R. Katzer\*  
Center for Catalytic Science and Technology  
Department of Chemical Engineering  
University of Delaware  
Newark, Delaware 19711

<sup>1</sup>Air Products and Chemicals, Inc.; P.O. Box 538, Allentown,  
Pennsylvania 18105

\*To whom correspondence should be addressed. (302) 738-8056

## CATALYST DEACTIVATION IN HYDROTREATING COAL-DERIVED LIQUIDS

### Introduction

Coal liquefaction processes are likely to be commercialized within the next decade. Coal-derived liquids contain larger fractions of heteroatoms (sulfur, nitrogen, oxygen) than petroleum liquids. Hydroprocessing of these liquids will become necessary to improve the quality of the products. Considerable work has been done in determining catalyst deactivation rates in petroleum hydroprocessing. However, coal-derived liquids differ considerably from petroleum liquids in their aromaticity, metals content and C/H ratio. Coal-derived liquids are much harder to hydroprocess, cause more rapid catalyst deactivation, and represent a step upward in terms of difficulty of hydrotreating.

Characterization studies on aged catalysts can provide an understanding of the causes for catalyst deactivation and may lead to optimum design of reactors and improved catalysts. Characterization of three different coal-liquefaction catalysts that have been in direct contact with coal have been performed earlier in this laboratory (1,2,3). However, in the present study a catalyst that had been used to hydrotreat a coal-derived liquid is characterized.

### Experimental

Ni-Mo/Al<sub>2</sub>O<sub>3</sub> catalyst samples were obtained from a laboratory-size trickle-bed reactor that was used to hydrotreat an equal

volume mixture of raw anthracene oil and sýnthoil liquid. The properties of this particular feedstock is given in Table I. The feed oil had a sulfur content of 0.54 wt %, a nitrogen content of 1.21 wt % and 1.05 wt % ash. Table II presents the operating conditions in the trickle-bed reactor for the particular run from which the catalyst samples were obtained. At the end of the run, the reactor was shut down and the reactor was cut into three different sections and catalyst samples were obtained from the top, middle and bottom sections of the reactor. The spent catalyst pellets from the three different sections were analyzed with a scanning electron microscope (SEM) equipped with an energy dispersive x-ray analyzer (EDAX) and with an electron microprobe. In addition spent catalysts were regenerated (coke burnt off) and the hydrodesulfurization (HDS) and hydrodenitrogenation (HDN) activities of the fresh, spent and regenerated catalysts were compared.

#### Microscopy Studies

Most of the catalyst samples used in the microscopy studies were prepared by sectioning the catalyst; mounting the catalyst in potting material on a SEM sample holder, and then grinding the exposed surface flat with various grits down to 0.25 $\mu$  diamond dust. The lapped samples then were carbon shadowed. These samples then were inspected in light microscopy, SEM and the electron microprobe.

The SEM with EDAX was used in two modes, first conventional inspection of the surface coupled with spot analyses of distinctive

features. The second mode was to scan the surface for specific elements. The microprobe was used in three modes, inspection of the surface elemental scans (these scans are superior to the EDAX elemental scans), and finally to find the elemental response along a 100 x 0.5 micron line parallel to a tangent to the catalyst surface. The line scan was mechanically driven to sweep an area near the catalyst exterior surface.

Samples also were then prepared by cleaving the catalyst, mounting on an SEM post and then removing surface "coke" by plasma etching. This preparation method reveals the distribution of mineral matter on the catalyst surface.

#### Activity Studies

In order to determine the activity decay of the spent catalysts, the spent catalysts were regenerated and the activities of the spent catalysts were compared with that of the fresh and regenerated catalysts for hydrodesulfurization and hydrodenitrogenation using a mixture of dibenzothiophene and quinoline dissolved in hexadecane as a feedstock in a batch autoclave reactor. Earlier experiments by Chiou and Olson (2,3) were done by crushing the spent pellets to 140 mesh. For this work, in order to find out the effect of crushing the spent catalysts, it was decided to conduct experiments using crushed particles as well as using the spent catalysts as received (8/10 mesh).

A mixture of spent catalysts from all three sections of the reactor was obtained and this mixture was divided into two halves.

One half of this mixture was ground to a size of 140 mesh. Both halves were regenerated by controlled combustion of the coke deposited on the catalyst. The regeneration process was done by passing a 2% oxygen in helium over the spent catalysts at a temperature of 450°C at a flow rate of 100 cc/min. The burning process was continued until the weight of residual catalyst became constant.

All the experiments were conducted in a 300 cc standard autoclave reactor (Autoclave Engineers, Erie, PA) equipped with a variable speed magnadrive; the autoclave was operated in batch mode. A special injection system was used to inject a slurry of catalyst, reactants and carbon disulfide in a small amount of carrier oil into the reactor after it had been stabilized at reaction temperature. This technique allowed the precise definition of zero time and eliminated complications including reaction and possible catalyst activity changes arising from long heat-up times. The system has been described elsewhere (4). However, the above technique could not be utilized in runs involving catalyst pellets. For these runs a special basket was designed that held the catalyst in place inside the autoclave reactor. For the pellet runs, the reactants and carbon disulfide in carrier oil were injected after the reactor had reached the operation temperature. Two blank runs not containing catalyst were made to determine the effect of reactor walls and the catalyst basket.

Table III presents the operating conditions for the batch autoclave reactor for all the runs used in this study. N-hexadecane

was used as a carrier oil. All catalysts were presulfided, and in order to maintain the catalyst in the sulfided form during the reaction, an amount of  $\text{CS}_2$  equivalent to 0.05 wt % of the carrier oil was added to the injection tubing together with catalyst and reactants. Under the operating conditions carbon disulfide was rapidly converted to hydrogen sulfide and methane. The amount of  $\text{CS}_2$  created 1.4% higher concentration of  $\text{H}_2\text{S}$  than that required to keep the catalyst in the sulfided form. Liquid samples were analyzed using a gas chromatograph equipped with a glass capillary column (OV101, 75 m).

#### Results of Microscopic Investigations

The prior part of this section presents a fairly detailed narrative of the SEM results for the sample taken from the top (nearest the entrance) of the reactor and then less complete descriptions for the data gathered for the middle and bottom samples. This is followed by a presentation of the results from the microprobe investigations and plasma etching. The various experimental methods yield a reasonably consistent description for the deposition of mineral matter and coke at the catalyst surface.

#### SEM - Top Sample

Figures 1A and B are conventional photo micrographs of the polished cross section of the catalyst pellet. These two figures show the deposition of an irregular crust about 75 microns thick around the entire exterior surface of the catalyst. In addition there is a thin region about 10 microns thick which

appears on about one-third of the catalyst. The catalyst also has many circular regions about 40 microns in diameter which appear distinct from the polished section of the catalyst. Finally the zone near the surface contains many cracks with a thickness of 1-5 microns. The roughness of the catalyst exterior surface suggests that a small portion of the catalyst may have spalled away. The smaller boxed area in Figure 1B corresponds to a zone which was examined with scanning electron microscopy. The larger rectangle corresponds to a zone evaluated with the electron microprobe analyzer.

Figure 2A shows the surface of the catalyst pellet as seen with a scanning electron microscope. In contrast to the light microscope, the outer crust is seen to contain many large (~1 micron) cracks. In addition the outer crust contains about 20 percent of small particles (~0.5 micron) embedded in an indistinct matrix. The inner crust also is seen to contain many voids and cracks; this zone appears to be made by aggregation of small crystals. The catalyst support contains a number of extended large cracks near the external surface. In addition there are a number of shallow depressions, 40 microns in the largest dimension which will be described more completely later. In summary the surface has two distinct crusts and a zone containing large fissures near the exterior surface.

Figure 2B is an aluminum area scan made by recording the aluminum signal from the EDAX. Figures 2B and 2A correspond.

There are three distinct zones for the aluminum signal, the upper zone for potting material, the middle zone for the crust, and the bottom zone of the catalyst support. Closer inspection reveals that the cracks seen clearly in the backscatter electron scan also appear, although less distinctly, in the aluminum scan. The aluminum scan shows that the inner and outer crust regions contain aluminum and that the catalyst exterior surface has been roughened in the process.

Figure 3A is a SEM-EDAX area scan for silicon. This scan shows that the exterior crust contains a high concentration of silicon; the gray (intermediate) zone on Figure 2B corresponds exactly with the bright zone of Figure 3A. In addition there is some penetration of silicon into the interior of the catalyst near the exterior surface. Careful examination of the crust region identifies a few zones (~15 microns across) of very high silicon concentration.

Figure 3B is a SEM-EDAX area scan for calcium. The calcium signal in the catalyst is only slightly greater than background, and therefore the zones are far less distinct. However the high-silicon region of Figure 3A has a corresponding but less distinct zone on the calcium scan. In addition, the major cracks appear faintly. Some zones of high silicon concentration in the crust region of Figure 3A appear as voids in the calcium scan on Figure 3B. Finally there is a small calcium signal in the catalyst support; however the calcium signal in the catalyst is barely above background.

Figure 4A, the SEM-EDAX Area Scan for Sulfur, and Figure 4B, the SEM-EDAX Area Scan for Iron, will be discussed together. The demarcation between the catalyst and the crust can be seen on both figures but is far clearer on the iron scan. The catalyst is sulfided, and therefore there should be a distinct sulfur signal in the interior of the catalyst. The cracks seen clearly on Figure 2A appear faintly on the sulfur area scan. The crust region gives a near-perfect correlation between the two signals. Further, the high section zones are seen as voids in the two figures. There is a fairly distinct zone of higher sulfur concentration in the crust located in the center of the figure which also appears, although less clearly, in the iron scan. Thus the exterior and the interior crusts contain an iron-sulfur compound. There is some penetration of iron into the catalyst, and sulfur appears throughout the catalyst interior.

Figure 5A is a titanium SEM-EDAX scan of the area. The interior crust region of Figure 2A is seen to contain a high concentration of titanium. In addition there is a significant concentration of titanium in the exterior crust. Finally there is some penetration of titanium into the near surface of the catalyst.

Figure 5B shows a molybdenum SEM-EDAX scan of the catalyst. Molybdenum is the major active element in the catalyst. The molybdenum signal correlates with the intense aluminum signal of Figure 2B. The cracks in the catalyst can be seen as voids in the molybdenum signal.

The area scanned in Figures 2A-5B were also examined for nickel and zinc. These scans gave no signal above background even though EDAX spot and line analyses showed that these elements are present. Indeed, the catalyst contains nickel as a hydrogenation promoter.

Figure 6A is an electron backscatter readout taken in the microprobe analyzer prior to making the line scans. This area appears as the large rectangle on Figure 1B. Consistent with Figure 2B, the figure shows an outer and inner crust, major cracks in the catalyst near the surface, and several flat depressions about 40 microns in diameter. The line in the crust region corresponds to the orientation of the 60 micron line scan used to find the average composition of the crust.

Figure 6B is the titanium microprobe area scan which corresponds to Figure 6B. The microprobe area scan for titanium is much more sensitive than the SEM-EDAX area scan, and therefore more details emerge: the inner crust is seen to produce a very high titanium signal. The dense exterior crust contains an intermediate concentration of titanium; however the crust in the upper left portion of the figure appears to be nearly free of titanium. The shallow craters and the cracks in the catalyst interior are decorated with titanium. Thus the titanium is distributed in a complex way throughout the crust region of the catalyst.

### SEM - Middle Sample

Figures 7A and 7B are conventional micrographs of the polished section of a catalyst pellet taken from the middle of the reactor. Consistent with the top sample, there is an irregular crust about 75 microns thick which completely covers the catalyst. Likewise there is a thin inner crust which covers about one-quarter of the surface. Again the surface region of the catalyst has many fissures, and the spent catalyst has many ponds which have been decorated with process material. The rectangular region on Figure 7B locates the region examined more closely with the SEM-EDAX and the microprobe. The region was chosen because the thin crust is unusually flat there.

Figures 8A and 8B are the SEM inspections of the sectioned catalyst. Owing to the greater depth of field of the SEM than for the light microscope, the cracks and the round depressions of the surface can be seen more clearly. Figure 8B, taken at 800X corresponds to the region examined by SEM-EDAX area scans. The latter data are recorded in Figures 9A-11B.

In harmony with the top sample the exterior crust has a high silicon concentration (Figure 9A) and contains grains of extremely high silicon concentration. The silicon density in the third of the crust nearest to the surface is greater than for the outer two-thirds; this density variation also can be seen in the SEM micrographs. The calcium concentration (Figure 9B) is fairly

uniform in both the crust and the catalyst interior. There is more calcium in the crust than in the catalyst.

The sulfur (Figure 10A) and iron (Figure 10B) area scans show a very high correlation for these two elements in the crust, a very low concentration of iron in the catalyst, and an intermediate concentration of sulfur in the catalyst. These results are similar to the top sample.

The titanium scan (Figure 11A) shows a very high concentration of this element in the inner crust, a high concentration in the outer crust, and decoration of the two shallow depressions on Figure 8B with titanium. In addition the small piece of material sitting on the surface of the catalyst at the extreme left is high in titanium. This speck appears to be a piece of inner crust which may have been displaced during sample preparation.

#### Bottom Sample

Figures 12A and 12B are conventional photo micrographs of the sectioned and polished catalyst sample taken from the bottom of the reactor. The small square shown on Figure 12A is examined at higher magnification with SEM; the micrographs are given in Figures 14A and 14B. The large rectangle area in Figure 12B was given SEM-EDAX scans; the data are given on Figures 15A-17B.

The bottom sample is distinctly different from the top and middle samples. First, the cemented exterior crust does not cover the entire surface, but instead appears to have filled in

regions where the surface of the catalyst has spalled away. Second, there is no titanium-rich inner crust on the catalyst in all of the samples investigated.

Figures 13A and 13B show two magnifications of the catalyst area in a zone where crust has formed. The enhanced depth of the field shows very large cracks and several round, shallow pits in the catalyst support. These features of the bottom sample are identical to the other two samples.

Figures 14A and 14B are two pictures at 1000x of the small square identified on Figure 12A. These pictures show that the flat crater is filled with polycrystalline material smaller than 0.5 microns which is similar to the inner crust material. A spot EDAX analysis shows that this zone contains significant quantities of titanium.

The SEM-EDAX area scans for the bottom sample are shown in Figures 15A-17B. The results for the six elements Si, Ca, S, Fe, Ti and Mo are identical effectively to the middle sample with the following exceptions:

- a) there are no particles very high in sulfur in the crust,
- b) there is less difference between the sulfur concentration in the crust and in the catalyst,
- c) the titanium concentration in the outer crust is very distinct, and there is significant but lower concentration of titanium in the catalyst close to the surface,
- d) the molybdenum is clearly conferred to the catalyst.

### Microprobe Results

The electron microprobe results are displayed on Figures 18A, B, and C; this figure is arranged to permit an easy comparison of the three samples for the several elements considered. Figure 18A is the top sample, 18B the middle sample and 18C the bottom sample. These elements were examined in each scan and the data are referenced to the aluminum signal. The amplitude of the signal is proportional to the line averaged concentration of the element.

Molybdenum and nickel are the active elements in the catalyst. The molybdenum signal in the crust is only slightly greater than background, and therefore there does not appear to be migration of this element. The nickel signal was amplified far more than molybdenum and therefore the signal has far more noise. Nickel is above background in the crust in 18A, B, and C and the broadened transition of the profile between the interior and the crust suggest that nickel has migrated slightly.

Iron and sulfur are found in the exterior crust of 18A and 18B and in the crust of 18C. Previous work has established that this crust is nonstoichiometric ferrous sulfide. This material appears in surprisingly large quantities in this investigation; obviously the coal-derived liquid carries all of the mineral found in coal. On the other hand in the interior the iron signal decays to background level within 125 microns of the surface while the sulfur stabilizes on the value appropriate to the sulfided catalyst.

Whenever there is a void in the catalyst (18B has a clear example) the aluminum and sulfur signal will decrease together.

Titanium, calcium and silicon are elements found in the mineral matter of coal. The titanium signal in 18A and 18B shows clearly the inner crust; the concentration of titanium in the inner crust is about twice as high as in the exterior crust of 18A and 18B or the outer crust of 18C. Thus the laydown of the inner crust appears to occur by a different mechanism than the outer crust. There is a surprisingly large penetration of titanium into the interior of the catalyst. The decoration of cracks and voids with titanium is seen as an irregular but diminishing penetration of titanium into the catalyst interior.

Silicon is a major component in the outer crust of 18A and B and in the crust of 18C. Further there is a substantial penetration of this element into the catalyst interior. Since silicon is found in the cracks near the surface, it is apparent that the catalyst is spalling away by interactions of the mineral matter. Calcium, on the other hand, has only a very weak signal in the interior of the catalyst. Further calcium and silicon apparently exclude each other in the surface crust and interior deposition.

The zinc signal shows the deposition of very low quantities of this material near the catalyst surface, particularly in the top sample. Thus the catalyst appears more active for deposition in the early part of the run; this activity is lost down the reactor.

These microprobe results are consistent with the SEM and electron microprobe area scans. The inner crust is a real phenomena, and the refractory components of the clay mineral matter are small enough to penetrate a significant way into the catalyst.  $\text{FeS}_x$  remains in the feed slurry and becomes firmly attached to the catalyst exterior. These deposits diminish the extent to which the catalyst can be regenerated.

#### Plasma Etched Samples

Figures 19A and 19B are two magnifications of a catalyst sample which has been plasma etched to remove oxidizable material "coke" and then reveal the firmly attached exterior crust. Figure 18A shows two cleavage planes through the catalyst and the irregular surface at the left of the picture. The exterior surface is covered with waves of deposited material. Figure 18B shows the marked rectangle on 18A at higher magnification. The surface contains aggregates of crystalline material with an 0.5 to 2.0 micron crystal size. (The largest crystal in the figure was used as a marker. This crystal appears to be a chip held to the surface electrostatically.)

Figure 20B is a view along the transverse axis of a pellet cleaved on the radial plane. The sample was taken from the bottom of the reactor where the external crust is irregular. After plasma etching no residual crust was found. However the radial plane is dotted with round pits and plateaus which have been observed in all of the polished sections. The pits near the

surface occasionally are partially filled with deposited mineral matter. Further the exterior surface of the catalyst has eroded to become quite rough. This micrograph shows that the round pits seen in all of the micrographs are not an artifact of sample preparation.

#### Catalyst Activity Results

A total of eight experimental runs were conducted. Table IV presents the catalysts used in each run. Two of the runs were blank runs to determine the background activity of the reactor. The fresh, spent and regenerated catalysts were used in two different sizes comprising of the other six runs. All experiments were conducted at the same operating conditions presented in Table III. However the duration of the runs varied.

Figures 21 and 22 show the total nitrogen removal and the total sulfur removal for crushed catalyst run in the fresh, spent and regenerated states. These figures show that these reactions follow pseudo first-order kinetics over limited ranges of element removal. Equivalent plots are obtained for runs made with the three states of pelleted catalysts.

Table V presents the first-order rate parameters corrected for background activity. This table shows that the pelleted catalysts have either equal or larger activities than the corresponding crushed catalyst; these results are contrary to the usual effect of isothermal transport limitations in catalysts. These results will be described more fully below.

Figure 23 shows the network for the hydrogenolysis of quinoline developed by Shih *et al.* (4). The individual rate constants for this network are obtained as pseudo first-order rate parameters using the techniques developed by Himmelblau *et al.* (5). The experimental data were analyzed using three different weighting schemes and the best weighting scheme was chosen based on the overall fit of the data and the reduction of the sum square error. Figures 24 and 25 show a comparison of the data with the parametric representation. These figures show reasonable agreement between the model and the data; the pseudo first-order form provides a simple and adequate representation of the network.

The individual rate parameters for this network analysis, corrected for background reactivity, are presented in Table VI. The rate parameters for pellets are lower than those for crushed catalyst in the three states, fresh, spent and regenerated for all parameters except  $k_6$ . The parameter  $k_6$  governs the conversion of 1,2,3,4-tetrahydroquinoline to orthopropylaniline; the rate parameter for subsequent step for nitrogen removal cannot be obtained reliably from the data, and thus this step represents an apparent dead end for nitrogen removal. Hence it is useful to calculate the concentration of all intermediate nitrogen compounds using the parameters of the reaction network.

Figure 26 compares the data for total nitrogen concentration with the values predicted by the model for fresh crushed catalyst; the model represents the data adequately. Similar comparisons

were made with the other five cases, and the experimental data are represented with equivalent acceptability. Thus the network representation is consistent with the overall rate of nitrogen removal for all cases.

There is direct evidence that some of the reaction rates in pellets are inhibited by transport considerations. Figure 27 shows the 1,2,3,4-tetrahydroquinoline (1THQ) and quinoline concentrations as a function of time for fresh crushed and pellet catalysts runs under otherwise identical conditions. Consistent with the lower forward apparent rate parameter for the reversible reaction, the pellet data show a higher concentration of quinoline, a lower concentration of 1THQ, than for crushed catalyst. In addition the maximum in the 1THQ concentration occurs earlier for the crushed catalyst than for the pelleted run. Therefore the pellets exhibit direct evidence for transport limitations in the catalyst.

The utility of this assumption can be tested by calculating the effectiveness factor for the pellet catalyst based upon the crushed catalyst parameters. This calculation assumes that the crushed catalyst is small enough to give intrinsic rates for all rates; this assumption can be examined later. Table VII outlines the results of the calculation.

The parameter values for the pellet catalyst agree reasonably well with the calculated values; the exceptions are  $k_6$  and  $k_8$ .

A similar calculation for the regenerated (Table VIII) catalyst shows that again with the exception of  $k_6$  the calculated values for the pellet catalyst are too high in comparison to the data.

The low values found for the pellets show that there is a significant loss in the effective diffusivity for the pellets. This loss is the result of deposition of mineral matter on the exterior of the pellets; this transport resistance is removed (or avoided) when the regenerated catalyst is crushed.

Table IX gives the percentage activity remaining in the five catalyst forms relative to fresh crushed catalyst. The values observed stem from several causes: 1) intrinsic loss in kinetic activity, thus the spent catalyst has about 3-4 percent of the fresh catalyst activity and the regenerated catalyst has circa 60 percent of the original activity; 2) internal diffusional transport losses; 3) contributions from the external and near surface mineral material on the pellets, and 4) an abnormal enhancement of the  $k_6$  and  $k_8$  rate parameters in pellets. With reference to the latter, Bhinde (6) has shown that the hydrogenolysis rate has the approximate form  $\text{rate} = kKC/(1+KC)^2$ , where  $C$  is the reactant concentration and  $K$  is the adsorption term. This rate expression is negative order for  $KC$  greater than one, and thus a decreasing concentration profile to the center of the pellet will increase the effective reaction rate. Thus the enhanced overall rate for HDN in pellets is in part the result of coupling transport limitations with the very strong adsorption equilibrium of nitrogen hetrocycles.

The reaction network shown in Figure 28 for dibenzothiophene hydrodesulfurization has been determined earlier by Houalla *et al.* (7). However, their reaction network was determined using only dibenzothiophene as a reactant. In this study, dibenzothiophene and biphenyl were observed for the crushed particles, and runs using pellets contained traces of cyclohexyl benzene in addition to the above two products. Concentration profiles suggested that cyclohexyl benzene is a secondary product. Bhinde (6) found that quinoline inhibits the hydrogenation steps in the dibenzothiophene network strongly, and in our experiments the concentration of quinoline was very high.

Based on all the above information the dibenzothiophene HDS data were analyzed using the following network:

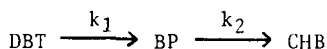


Table VIII presents the individual rate constants. The table shows that spent catalyst had a very low activity. However, unlike nitrogen removal, the spent catalyst is not totally non-reactive. For fresh catalyst the pellets are significantly more active than crushed pellets. Further cyclohexyl benzene, a hydrogenated product from biphenyl, was found only in the pellet runs. Broderick (8) and Sapre (9) have studied biphenyl hydrogenation and have shown that biphenyl hydrogenation is extremely slow and is severely inhibited by the presence of quinoline. This observation can be explained in terms of transport limitations in pellet runs in two

different ways. Since transport limitations exist in the case of pellets, the biphenyl concentration will probably be higher in the interior of the catalyst particles than for crushed catalyst. The higher concentration of biphenyl and the significantly longer residence time in the catalyst couple to increase the probability of formation of cyclohexylbenzene. The concentration profile for nitrogen hetrocycles in the catalyst interior also contributes to the observed difference between pellets and crushed catalysts. The catalyst pellets have a lower interior concentration of quinoline and THQ as opposed to the crushed particles, and hence the inhibiting effects of quinoline on dibenzothiophene is lower in the case of pellets. Thus the interior reactivity is higher for pellets, but the overall rate is lower than would be observed if quinoline were absent.

### Discussion

The photomicrograph data provides detailed information on the deactivation of catalyst and an opportunity to compare the hydroprocessing of a coal-derived liquid with the hydroprocessing of coal. These data supplement the results from the activity studies.

The one percent suspended minerals in the feed is very significant in the deactivation of the catalyst. These suspended material are very finely divided and therefore can penetrate rather easily into the interior of the catalyst. Hence silicon, which is a major constituent of the clays in coal, is found in the interior 100 microns of the catalyst in all three samples.

This observation is consistent with the behavior of coal hydro-processing experiments.

The catalyst is deactivated by the laydown of coke. The plasma etching experiments show that the exterior crust is largely coke, and regeneration by burning decreases the sample weight by twenty percent. Thus a significant fraction of the activity can be regained by burning away the coke deposits as evidenced by the results from activity studies, however the deposited mineral matter remains.

The exterior crust also contains  $\text{FeS}_x$ ; previous studies have shown that these deposits are  $\text{FeS}_{1.1}$ . The crystal size of  $\text{FeS}_x$  is smaller in this system than for the synthoil catalyst. There is no evidence that the  $\text{FeS}_x$  was formed in the trickle-bed reactor; the weak penetration of iron into the catalyst correlates with the penetration of silicon, and it therefore appears that  $\text{FeS}_x$  is cemented on the catalyst with coke.

The nickel profiles indicate a small migration of this element away from the catalyst support into the crust on the surface. The migration of this promoter may affect catalyst function; in particular the effect of nickel upon the rate of coking may change.

The most unique feature of these studies is the formation of the titanium-rich inner crust on the top and middle catalyst samples.

Spent catalyst was found to be essentially non-reactive for both sulfur and nitrogen removal. Network analysis for quinoline HDN and dibenzothiophene HDS indicate that the laydown of coke seems to affect both hydrogenation and bond-breaking steps in the same way. The results from the experiments using the regenerated catalysts show that half of the activity was recovered by the regeneration process. A comparison of the runs using catalyst pellets and crushed particles shows that the catalyst interior is filled with coke and inactive. These results also raise some interesting questions on the interplay between diffusion limitations and the interactions between nitrogen and sulfur-containing compounds upon the intrinsic kinetics.

The results presented here are similar to the ones observed from characterization studies performed on catalysts that have been in direct contact with coal, except for a few minor differences.

Since 50 to 60 percent of the catalyst activity can be recovered by burning the coke, the mineral matter is secondary in the direct deactivation of the catalyst. However, the deposited mineral matter is a potential catalyst for coke formation; thus the effective lifetime for the regenerated catalyst may be less than that for a fresh catalyst.

#### Acknowledgements

This work was supported by a grant from the Department of Energy.

### Literature Cited

1. Stanulonis, J. J., Gates, B. C., and Olson, J. H., AICHE J., 22, 576 (1976).
2. Chiou, M. J. and Olson, J. H., Am. Chem. Soc., Div. Pet. Chem., Prepr., 23 (4), 1421 (1978)
3. Chiou, M. J. and Olson, J. H., 'Catalyst Deactivation in Coal Liquefaction Processes,' submitted to AICHE J.
4. Shih, S. S., Katzer, J. R., Kwart, H., and Stiles, A. B., Am. Chem. Soc.; Div. Pet. Chem. Prepr., 22(3), 919 (1977).
5. Himmelblau, P. M., Jones, C. R., and Bischoff, K. B., Ind. Eng. Chem. Fundam. 6, 539 (1967).
6. Bhinde, M., Ph.D. Thesis, University of Delaware, 1979.
7. Houalla, M., Nag, N. K., Sapre, A. V., Broderick, D. H., and Gates, B. C., AICHE J. 24, 1015 (1978).
8. Broderick, D. H., Ph.D. Thesis, University of Delaware, 1979.
9. Sapre, A. V., Ph.D. Thesis, University of Delaware, in preparation.

TABLE I

Feed Oil Properties

Equal Volume Mixture of Raw Anthracene Oil and  
Synthoil Liquid

Carbon, wt %	84.92
Hydrogen, wt %	6.57
Sulfur, wt %	0.54
Nitrogen, wt %	1.21
Ash, wt %	1.05

TABLE II

Operating Conditions in the Trickle-Flow Reactor

Temperature -	371°C
Pressure -	.1500 psig
Liquid Volume	
Hourly Space Time -	1.25 hrs
H <sub>2</sub> /Oil Ratio -	7500 scf/bbl
Run Duration -	674 hours

TABLE III

Operating Conditions in Batch Autoclave Reactor

Temperature -	350°C
Pressure -	36 atm
Catalyst Concentration -	0.5 wt %
CS <sub>2</sub> Concentration -	0.05 wt %
Carrier Oil -	Hexadecane
Quinoline Concentration -	2 wt %
Dibenzothiophene Concentration -	1 wt %

TABLE IV

Catalysts Used in Batch Experimental Runs

<u>Run No.</u>	<u>Catalyst Used</u>	<u>Catalyst Size</u>	<u>Duration, minutes</u>
1	Fresh	140 mesh	600
2	Spent	140 mesh	1280
3	Regenerated	140 mesh	1260
4	Fresh	8/10 mesh	1200
5	Spent	8/10 mesh	1800
6	Regenerated	8/10 mesh	1250
7	Blank run without boat		600
8	Blank run with boat		2500

TABLE V

Total Nitrogen and Sulfur Removal  
Pseudo First Order Rate Constants,  $\frac{\text{g of oil}}{\text{g of cat. minutes}}$

	<u>Fresh</u>		<u>Spent</u>		<u>Regenerated</u>	
	C	P	C	P	C	P
Nitrogen	0.195	0.214	0	0	0.116	0.165
Sulfur	0.333	0.491	0.333	0.222	0.168	0.165

TABLE VI

Individual Reaction Rate Constants  
for the Quinoline Network,  $\frac{\text{g of oil}}{\text{g of cat. minutes}}$

	<u>Fresh</u>		<u>Spent</u>		<u>Regenerated</u>	
	C	P	C	P	C	P
k <sub>1</sub>	81.19	9.045	0.908	0	46.07	3.566
k <sub>2</sub>	12.92	1.835	0.135	0	10.96	0.620
k <sub>3</sub>	1.120	0.676	---	0.042	0.627	0.216
k <sub>4</sub>	0.167	0.114	0.0042	0	0.153	0.121
k <sub>5</sub>	0.727	0.422	---	0	0.182	0.025
k <sub>6</sub>	0.101	0.218	0.0042	0	0.064	0.107
k <sub>7</sub>	---	---	---	0	---	---
k <sub>8</sub>	1.752	1.66	0	0	1.372	0.170

TABLE VII

Theoretical Calculation of Rate Parameters for Fresh Pellets

	<u>Crushed Rate</u> <u>g oil/g cat min)</u>	<u>Thiele Modulus</u>	<u><math>\eta</math></u>	<u>P<sub>cal.</sub></u>	<u>P<sub>found</sub></u>
k <sub>1</sub>	81.19	13.51	0.074	9.27	9.045
k <sub>2</sub>	12.92	5.39	0.185	2.39	1.83
k <sub>3</sub>	1.12	1.59	0.58	0.65	0.68
k <sub>4</sub>	0.167	0.61	0.89	0.15	0.11
k <sub>5</sub>	0.727	1.28	0.67	0.49	0.422
k <sub>6</sub>	0.101	0.48	0.93	0.093	0.218
k <sub>8</sub>	1.752	1.98	0.49	0.85	1.66

TABLE VIII

Theoretical Calculation of Rate Parameters  
for Regenerated Pellets

	<u>Crushed Rate</u> <u>(g oil/g cat·min)</u>	<u>Thiele</u>	<u><math>\eta</math></u>	<u><math>P_{calc}</math></u>	<u><math>P_{found}</math></u>
$k_1$	46.1	10.18	0.098	4.53	3.57
$k_2$	11.0	4.97	0.20	2.21	0.62
$k_3$	0.63	1.19	0.70	0.44	0.22
$k_4$	0.15	0.587	0.90	0.134	0.121
$k_5$	0.18	0.637	0.88	0.16	0.025
$k_6$	0.064	0.40	0.95	0.058	0.107
$k_8$	1.372	1.76	0.53	0.74	0.170

TABLE IX

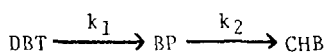
Rate Constants in the Quinoline NetworkRelative to Fresh Catalyst, %

	$k_1$	$k_2$	$k_3$	$k_4$	$k_5$	$k_6$	$k_7$	$k_8$
Spent pellets	0	0	6	0	0	0	--	0
Spent particles	1	1	0	3	0	4	--	0
Regenerated Pellets	39	33	32	100	6	49	--	10
Regenerated particles	57	85	56	92	25	63	--	78

TABLE X

Individual Rate Constants for  
 Dibenzothiophene Hydrodesulfurization,  $\frac{\text{g of oil}}{\text{g of cat} \cdot \text{minutes}}$

	Fresh		Spent		Regenerated	
	C	P	C	P	C	P
$k_1$	0.333	0.491	0.033	0.022	0.168	0.163
$k_2$	---	0.008	---	---	---	0.007



## LIST OF FIGURES

### Figure

- 1 Light microscopy of top sample A. 100x; B. 200x.
- 2 SEM top sample A. backscatter electron; B. aluminum EDAX.
- 3 SEM-EDAX of top sample A. silicon; B. calcium.
- 4 SEM-EDAX of top sample A. sulfur; B. iron.
- 5 SEM-EDAX of top sample A. titanium; B. molybdenum.
- 6 Microprobe area scans A. backscatter electron;  
B. titanium.
- 7 Light microscopy of middle sample A. 100x; B. 200x.
- 8 SEM of middle sample A. 400x; B. 800x.
- 9 SEM-EDAX of middle sample A. silicon; B. calcium.
- 10 SEM-EDAX of middle sample A. sulfur; B. iron.
- 11 SEM-EDAX of middle sample A. titanium; B. molybdenum.
- 12 Light microscopy of bottom sample A. 100x; B. 200x.
- 13 SEM of bottom sample A. 200x; B. 400x.
- 14 SEM of interior spot A. backscatter electron;  
B. ground current.
- 15 SEM-EDAX of bottom sample A. silicon; B. calcium.
- 16 SEM-EDAX of bottom sample A. sulfur; B. iron.
- 17 SEM-EDAX of bottom sample A. titanium; B. molybdenum.
- 18 Electron microprobe results for the three samples  
A. top; B. middle; C. bottom.
- 19 SEM of plasma etched surface of top sample A. 200x;  
B. 2000x.
- 20 SEM of plasma etched surfaces A. 200x middle sample;  
B. 100x bottom sample.
- 21 Comparison of total nitrogen removal for fresh, spent  
and regenerated catalysts.

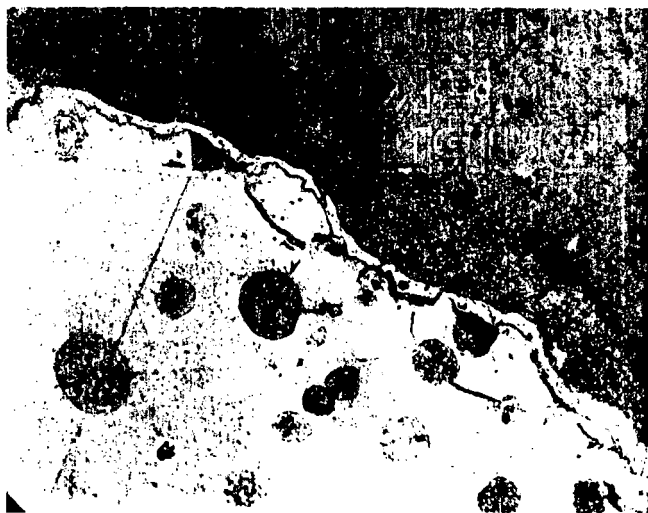
Figure

- 22 Comparison of total sulfur removal for fresh, spent and regenerated catalysts.
- 23 Network for quinoline hydrodenitrogenation.
- 24 Comparison of experimental data and predicted values for quinoline and 1,2,3,4-tetrahydroquinoline concentrations.
- 25 Comparison of experimental data and predicted values for orthopropylaniline, 5,6,7,8-tetrahydroquinoline and decahydroquinoline concentrations.
- 26 Comparison of experimental data and predicted values for total nitrogen removal for fresh catalysts.
- 27 Effect of catalyst particle size on quinoline and 1,2,3,4-tetrahydroquinoline concentration.
- 28 Network for dibenzothiophene desulfurization.

Light Microscopy—top sample



100x



200x

Scanning Electron Microscopy - top sample



400x  
Backscatter  
Electron

SEM-EDAX Area Scan - top sample



400x  
Aluminum  
EDAX

SEM - EDAX Area Scans - top sample

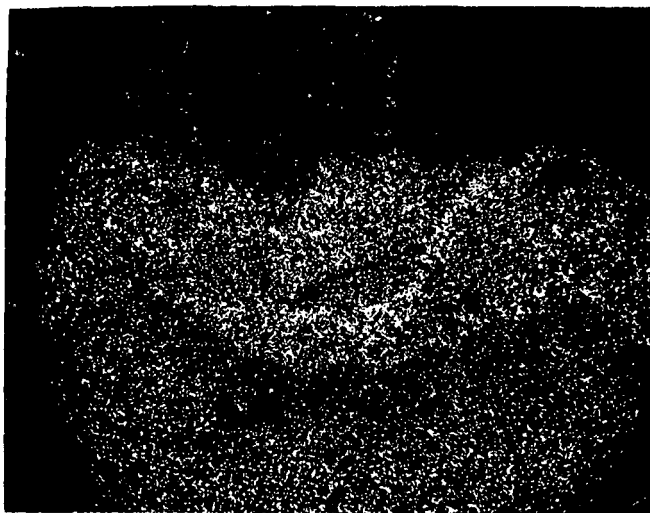


400x  
Silicon

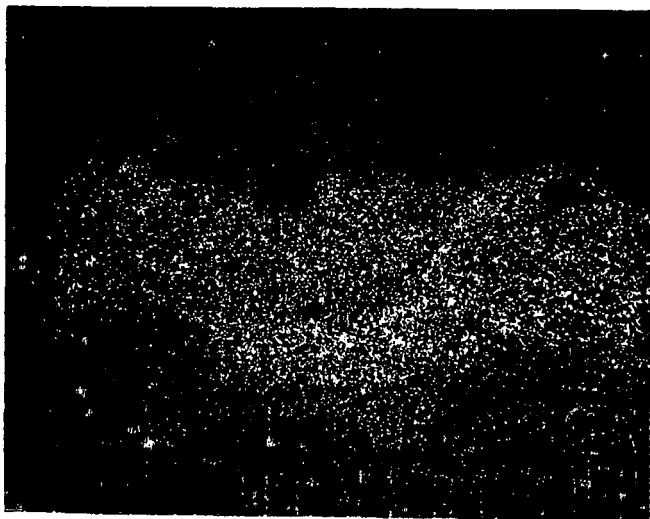


400x  
Calcium

SEM-EDAX Area Scans - top sample



400x  
Sulfur



400x  
Iron

# SEM-EDAX Area Scans - top sample

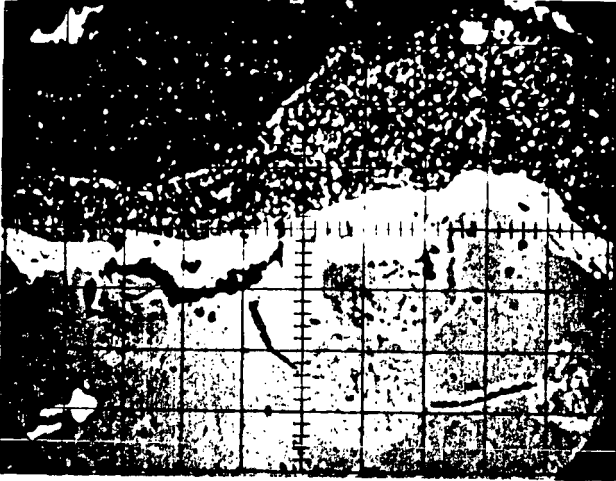


400x  
Titanium



400x  
Molybdenum

# Microprobe Scans - top sample

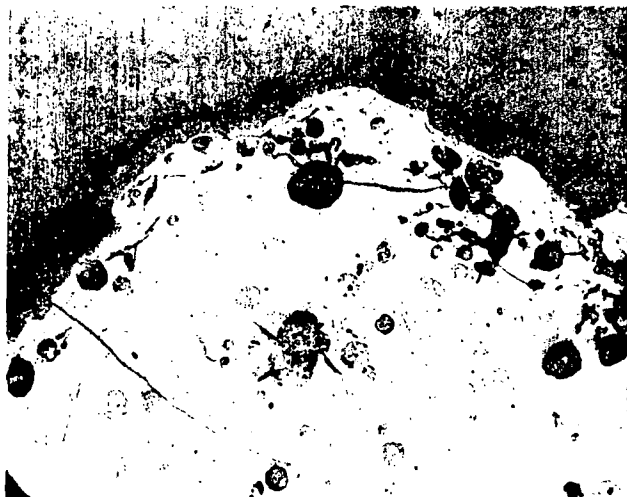


500x  
Backscatter  
Electron



500x  
Titanium

# Light Microscopy – middle sample



100x



200x

Scanning, Electron Microscopy – middle sample

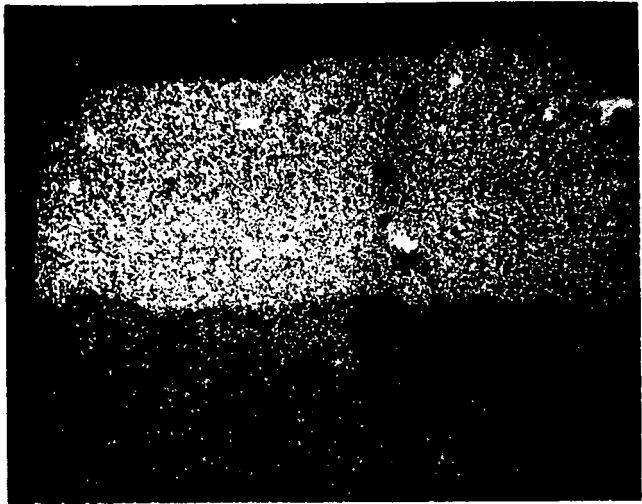


400x

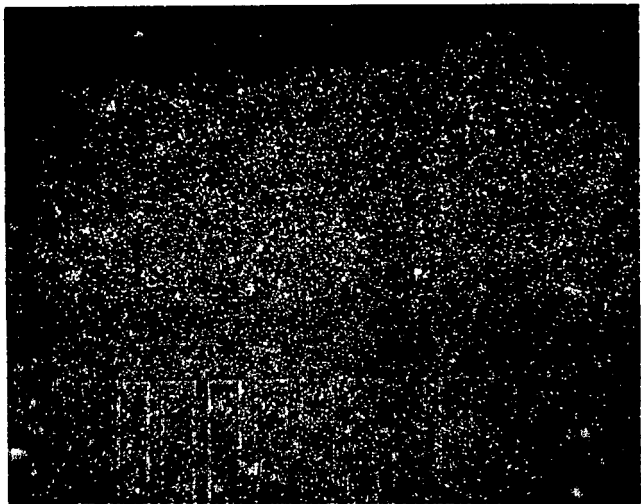


800x

SEM - EDAX - Area Scans - middle sample

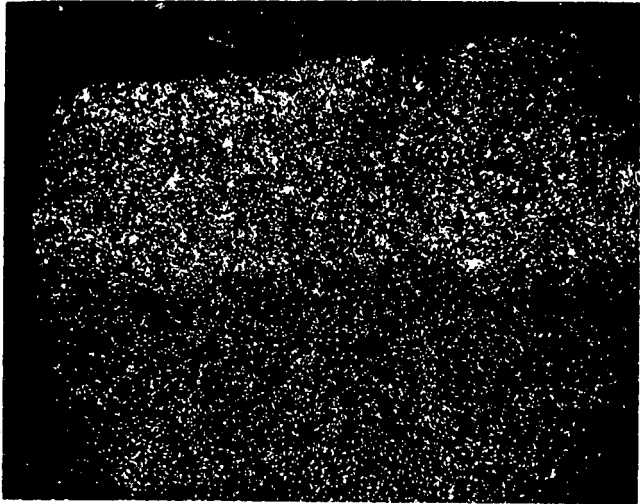


800x  
Silicon

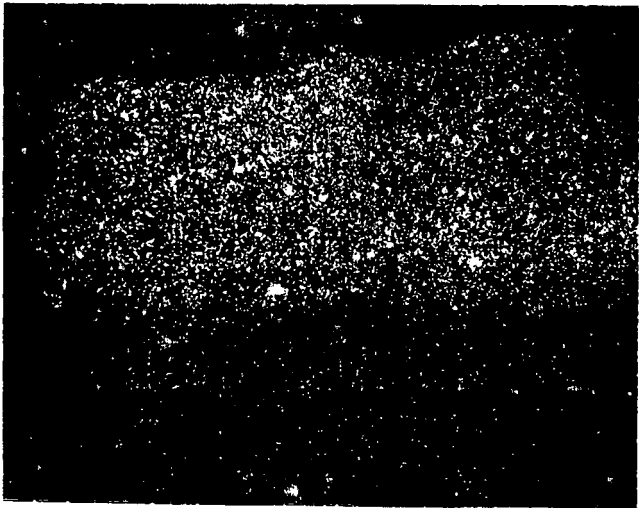


800x  
Calcium

SEM - EDAX Area Scans - middle sample

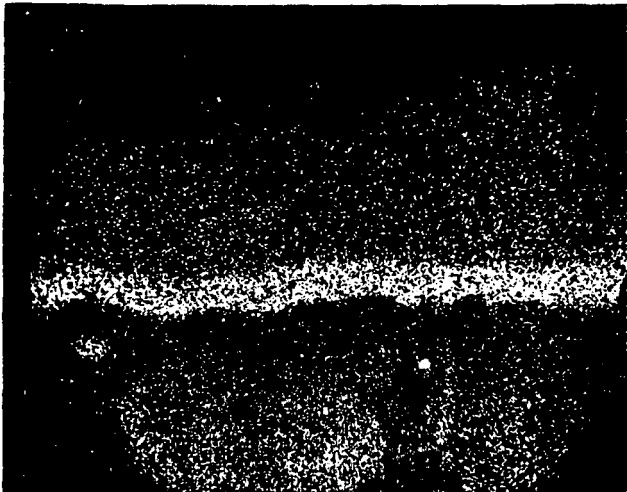


800x  
Sulfur

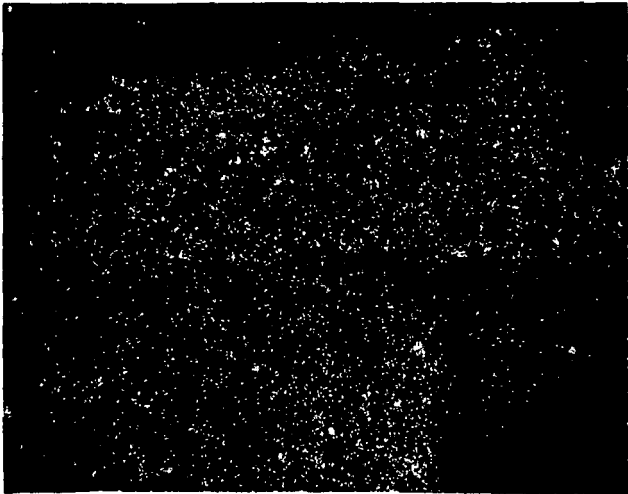


800x  
Iron

SEM-EDAX Area Scans - middle sample



800x  
Titanium



800x  
Molybdenum

Light Microscopy - bottom sample



100x



200x

Scanning Electron Microscopy - bottom sample

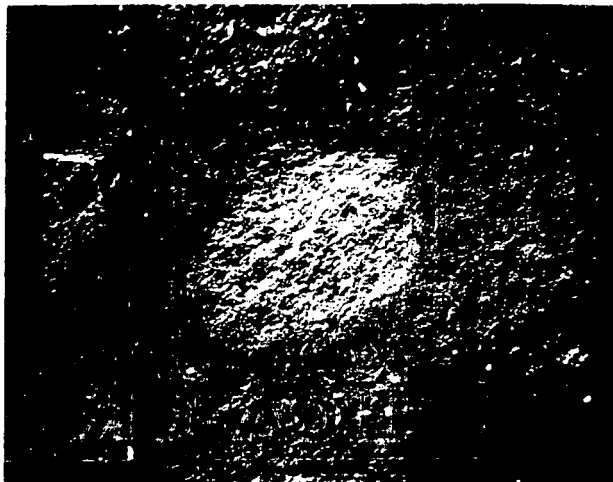


200x

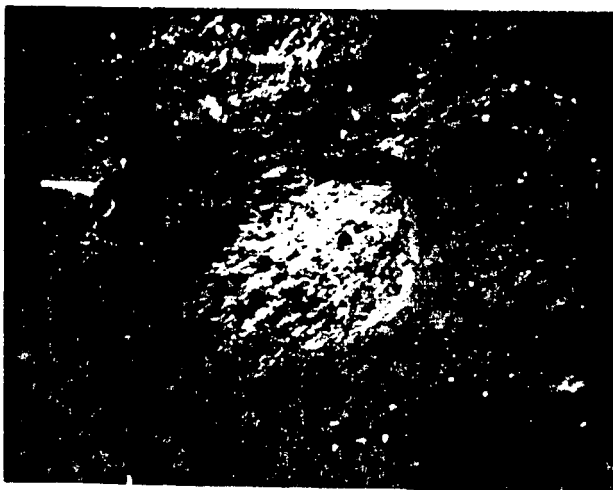


400x

Scanning Electron Microscopy  
Interior Spot - 1000x, 45° tilt

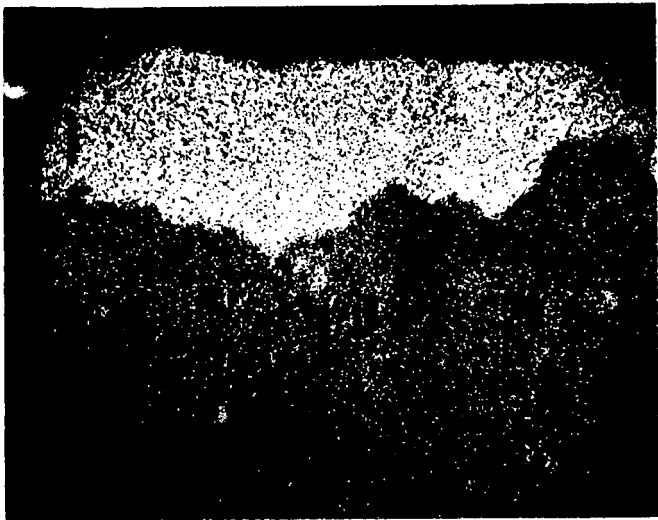


Backscatter  
Electron

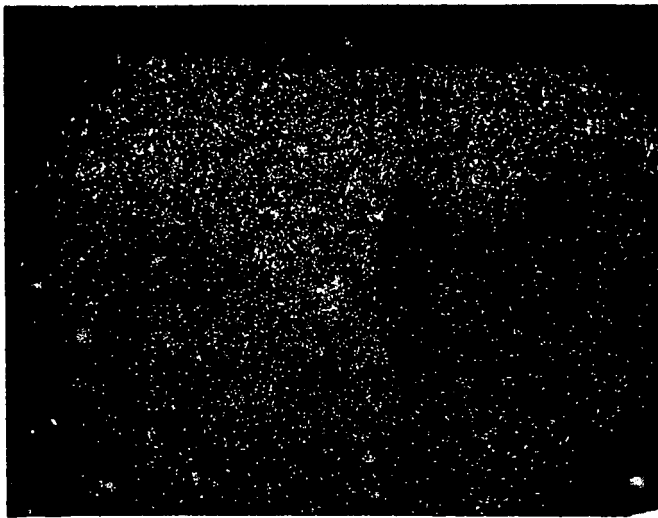


Ground  
Current

SEM-EDAX Area Scans - bottom sample

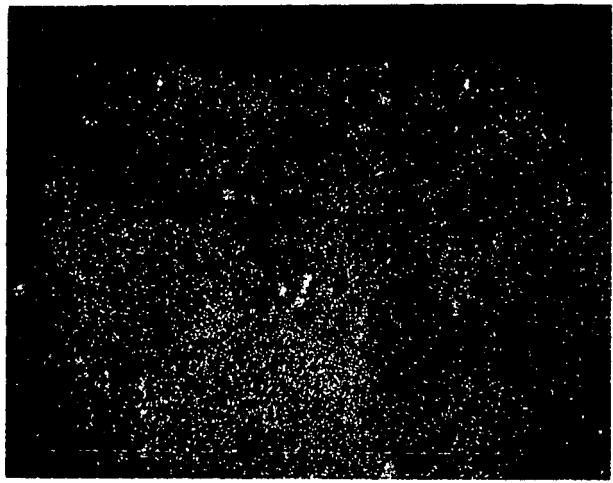


400x  
Silicon

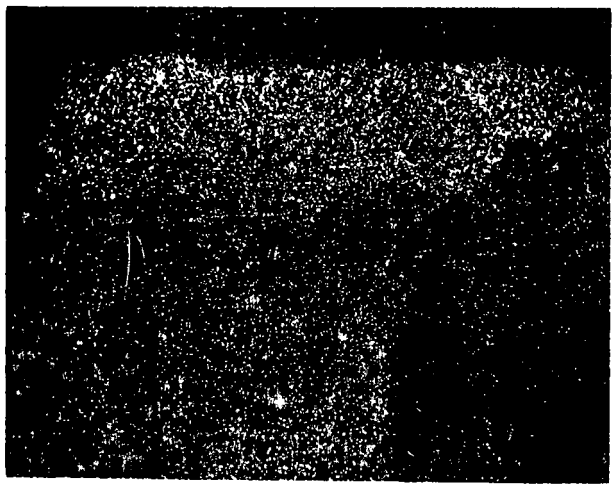


400x  
Calcium

SEM-EDAX Area Scans - bottom sample

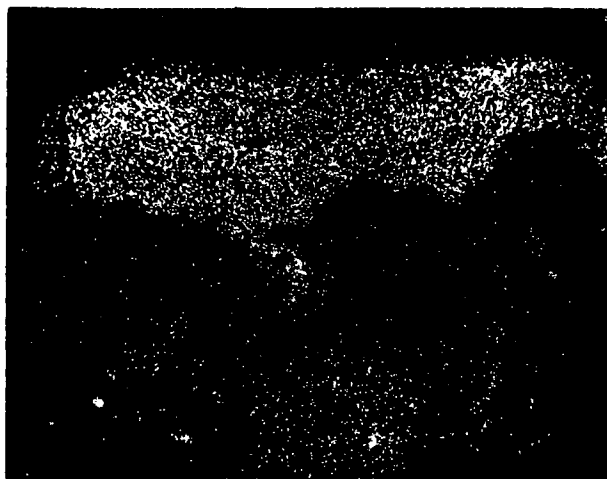


400x  
Sulfur

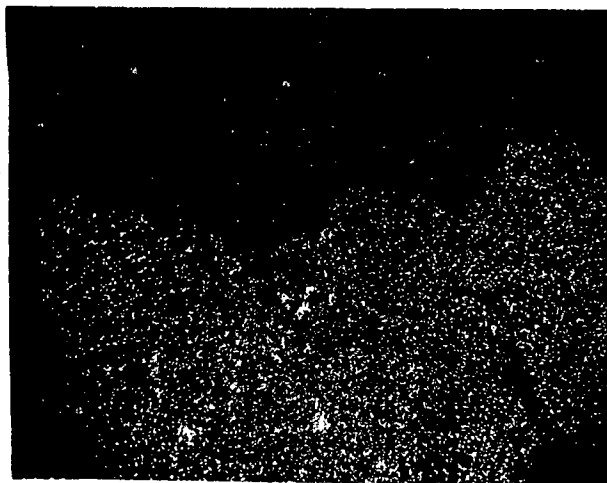


400x  
Iron

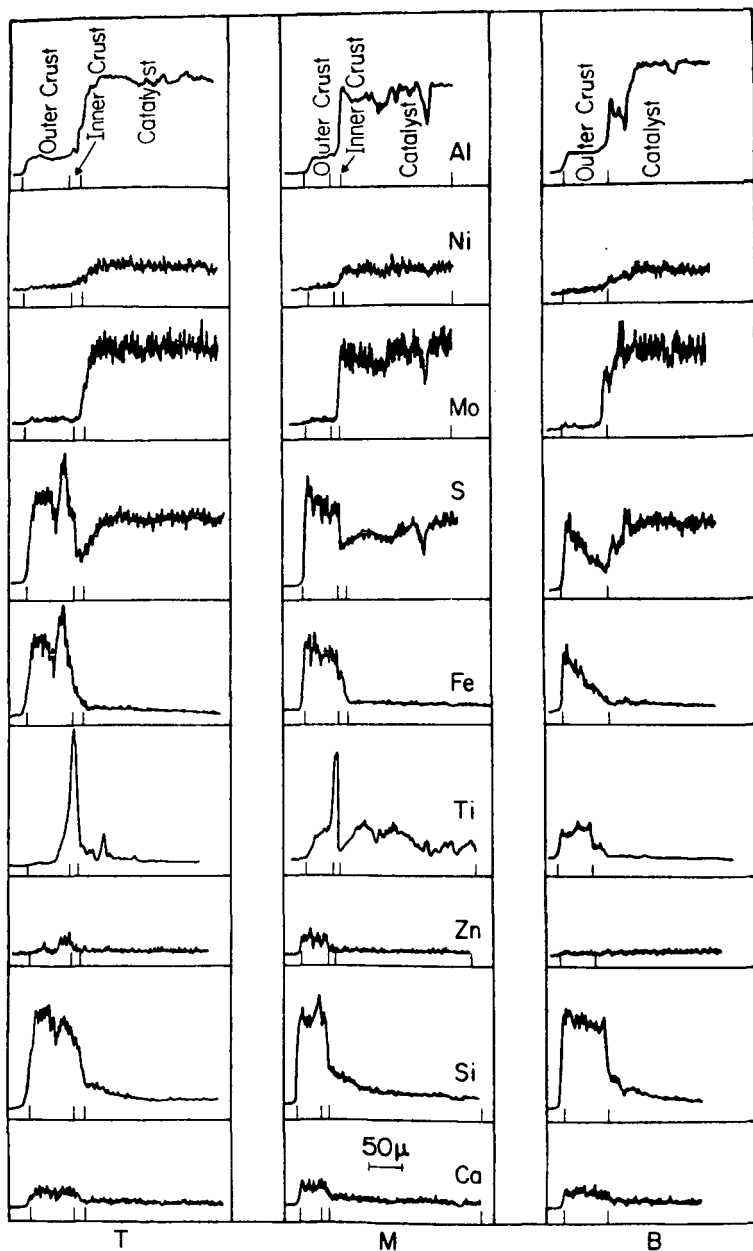
SEM-EDAX Area Scans - bottom sample



400x  
Titanium

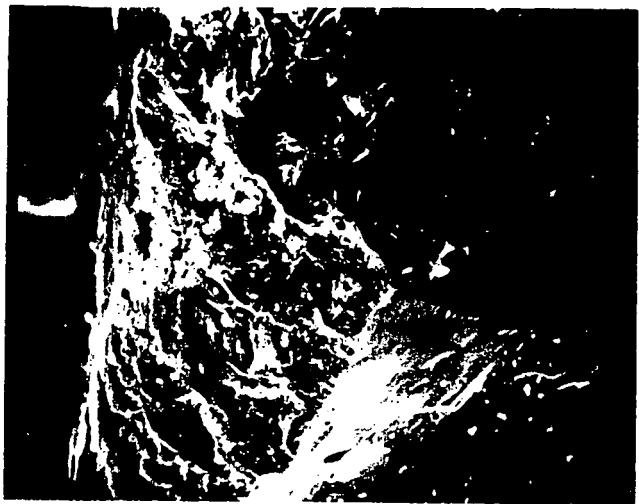


400x  
Molybdenum

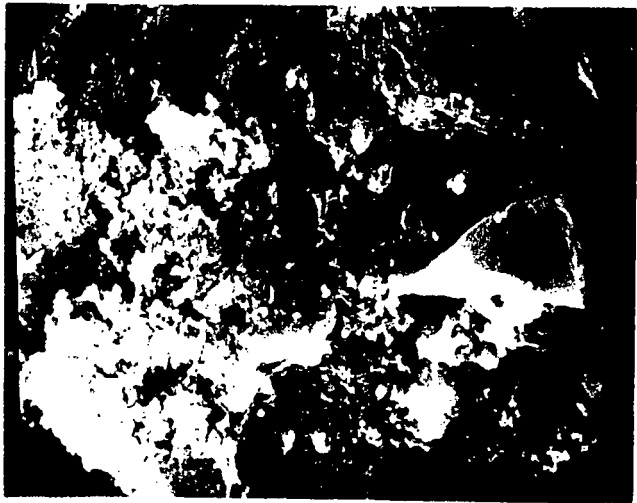


RELATIVE CONC PROFILES

SEM Plasma Etched Surface - top sample

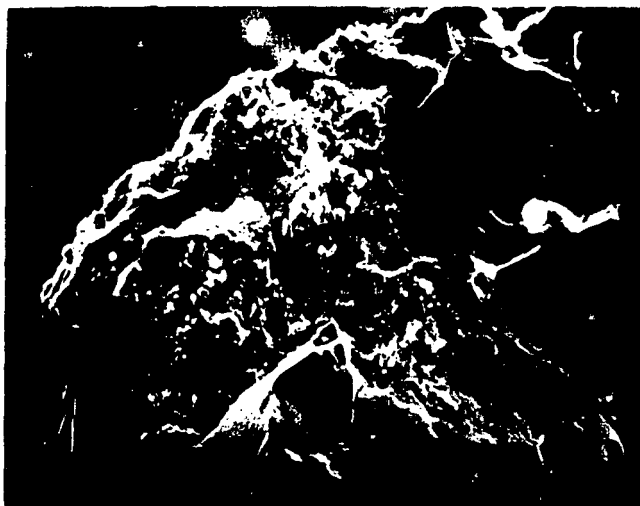


200 x



2000 x

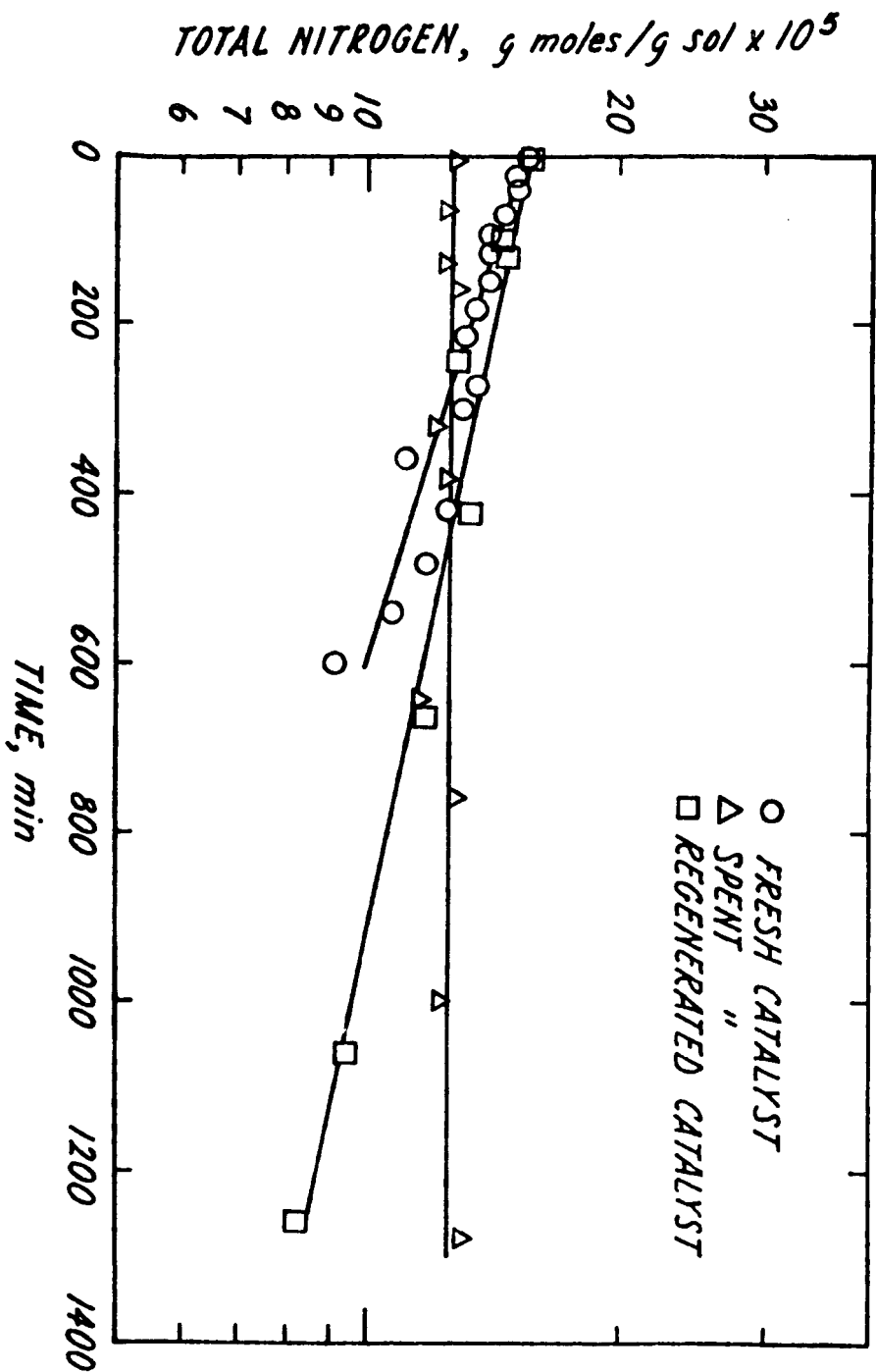
## SEM Plasma Etched Surfaces

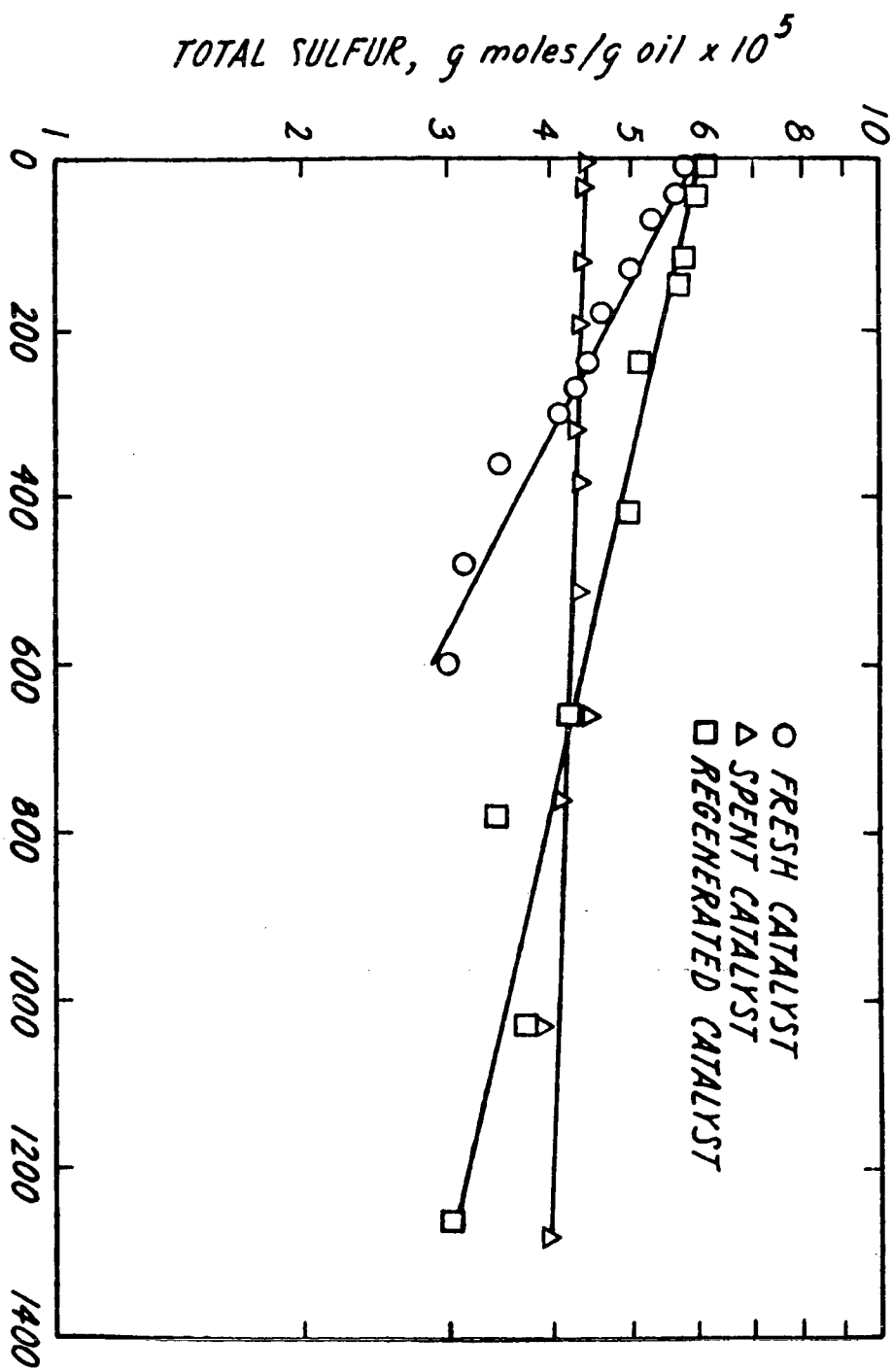


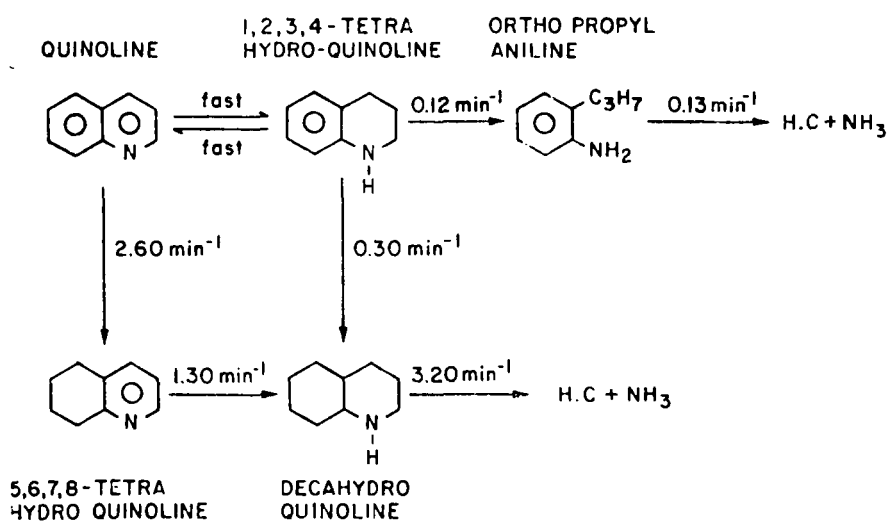
200x  
Middle  
Sample

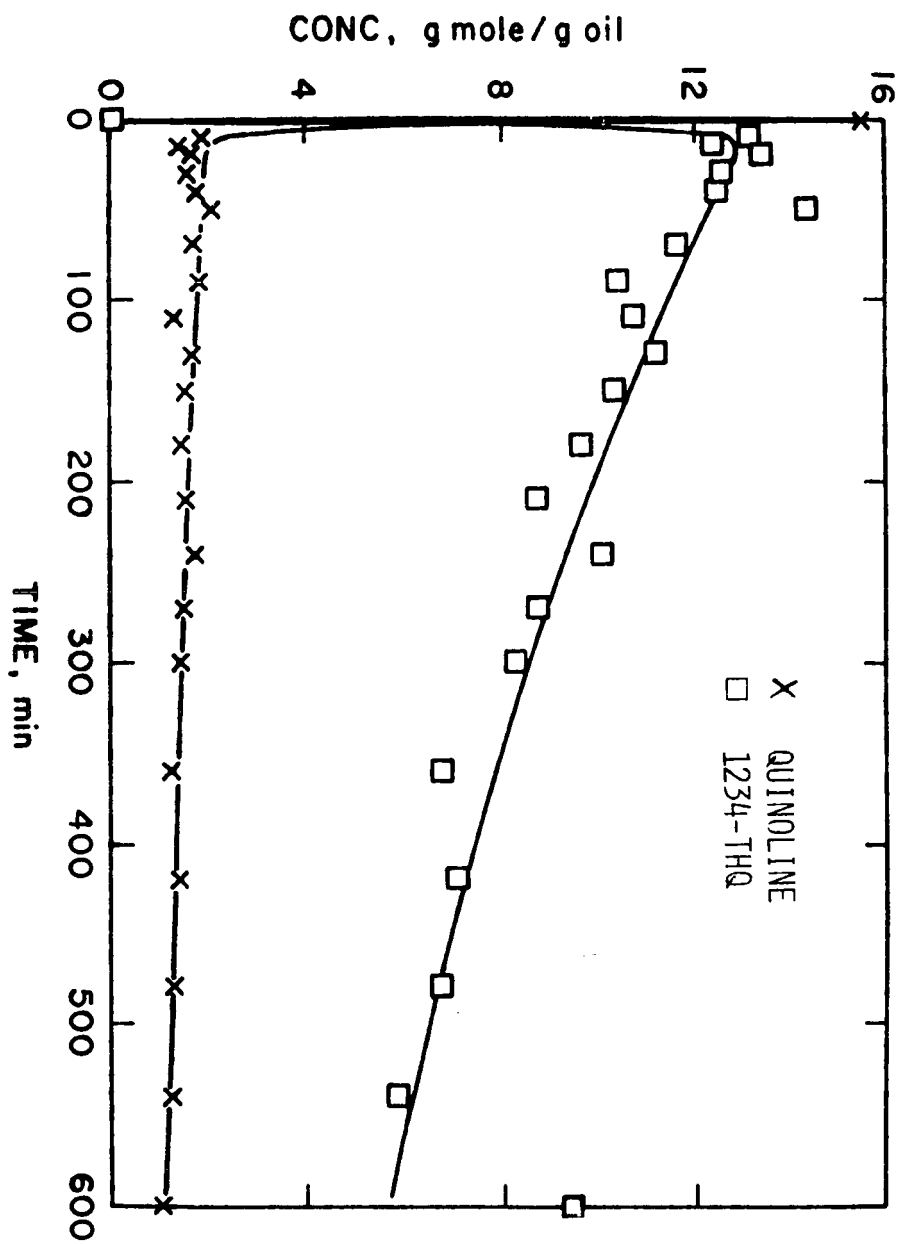


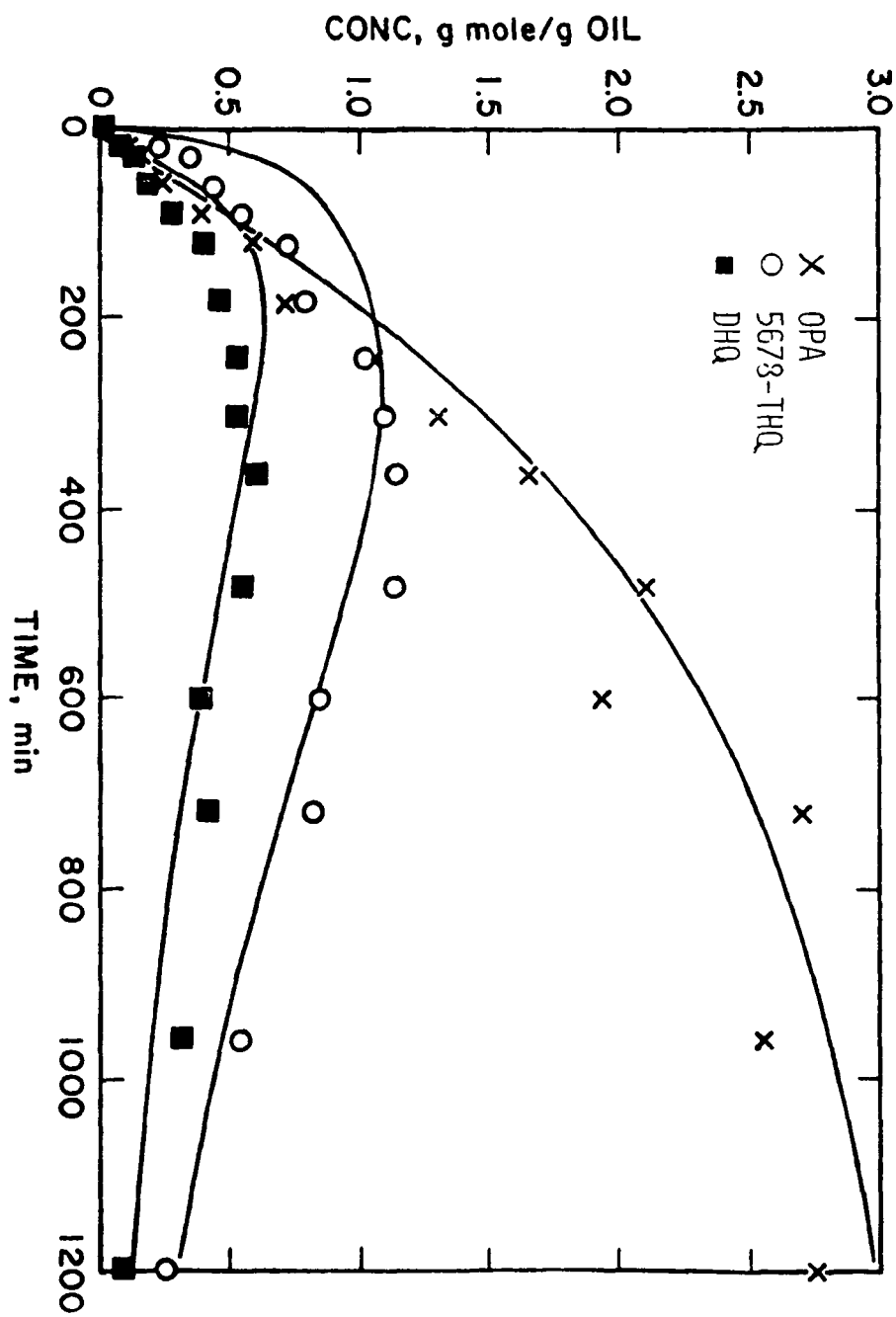
100x  
Bottom  
Sample

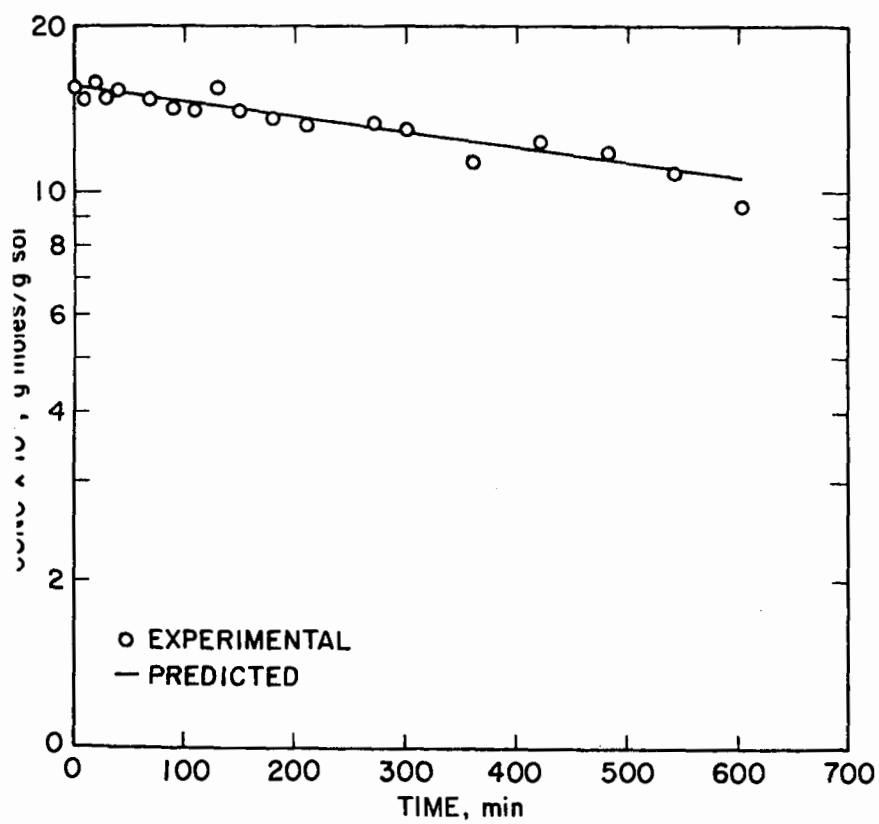


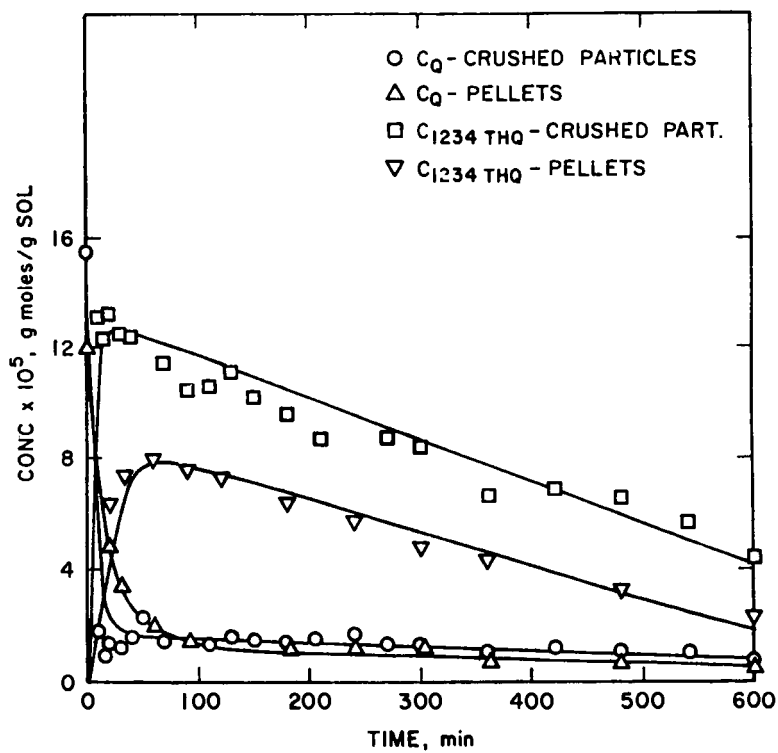


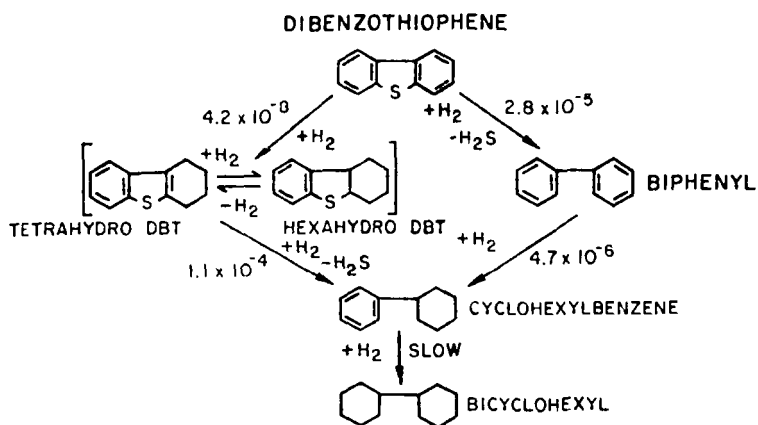












CATALYST DEACTIVATION IN HYDROTREATING COAL-DERIVED LIQUIDS by R. Sivasubramanian, J.H. Olson and J.R. Katzer. Center for Catalytic Science and Technology, Department of Chemical Engineering, University of Delaware, Newark, Delaware 19711.

Ni-Mo/Al<sub>2</sub>O<sub>3</sub> catalysts aged in hydrotreating coal-derived liquids were characterized by scanning electron microscopy, electron microprobe, and catalytic activity. Aged catalyst from three different sections of the trickle-bed reactor used for the hydroprocessing were plasma etched to remove the carbon coating and were then examined. An inner crust and an outer crust were observed on the exterior of the catalyst particles; the inner crust was not present on catalyst near the reactor exit. The inner crust was composed principally of titania; whereas the outer crust contained ferrous sulfide, silica, and traces of other metals. Titania was also deposited within the interior of the catalyst. The activities of fresh, aged, and regenerated (coke burnt off) catalysts were compared for hydrodesulfurization (HDS) and hydrodenitrogenation (HDN) using a mixture of dibenzothiophene and quinoline in n-hexadecane in a batch autoclave reactor. The aged catalyst was inactive for HDN and had very low activity for HDS. Burning the carbon off the catalyst resulted in approximately 60% recovery of the HDN activity and 50% recovery of the HDS activity compared to that of the fresh catalyst. Pseudo first-order rate constants were determined for each of the reactions in the quinoline and dibenzothiophene reaction networks.

Refining of Coal and Shale Derived Syncrudes

R. H. Fischer and R. E. Hildebrand

The Department of Energy is funding a program in refining of syncrudes with the objective of assessing the ability of existing technology to process syncrude, developing new more efficient technology designed especially for syncrude and determining the relationship between refining severity and product end use performance and toxicity. Also the Air Force sponsors a program that is developing new methods of refining shale oil. The achievements of these programs in 1979 will be reviewed and the Department's plans for 1980 and 1981 will be discussed.

APPLICATION OF LC-FINING TECHNOLOGY FOR UPGRADING SRC IN TWO-STAGE LIQUEFACTION  
CONCEPT. J. D. Potts, K. E. Hastings, and R. S. Chillingworth, Cities Service  
Co., Box 300, Tulsa, OK 74102; H. Unger, C-E Lummus Co., 755 Jersey Ave.,  
New Brunswick, NJ 08902; E. M. Phillips, Air Products and Chemicals, Inc.,  
Box 538, Allentown, PA 18105

The concept of Two-Stage Liquefaction (TSL) hinges on recognition of the fact that the deashed solid Solvent Refined Coal (SRC), obtained from a first stage coal dissolution, is a high boiling residual type hydrocarbon stream. This material can be efficiently upgraded to liquid fuels by a second stage application of conventional hydrocracking or hydroprocessing technology extensively developed and demonstrated in the petroleum industry over the last twenty years (LC-Fining). That is, by judicious hydrocracking of the SRC product from the first stage, in the presence of a selective catalyst and under optimum conditions of temperature, space velocity, and reactor pressure, the production of middle distillate liquid fuels can be enhanced, the formation of light hydrocarbon gases can be minimized, and the overall utilization of hydrogen is optimized. In addition, the operation of a separate stage of LC-Fining provides wide operating latitude to tailor the overall product slate distribution (i.e., ratio of liquids to solids) and the product quality to both current and future market product requirements.

This study will also present the results of additional PDU runs which will delineate the effects of total reactor pressure and space velocity on the hydrotreating of coal extracts.

## CATALYST ASSESSMENT FOR UPGRADING SHORT CONTACT TIME SRC TO LOW SULFUR BOILER FUELS

S. S. Shih, P. J. Angevine, R. H. Heck and S. Sawruk

Mobil Research and Development Corporation  
Paulsboro, New Jersey 08066

### Introduction

Solvent refined coal (SRC) can be upgraded via catalytic hydroprocessing into low sulfur fuels (1,2). Reduced process cost can be effected by several factors, including the following: higher catalyst activity, improved utilization of hydrogen, and optimized SRC concentration in the feedstock. To this end, a series of commercial and proprietary catalysts was evaluated for the hydroprocessing of 50 wt % W. Kentucky short contact time SRC (SCT SRC). The commercial catalysts tested were alumina-based and were known to have good hydrotreating activity for heavy petroleum or coal-derived liquids. The rates of hydrogenation and pore size distribution will be discussed. A developmental catalyst with relatively high desulfurization and efficient hydrogen utilization was tested in a constant temperature aging run to establish process conditions needed to produce 0.4 wt % sulfur boiler fuels.

### Experimental

The experiments were conducted in a continuous down-flow fixed bed pilot unit. The feedstock, 50 wt % W. Kentucky/SRC recycle solvent blend, was prepared in a charge reservoir and transferred to a weigh cell by gravity flow. Both the charge reservoir and weigh cell were kept at 350°F. After the reactor, hydrogen and light gases were separated from hydrotreated oil through high (300°F) and low (75°F) temperature separators in series. To maintain fluidity of the high SCT SRC concentration blend, all lines and valves from the charge reservoir to the high temperature separator were heat-traced to 340-420°F. The detailed description of the pilot unit is available elsewhere (1). The selection of SCT SRC as the feed was based on a recent finding that the hydrogen utilization efficiency for production of hydrogen-rich coal liquids can be improved by coupling mild short resident time hydroliquefaction (to produce SCT SRC) with catalytic hydroprocessing (3).

The catalysts were presulfided with a 10% H<sub>2</sub>S/H<sub>2</sub> mixture and tested at a reactor pressure of 2000 psig and a hydrogen circulation of 5000 scf/B. Each catalyst was subjected to a standard sequence of temperatures and liquid hourly space velocities, ranging from 720-800°F and 0.5-2.0 hour<sup>-1</sup>, respectively.

### Results and Discussions

Fresh Catalyst Properties - Three Mobil catalysts were tested and have been identified as HCL-1, -2, and -3. Because of the proprietary nature of these catalysts, properties have been excluded. The major properties of the four commercial and two developmental catalysts are shown in Table 1. The four commercial catalysts evaluated were NiMo/Al<sub>2</sub>O<sub>3</sub>: Harshaw's 618X and HT-500, and American Cyanamid's HDN-1197 and HDS-1443. The NiMo catalysts were

tested in a greater number than the CoMo catalysts because it had been thought that improved hydrogenation activity was needed to treat the highly refractory SRC. Also, nickel-promoted hydroprocessing catalysts form less coke than cobalt-promoted catalysts, possibly resulting in better stability. The 618X, HT-500, and HDS-1443 catalysts all have similar metals loading; their major difference is found in surface area, going from relatively low to medium to high, respectively. The shift in surface area can also be seen in the different pore size distributions. Harshaw 618X has a well-defined distribution with 77% of its pore volume in the 100-200Å diameter region. HT-500 has a broader distribution and smaller median size, having half of its pore volume in the 80-100Å region. HDS-1443 has a bimodal distribution: it has most of its pores in 30-80Å, but it also has some 200Å<sup>+</sup> pores. HDN-1197 has a higher metals loading than the other NiMo catalysts and also has most of its pores in the 30-80Å region.

Two developmental catalysts were evaluated in this study. These include Amocat 1A and 1B, recently developed by Amoco for testing in the H-Coal<sup>®</sup> Process (4). Both catalysts were made of the same support and had primarily 100-200Å pores with some macropores (>1000Å). Amocat 1B is an unpromoted Mo/Al<sub>2</sub>O<sub>3</sub> while 1A is CoMo/Al<sub>2</sub>O<sub>3</sub>.

Fresh Activity Comparisons - The nine catalysts have been divided into two groups in order to simplify the activity comparisons. Group A is made up of the more active desulfurization catalysts and includes Mobil HCL-2, Mobil HCL-3, American Cyanamid HDS-1443, and Amocat 1A. Group B includes Mobil HCL-1, Harshaw 618X, American Cyanamid HDN-1197, and Amocat 1B. For the activity comparisons, the heteroatom removals (and CCR reduction) are plotted versus reactor temperature at a liquid hourly space velocity of 1.0. Consequently, catalyst activity can be compared on the basis of temperature requirements for achieving specific liquid product heteroatom (or CCR) contents.

The comparisons of desulfurization activities are shown in Figure 1 and Figure 2 for Group A and Group B catalysts, respectively. At the 80% desulfurization level, Mobil HCL-2 is 10-15°F more active than HDS-1443, followed by HCL-3, Harshaw 618X, and Amocat 1A (Figure 1). Surface area and pore size distribution seem to be important parameters for the fresh catalyst activity. The relatively high fresh activity of HDS-1443 may be partially explained by its high surface area and presence of macropores (Table 1). The presence of macropores may be responsible for the improvement of the relative positions of HDS-1441 and Amocat 1A at more severe conditions (0.5 LHSV).

The importance of pore size distribution also explains the low activity of HT-500, which has 75% of its pore volume in the 100Å region. Cyanamid HDN-1197 seems to have a high desulfurization activity (Figure 2). However, it yields an inhomogeneous product, probably due to its high hydrogenation activity coupled with its small pore size. Inhomogeneous products have also been observed in the upgrading of regular SRC by small pore catalysts (1). The SCT SRC, with its high polar asphaltene content, is particularly susceptible to "front end, back end" incompatibility.

The ranking of deoxygenation activity was very similar to that of the desulfurization activity (Figure 3). The results may suggest that, like desulfurization, the deoxygenation reaction could occur without pre-hydrogenation. The comparison of denitrogenation activities is shown in Figure 4. Mobil HCL-3 was the most active catalyst followed by Mobil HCL-2 and Harshaw 618X.

The CCR reduction activity for the nine catalysts is similarly plotted as a function of temperature in Figure 5 and Figure 6. Mobil HCL-2, HCL-3, and Amocat 1B are the most active catalysts. Generally, heteroatom removal can be achieved with only minor changes in chemical structure. However CCR reduction in SCT SRC occurs with significant alteration of GEC classes, primarily toward the formation of less polar compounds. The classes of W. Kentucky SCT SRC, separated by GEC (gradient elution chromatography), are given in Table 2 and show that 75% of the SRC is polar and non-eluted polar asphaltenes.

Table 2: GEC Analyses of W. Kentucky SCT SRC

Saturates	0.3 wt %
Aromatic Oils	0.4 wt %
Resins/Asphaltenes	24.8 wt %
Polar Asphaltenes	45.1 wt %
Non-Eluted Asphaltenes	29.4 wt %
	100.0

The conversion of polar asphaltenes (lumped with non-eluted asphaltenes) as a function of process severity, expressed by hydrogen content in the liquid product, is shown in Figure 7. Amocat 1B and HDS-1443 show a significantly high conversion of polar asphaltenes at a given process severity. It is worth noting that Amocat 1B and HDS-1442, the Co-Mo version of HDS-1443, have been found to be active catalysts for coal hydroliquefaction (4).

Hydrogen consumption is a major economic factor in any coal liquid hydroprocessing operation. In Figure 8, the total hydrogen consumption is plotted vs. total liquid product (TLP) sulfur content. Three selectivity curves have been drawn from Figure 8: the solid curve represents Harshaw 618X, and the dashed curves are for Amocat 1A and 1B. To a rough approximation HCL-2, HDS-1443, and Amocat 1A are "low" hydrogen consumption catalysts; Harshaw 618X and Mobil HCL-3 are relatively "high" hydrogen consumption catalysts. At the same level of desulfurization Harshaw 618X uses approximately 500 scf/B more than Amocat 1A. However, Amocat 1B, a low desulfurization activity catalyst, shows a very high hydrogen consumption.

Analyses of Used Catalysts - The analyses of five used catalysts tested with 50% W. Kentucky SCT SRC are given in Table 3. The coke and iron depositions appear to be strongly dependent upon catalysts; Harshaw 618X and HDS-1443 are high, but Amocat 1A and 1B are low in coke deposition. Since surface area measurements can include contribution by contaminants (particularly coke), these values have no clearcut meaning. Besides the coke deposition, metal deposition on the catalysts contributes to the catalyst deactivation.

Table 3: Used Catalyst Properties as Received

	Harshaw 618X	Harshaw HT-500	Cyanamid HDS-1443	Amocat 1B	Amocat 1A
Surface Area, M <sup>2</sup> /g	132	147	201	137	125
Pore Volume, cc/g	0.349	0.253	0.568	0.510	0.487
Pore Diameter, Å	106	69	113	149	156
Iron, Wt Pct	0.61	0.30	0.35	0.77	0.61
Coke, Wt Pct	20.6	23.0	18.0	12.8	13.0

The deposition of metal contaminants on a used Harshaw 618X catalyst was analyzed with a scanning electron microscope (SEM). The SEM x-ray emission spectra for fresh and used catalysts at different locations in the catalyst particle are shown in Figure 9. The used catalyst, tested after our standard procedure, showed a large buildup of iron and titanium in a narrow band (<2 microns) of the catalyst exterior. Other contaminants (e.g., K, Ca, Si) were detected at lower concentrations. As shown in Figure 9(b), strong intensities of deposited metals were clearly shown in the x-ray emission spectrum taken near the extrudate external surface. The intensities were substantially reduced in analyses made away from the exterior edge, as shown in Figures 9(c) and 9(d). These results indicate that the hydroprocessing of coal liquids is well suited to ebullated bed reactors; the motion of the fluidized catalysts may provide a continuous, partial regeneration by mildly abrading the metals-rich pellet exterior.

Aging Run - Based on the fresh activity evaluation, Amocat 1A was tested in an aging run for the hydroprocessing of 50% W. Kentucky SCT SRC. The run was made at constant conditions (2000 psig, 775°F, 0.5 LHSV) and was smoothly operated for 15 days. The run was then terminated due to incipient plugging in the reactor. The results are shown in Figure 10, where sulfur content in the liquid products has been plotted vs. days-on-stream. During this first four days the temperature was varied to obtain an activation energy estimation, and these data have been omitted.

A simple deactivation equation was used for a fixed bed reactor:

$$\frac{1}{C_A} - \frac{1}{C_{AO}} = \frac{k_0 e^{-E/RT_e - t/\tau}}{\text{LHSV}}$$

where  $C_{AO}$  and  $C_A$  are the initial and final concentrations of reactant (i.e., heteroatom or CCR). Here,  $k_0$  is the fresh pre-exponential factor, LHSV is liquid hourly space velocity,  $E$  is activation energy,  $T$  is reaction temperature,  $t$  is time on-stream and  $\tau$  is catalyst deactivation time constant. The estimated values for  $\tau$ ,  $k_0$ , and  $E$  are as follows:

	$\frac{k_0}{1}$ Wt %-hr	$\frac{E}{\text{Btu}}$ lb mole	$\frac{\tau}{\text{Days}}$
Sulfur	$1.992 \times 10^{13}$	69,900	18.3
Nitrogen	$3.368 \times 10^5$	34,600	36.1
Oxygen	$6.895 \times 10^9$	57,800	8.9
CCR	$2.553 \times 10^7$	50,400	21.9

The temperature rise necessary to maintain a constant product sulfur concentration is about 2-3°F/day. The measured and model-predicted values for sulfur and CCR are shown in Figure 10.

The simulated operating conditions for the fixed bed reactor to produce a 900°F<sup>+</sup> fuel with a sulfur content of 0.4 wt % are shown in Figure 11, using a charge of 50% W. Kentucky SCT SRC. Figure 11 shows the reactor temperature required to achieve these sulfur levels as a function of days-on-stream and LHSV. The temperature rise is 2.5-3.0°F/day. The cycle length, a function of both LHSV and the limit of reactor temperature, can be determined from Figure 11. For example, at 0.3 LHSV and a maximum reactor temperature of 850°F, the cycle length is 60 days.

### Conclusions

Short contact time SRC can be upgraded via catalytic hydroprocessing into low sulfur boiler fuels. However, the solid SCT SRC feedstock requires solvent dilution to reduce its viscosity. Furthermore, even for a 50 wt % W. Kentucky SCT SRC blend, all pilot unit lines and valves have to be heat-traced above 350°F in order to achieve smooth mechanical operations.

Catalytically, the SCT SRC is more susceptible to form an inhomogeneous product than the regular SRC, particularly where small pore catalysts are used. The upgrading costs can be significantly reduced through increased activity as well as efficient hydrogen utilization. A proprietary catalyst, Mobil HCL-2, and a developmental catalyst, Amocat 1A, were observed to have these two important properties. For hydroprocessing of the 50 wt % W. Kentucky SCT SRC blend, the aging rate was moderate with a 2-3°F/day of temperature rise required to keep constant desulfurization activity. The catalysts are believed to be deactivated by coke and metal depositions on the surface. A large buildup of iron and titanium was found in a narrow band of the catalyst exterior of a spent catalyst. Improved catalyst aging is likely to occur by the use of an ebullated bed reactor, primarily by decreased interparticle coke formation as well as by mild abrasion of metal contaminants.

### Acknowledgement

This work was performed under EPRI/Mobil research project RP 361-2. Dr. W. C. Rovesti is the EPRI project manager.

### Reference

- (1) Stein, T. R., et al, Annual Report, EPRI Contract No. AF-873 (RP 361-2). Mobil Research and Development Corporation, December 1978.
- (2) Givens, E. N., Collura, M. A., Skinner, R. W., and Greskovich, E. J., Hydrocarbon Processing, 195, November 1978.
- (3) Mitchell, T. O., and Heck, R. H., Presented at AIChE 71st Annual Meeting, Miami Beach, Florida, November 13, 1978.
- (4) Bertolacini, R. J., Gutberlet, L. C., Kim, D. K., and Robinson, K. K., Final Report, EPRI Contract No. AF-1084 (Project 408-1), Amoco Oil Company, June 1979.

Table 1

## FRESH CATALYST PROPERTIES

<u>Compositions, Wt %</u>		<u>Harshaw</u>	<u>Harshaw</u>	<u>Cyanamid</u>	<u>Cyanamid</u>	<u>Amoco *</u>	<u>Amoco</u>
		618 X	HT-500	HDN-1197	HDS-1443	1 B	1 A
Ni		2.7	2.4	3.7	2.9	0	
CoO							2.9
MoO <sub>3</sub>		14.8	14.0	21.7	15.5	14.9	19.7
<u>Physical Properties</u>							
Surface Area, m <sup>2</sup> /g		140	193	130	306	167	154
Pore Volume, cc/g		0.60	0.511	0.379	0.764	0.67	0.662
Pore Diameter, Å		172	104	117	100	160	172
<u>Pore Size Dist., cc/g</u>							
0-30 Å		0.025	0.005	0.059	0.165	>	0.065
30-80 Å		0.037	0.125	0.123	0.355	0.027	0.046
80-100 Å		0.036	0.252	0.112	0.020	0.063	0.063
100-200 Å		0.464	0.123	0.035	0.033	0.419	0.385
200 Å +		0.038	0.007	0.050	0.192	0.153	0.103

\* Amoco's Analyses

Figure 1

COMPARISON OF DESULFURIZATION ACTIVITIES: GROUP A CATALYSTS

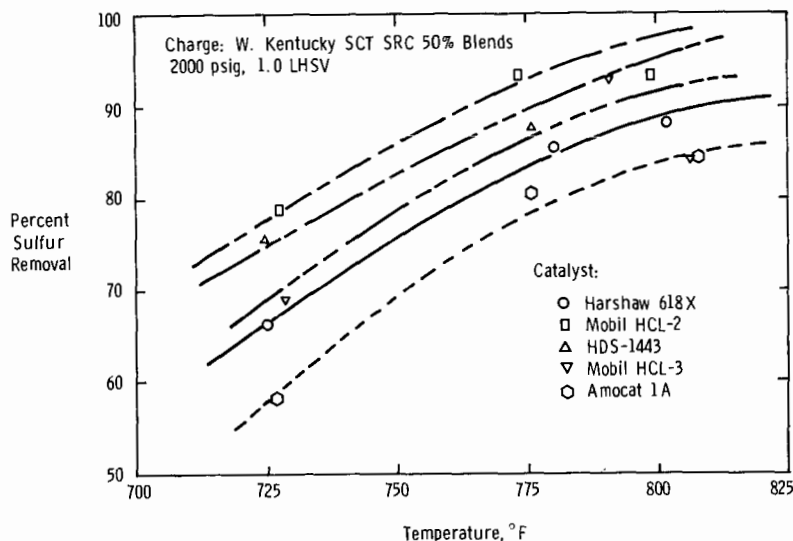


Figure 2

COMPARISON OF DESULFURIZATION ACTIVITIES: GROUP B CATALYST

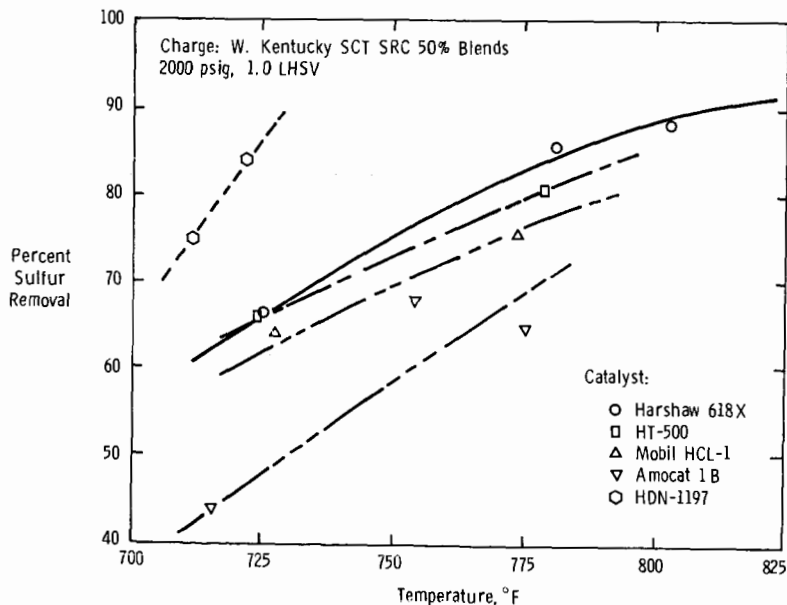


Figure 3

COMPARISON OF DEOXYGENATION ACTIVITIES: GROUP A CATALYSTS

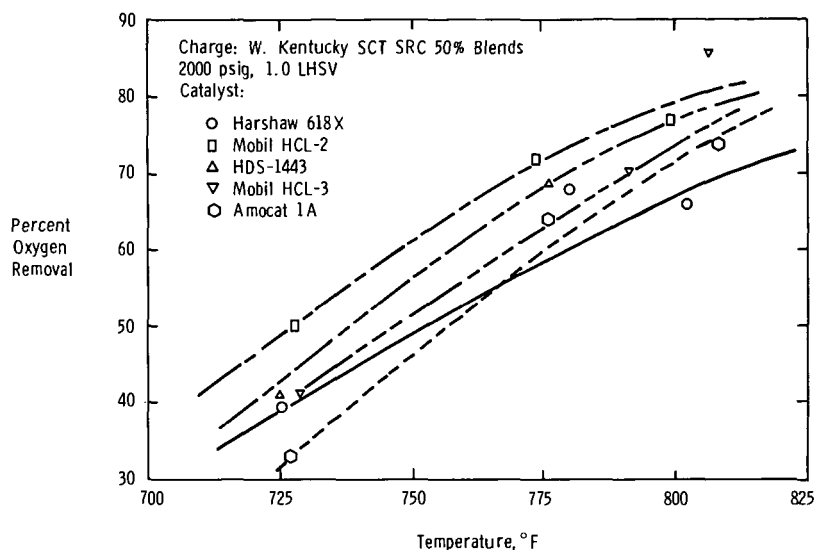


Figure 4

COMPARISON OF DENITROGENATION ACTIVITIES: GROUP A CATALYSTS

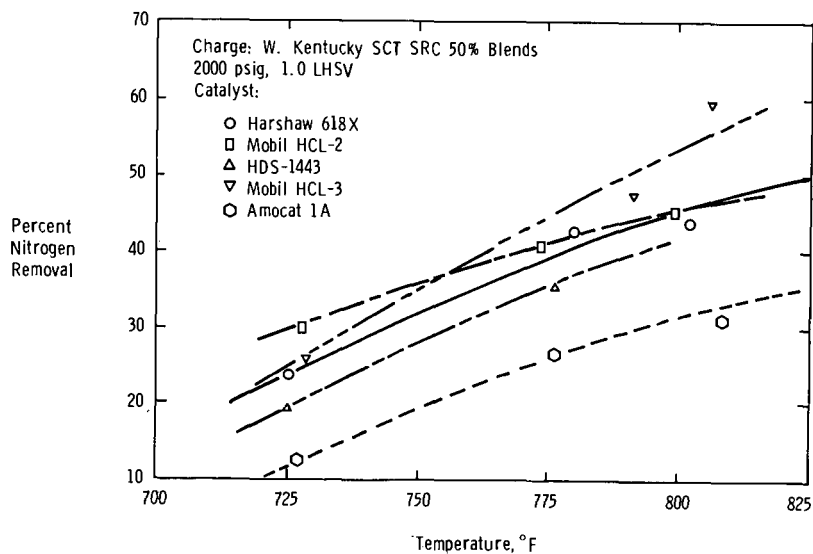


Figure 5

COMPARISON OF CCR REDUCTION ACTIVITIES: GROUP A CATALYSTS

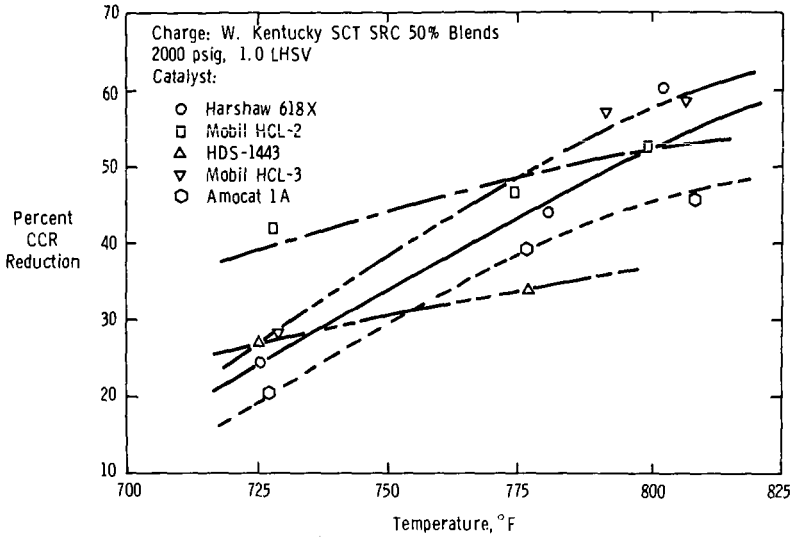


Figure 6

COMPARISON OF CCR REDUCTION ACTIVITIES: GROUP B CATALYSTS

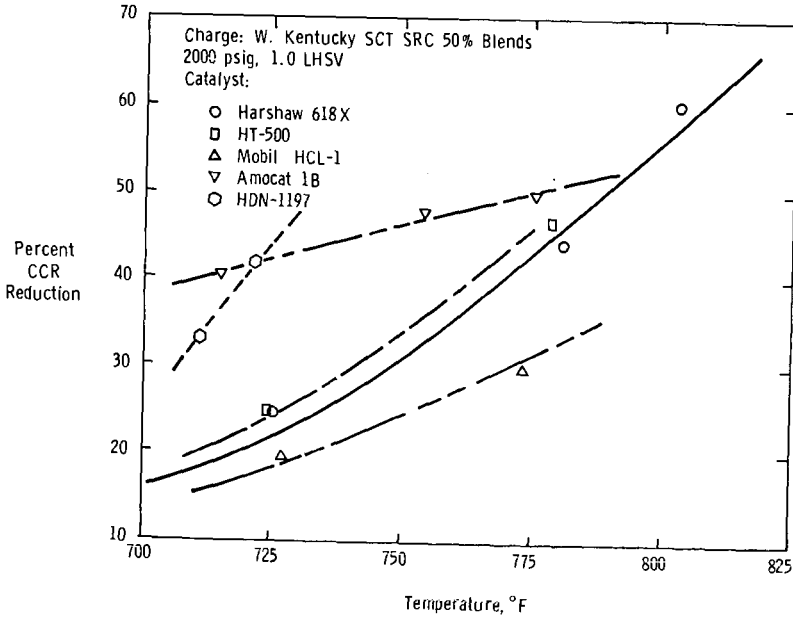


Figure 7

POLAR ASPHALTENES CONVERSION AS A FUNCTION OF HYDROPROCESSING SEVERITY

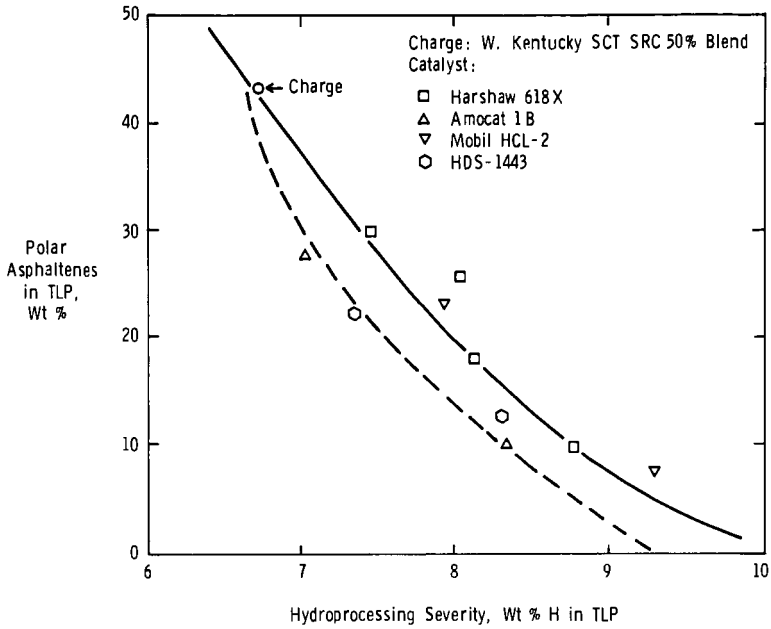
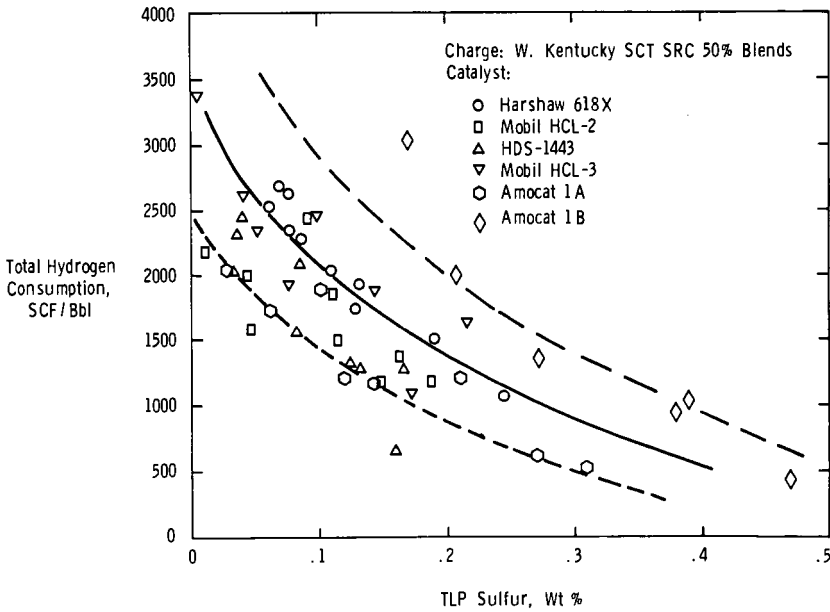
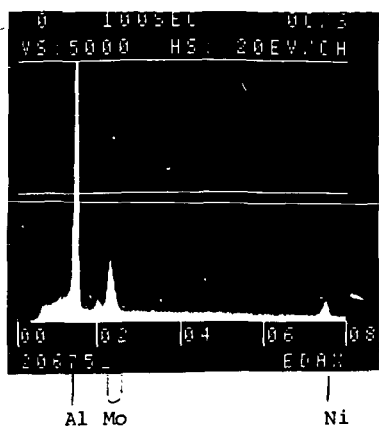


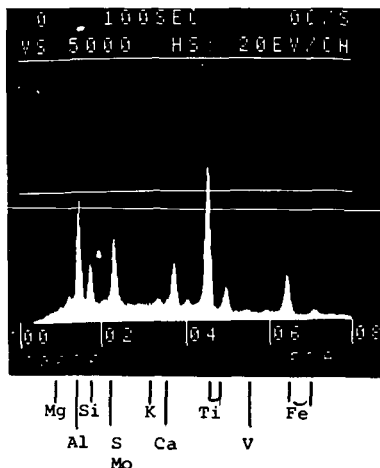
Figure 8

TOTAL HYDROGEN CONSUMPTION AS A FUNCTION OF SULFUR IN LIQUID PRODUCT

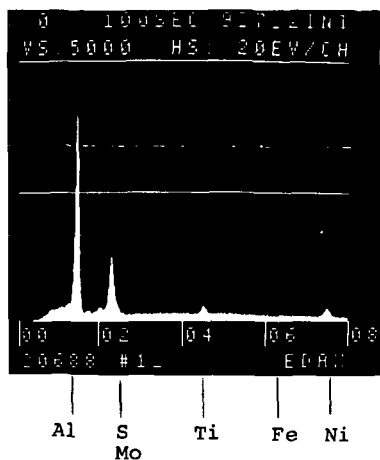




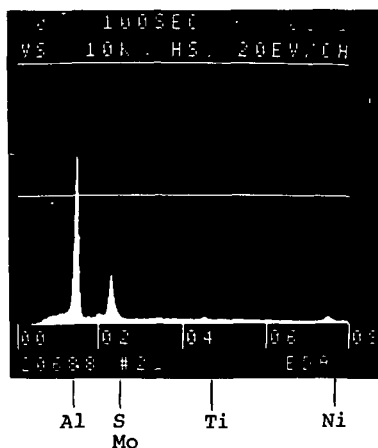
(a)



(b)



(c)



(d)

FIGURE 9: SEM Examination of Fresh and Used Harshaw 618X

- (a) X-ray emission spectrum taken of external surface of fresh catalyst showing presence of Al, Mo and Ni.
- (b) X-ray emission spectrum taken of external surface of used catalyst showing presence of Mg, Al, Mo, K, Ca, Ti, V and Fe.
- (c) X-ray emission spectrum taken at 0-20  $\mu$  from the edge of the cross section of used catalyst showing presence of Al, Mo, Ti, Fe and Ni.
- (d) X-ray emission spectrum taken at 60-80  $\mu$  from the edge of the cross section of used catalyst showing presence of Al, Mo, Ti and Ni.

Figure 10

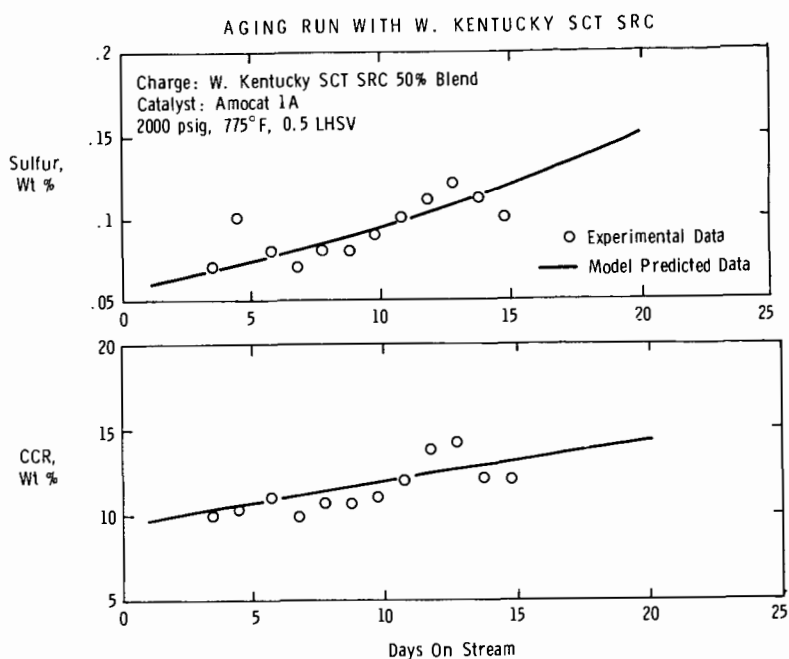
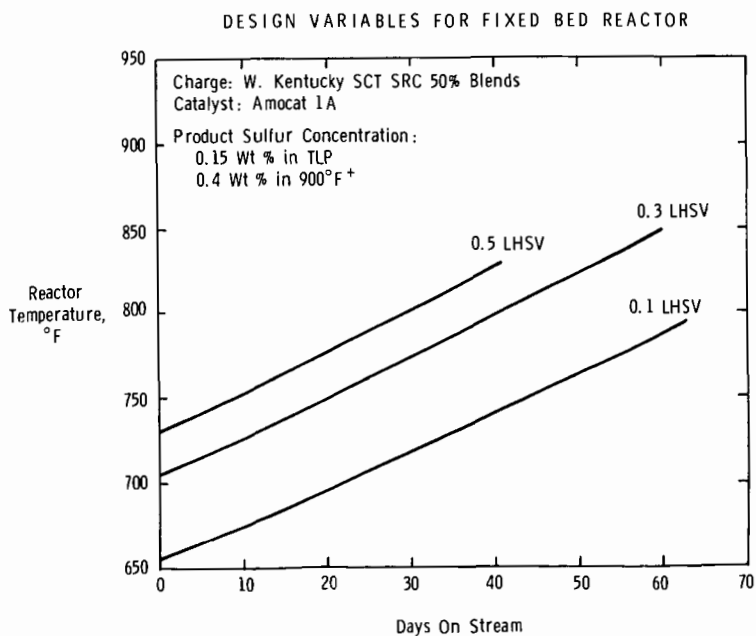


Figure 11



HYDROTREATING OF SRC I PRODUCT - OPTIMIZATION  
OF PROCESS VARIABLE SPACE

D. Garg, A. R. Tarrer,  
J. A. Guin, and J. M. Lee

Chemical Engineering Department  
Auburn University  
Auburn, Alabama 36830

INTRODUCTION

In the Solvent Refined Coal Process, coal is dissolved in a coal-derived solvent to produce a filterable liquid. This is accomplished by means of a mild liquid phase hydrogenation of the coal. The liquid is separated from the insoluble minerals and unreacted organic matter by filtration. The solvent is recovered for recycle by vacuum distillation, and the SRC is obtained as a black shiny solid at room temperature. Some of the sulfur present in the coal is removed in the form of hydrogen sulfide gas.

The present sulfur standards (0.97 percent sulfur in SRC) are being met by conventional SRC processing. New Source Performance Standards (NSPS) recently proposed by the Environmental Protection Agency (EPA) would require a sulfur content of 0.5 to 0.6 percent in SRC for most coals. The proposed NSPS could be met using the conventional SRC process with the application of severe operating conditions (e.g., a reaction temperature of 450°C, a H<sub>2</sub> pressure of 2,000 psig or 13.9 MPa and a long reaction time of 30 to 60 minutes. This would result in an unreasonably high hydrogen consumption and operating cost. Therefore, a modification of the conventional SRC process is necessary to meet the proposed NSPS with minimum hydrogen requirements.

For the coal studied here, a bituminous Western Kentucky #9/14 coal, dissolution of the coal has been shown to occur very rapidly, requiring less than 30 minutes to liquefy most of the coal (~90 percent). However, a relatively long reaction time (120 min.) is required to reduce its sulfur level low enough to meet even the current standards (1). A new short residence time two-stage SRC type process has been suggested by Auburn University (2) for solvent refining this coal. This process has been shown to have the potential of producing a low-sulfur solid SRC product that meets the proposed NSPS. It involves the dissolution of the coal (first stage) in the presence of an inexpensive mineral additive, and then subsequent hydrotreating of the filtered liquid from the first stage in the presence of a presulfided Co-Mo-Al catalyst.

The objective of the present work is to evaluate the effect of a wide range of process or reaction variables--reaction temperature, hydrogen partial pressure, catalyst loading, and reaction time--on hydrodesulfurization and hydrogenation of filtered liquid product (coal-derived liquid) obtained from the coal dissolution stage in the presence of a commercial presulfided Co-Mo-Al catalyst. The selectivity for desulfurization over hydrogenation (Se) is used to rate the effectiveness of the above mentioned process variables. Se is defined as the fraction of sulfur removal per unit (g) of hydrogen consumed, that is,

$$Se = \frac{\frac{S_f - S_o}{S_o}}{H_2 \text{ Used, g}}$$

where Se: Selectivity,

$S_o$ : Original sulfur content of the coal liquids, and

$S_f$ : Sulfur content of the hydrotreated coal liquids.

The purpose of this study is to identify a set of operating conditions for hydrotreating reactions at which maximum selectivity is attained for a specified sulfur content of the solid SRC product.

There are many different types of search routines used to locate optimum operating conditions. One approach is to make a large number of runs at different combinations of temperature, reaction time, hydrogen partial pressure, and catalyst amount, and then run a multivariable computer search routine (like the Hooke-Jeeves method or Powell method). A second approach is to formulate a mathematical model from the experimental results and then use an analytical search method to locate the optimum. The formulation of a mathematical model is not an easy task, and in many cases, this is the most critical step. Sometimes it is impossible to formulate a mathematical model for the system, as in the case of the system studied here, and an experimental search must be performed.

The experimental strategy used here is to perform a series of small experiments instead of a single comprehensive experiment. A univariate search was made in which only one variable was changed at a time. The information obtained in the earlier experiments performed during the univariate search was used to plan subsequent experiments. By doing so, the results were available quickly, and the experimental error was checked and minimized during the course of experimentation.

In the first step of the univariate search a series of experiments were performed in which base values were used for the initial hydrogen partial pressure, reaction time and reaction temperature, and only the amount of catalyst used was varied. The amount of catalyst which yielded the best performance (i.e. maximum selectivity) and best satisfied practical constraints was selected. In the next step a series of experiments was performed in which the selected amount of catalyst was used, base values were used for temperature and time, and only the initial hydrogen partial pressure was varied. An initial hydrogen partial pressure was selected as was done for the amount of catalyst in the first step.

The dependence of selectivity (Se) on the reaction time and temperature was modeled using empirical expressions for desulfurization and hydrogen consumption kinetics. The same values selected for initial hydrogen partial pressure and amount of catalyst in the first two steps of the univariate search were used in determining these kinetic expressions. The final step of the search procedure was to perform a series of experiments mapping the region close to the above determined optimum conditions for verification.

## EXPERIMENTAL

### Reagents and Materials

Light recycle oil (LRO) and Western Kentucky #9/14 coal were obtained from the Wilsonville SRC Pilot Plant, operated by Southern Company Services, Inc. The

LRO contains 0.26% sulfur, and the Western Kentucky #9/14 coal is analyzed to be 67% C, 4.9% H, 3.10% S, and 12 % mineral matter. The coal was dried overnight at 100°C and 25 inches Hg vacuum before use.

The coal liquid is obtained by reacting Ky #9/14 coal-LRO slurry for 60 minutes at 410°C in an autoclave reactor under 2000 psig (13.9 MPa) hydrogen pressure. The product from the autoclave is collected and filtered using Watman #51 filter paper to remove the mineral matter and undissolved coal. The liquid product is saved and used for further hydrotreating studies. The analysis of the filtered product from the coal dissolution step is given in Table I.

Co-Mo-Al is a commercial catalyst from Laporte Industries, Inc. (Comox 451). The catalyst was ground and screened to -325 mesh before use. Presulfided Co-Mo-Al was prepared by collecting the solid residue after reaction of creosote oil (S = 0.64 percent) with Co-Mo-Al in the autoclave reactor. The sulfur content of the pre-sulfided Co-Mo-Al was 2.76%.

Hydrogen gas cylinders (6000 psi grade) were supplied by Linde.

#### Equipment

A commercial 300 ml magnedrive autoclave (Autoclave Engineers) reactor was used for all reaction studies and has been previously described (3-6). Varian gas chromatographs (Model 920 and 1800) were used for analysis of gas samples and products from the hydrotreating reactions. A LECO sulfur determinator (Model 532) was used for analysis of sulfur in the products.

#### Procedure

One hundred grams of coal liquid was combined with a predetermined amount of presulfided Co-Mo-Al catalyst and charged to the autoclave. Reaction temperature for the runs varied from 360 to 435°C, depending on the run. A stirring setting of 1000 rpm was used, and the initial total pressure was varied from 1500 (10.4 MPa) to 2500 (17.3 MPa) psig. The heat-up rate was about 12 to 20°C/min, thus requiring a total heat-up time of about 20-25 min. After a specified reaction time, a gas sample was taken; the autoclave was cooled to below 100°C, and the reaction products were collected. The filtered liquid product was vacuum distilled under <1.0 mm Hg pressure to recover the process solvent added prior to the reaction. The 270°C + fraction obtained by vacuum distillation was defined as the solvent refined coal (SRC). A sulfur analysis was performed on each fraction.

The conversion of SRC to oil and gases is defined as

$$\text{SRC Conversion, \%} = \frac{(\text{Amount of SRC})_{\text{original liquid}} - (\text{Amount of SRC})_{\text{hydrotreated liquid}}}{(\text{Amount of SRC})_{\text{original liquid}}}$$

and is used as a constraint.

## RESULTS AND DISCUSSION

### Effect of Catalyst Loading

The effect of the amount of Co-Mo-Al catalyst present in the hydrotreating reaction is tabulated in Table II. It was observed that increasing the amount of Co-Mo-Al from 1 g to 15 g increases the sulfur removal by 52 percent, increases hydrogen consumption by 87 percent, and increases SRC conversion from 16 to 24 percent. Figure 1 shows the variation of selectivity versus the amount of catalyst used while keeping the other reaction variables constant. It can be seen that the maximum selectivity resulted when

10 g of Co-Mo-Al was used. However, the variation in selectivity for the different amounts of catalyst used was insignificant, that is, within the range of experimental error (standard deviation is only 3 percent). The change in SRC conversion to oil and gases, as shown in Table II, was also within the range of experimental error (standard deviation is less than 8 percent). The use of 1 g of Co-Mo-Al gave the lowest amount of SRC conversion (~16 percent). From the shape of the selectivity versus amount of Co-Mo-Al catalyst used curve (Figure 1), it appears that hydrodesulfurization is favored over hydrogenation in the range in which 1 g to 10 g of catalyst were used. However, increasing the Co-Mo-Al amount beyond 10 g tends to favor hydrogenation and a decrease in selectivity was observed. Thus 10 g of Co-Mo-Al was used throughout the remainder of the study. A search in the vicinity close to where maximum selectivity occurs (10 g of Co-Mo-Al) was not done because the insensitivity of selectivity and SRC conversion to the amount of catalyst used.

#### Effect of Pressure

Table III shows the effect of the initial hydrogen partial pressure on selectivity, sulfur removal, hydrogen consumption, and SRC conversion. It was observed that increasing the initial hydrogen partial pressure by 1500 psig (10.4 MPa) decreased the selectivity by 72 percent, increased hydrogen consumption by a factor of 2.6, enhanced sulfur removal by a factor of 1.9, and did not affect SRC conversion appreciably. For initial hydrogen pressures of 1500, 2000, and 2500 psig, the variation of selectivity was within the range of experimental error. Use of a 1000 psig hydrogen pressure gave the maximum selectivity. However, at 1000 psig the sulfur requirements set by the proposed NSPS (0.5 to 0.6 percent SRC sulfur) were not met (SRC sulfur content at 1000 psig is 0.66%). The use of a 2000 psig hydrogen partial pressure gave a slightly higher selectivity than was obtained with either 1500 or 2500 psig, and a sufficient amount of sulfur was removed. Therefore, a hydrogen pressure of 2000 psig was chosen for further studies.

#### Effect of Reaction Time and Temperature

The amount of catalyst (10 g of Co-Mo-Al in 100 g of coal liquids) and the initial hydrogen partial pressure (2000 psig) determined above were used to study the effect of reaction time and temperature. Hydrodesulfurization and hydrogen consumption kinetics were determined, as outlined in the following paragraphs.

In order to determine the rate equation for hydrodesulfurization, a semi-logarithmic plot of the total sulfur content with time was made (Figure 2). The plot indicated two independent first-order reactions with greatly different rate constants. This is in agreement with the findings of Gates et al. (7) and Pitts (3). A procedure similar to that of Pitts (3) was used to describe the hydrodesulfurization kinetics. The rate expression is given below

$$S_{\text{Total}} = S_{10} \exp [-K_{10} \exp (-\Delta E_1/RT) t] + S_{20} \exp [-K_{20} \exp (-\Delta E_2/RT) t]$$

The empirical parameters  $S_{10}$ ,  $S_{20}$ ,  $K_{10}$ ,  $K_{20}$ ,  $\Delta E_1$ , and  $\Delta E_2$  were determined by a numerical search routine. Figure 3 compares the theoretical curves with the experimental data and represents a satisfactory curve fit.

The amount of hydrogen gas present in the reactor was plotted against reaction time on a semi-logarithmic scale (Figure 4). This plot gave a straight line indicating a first-order rate expression. Pitts (3) also suggested a first-order rate expression

for hydrogen consumption. A procedure similar to that of Pitts (3) was used. The hydrogen consumption rate expression is given by

$$\frac{H_g}{H_{go}} = \text{EXP} [-K_o \text{EXP} (-\Delta E/RT)t]$$

A numerical search routine was applied to determine the value of  $K_o$  and  $\Delta E$ . Figure 4 compares the theoretical curve with the experimental data and represents a satisfactory curve fit. The total sulfur content and SRC sulfur content for hydro-treated product were plotted (Figure 5), and a linear relationship was shown to exist between them.

The rate expression for hydrodesulfurization and hydrogenation described above were used to compute selectivity. The optimum process conditions for different SRC sulfur contents (specifically, 0.6, 0.5, and 0.4 percent) were determined. The optimization procedure used is illustrated below for a specified SRC content of 0.5% or a total sulfur content of 0.23 % (see Figure 5).

The variation of the calculated total sulfur values versus reaction time and reaction temperature was plotted (Figure 6). A dashed line was drawn at a total sulfur level of 0.23 percent; the region above this line was labelled as being infeasible because, for a total sulfur content higher than 0.23 percent, the SRC content was more than 0.5 percent. So, the feasible region of search was that below the dashed line. The computed values of selectivity versus reaction time and temperature was plotted (Figure 7).

The maximum selectivity for each temperature was found to be located on the dashed curve shown in Figure 7, that is, at the boundary. The maximum selectivity values for each temperature were compared (Table IV). The highest temperature and the shortest reaction time used gave the maximum selectivity. The conversion of SRC to oil with reaction time and temperature were plotted also for comparison purposes (Figure 8). As shown in Table IV, the highest temperature and the shortest reaction time resulted in the lowest amount of conversion of SRC to oil. Similar analyses were performed for different SRC sulfur contents, and for each case, the highest temperature and the shortest reaction time gave the maximum selectivity and the lowest SRC conversion. A summary of the optimum reaction conditions obtained for different sulfur levels is given in Table V.

The optimization study discussed above suggests the use of a high temperature and a short-reaction time. Because of the heat-up and cool-down time limitations of the autoclaves used, this study was limited to reaction temperatures  $\leq 435^\circ\text{C}$ . Verification studies at higher temperatures ( $>435^\circ\text{C}$ ) are ongoing using micro-reactors. The present study should be supported by complementary catalyst aging studies to determine the maximum temperature limit below which serve deactivation and aging does not occur.

#### CONCLUSIONS

The proposed NSPS can be met by hydrotreating the coal liquids obtained by filtering the product from the coal dissolution stage. The desulfurization kinetics can be presented by two parallel first-order rate expression, and hydrogen consumption kinetics can be presented by a first-order rate expression. A linear relationship exists between total sulfur content and SRC sulfur content of the hydrotreated product. For

the Western Kentucky bituminous #9/14 coal studied here, the maximum selectivity and lowest SRC conversion to oil for a fixed SRC sulfur content are obtained using the highest reaction temperature (435°C) and the shortest reaction time (~ 7 min.).

#### ACKNOWLEDGEMENTS

This work was supported by the Department of Energy. The authors wish to acknowledge the technical assistance of Don Colgrove and David Watson of the Auburn University Chemical Engineering Department.

#### REFERENCES

1. Garg, D., Ph.D. Dissertation, Auburn University, Auburn, Alabama (1979).
2. Garg, D., Tarrer, A. R., Guin, J. A., Lee, J. M., and Curtis, C., Fuel Processing Technology, 2, 189-208 (1979).
3. Pitts, W. S., M.S. Thesis, Auburn University, Auburn, Alabama (1976).
4. Guin, J. A., Tarrer, A. R., Prather, J. W., Johnson, J. R., and Lee, J. M., Ind. Eng. Chem. Process Des. Dev. 17(2), 118 (1978).
5. Lee, J. M., Van Brackle, H. F., Lo, Y. L., and Tarrer, A. R., Am. Chem. Soc. Div. Fuel Chem., prepr., 22(6), 120 (1977).
6. Lee, J. M., Van Brackle, H. F., Lo, Y. L., Tarrer, A. R., and Guin, J. A., Symposium of the 84th National ALChE Meeting, Atlanta, GA, Feb. 26 - March 1, 1978 (516).
7. Gates, B. C., J. R. Katzer, J. H. Olson, H. Kwart, and A. B. Stiles, Quarterly Progress Report, Prepared for U.S. Dept. of Energy, No. EX-76-C-01-2028, (December 2, 1976 - March 20, 1977).

Table I. Analysis of the Liquid Product Used in Hydrotreating Stage

Distillation Product Distribution, %	
Distillate (Oil)	
SRC	61.6
	38.4
Sulfur Distribution, %	
Distillate (Oil)	0.21
SRC	0.97
	0.54
TOTAL LIQUID	0.24
Tetralin/Naphthalene Ratio	
Distillation is performed under <1 mm Hg pressure	
Distillate: 270°C - fraction of vacuum distillation	
SRC: 270°C + fraction of vacuum distillation	

Table II. Effect of Catalyst Amount on Hydrotreating of Kentucky #9/14 Coal Liquid  
Coal Liquid = 100 g, Time = 30 min., T = 410°C, P = 2000 psi (13.9 MPa)H<sub>2</sub>, 1000 RPM, Reactor - Autoclave

Amount of Catalyst	1.0	5.0	10.0	15.0
H <sub>2</sub> Used, g	0.11	0.17	0.18	0.21
Total Sulfur S <sub>f</sub> , %	0.36	0.22	0.20	0.17
So - Sf				
Se = $\frac{So}{So - Sf}$	2.8	3.3	3.4	3.2
H <sub>2</sub> Used, g				
SRC Conversion, %	16	21	22	24
So = 0.54%				

Table III. Effect of Hydrogen Partial Pressure on Hydrotreating of Kentucky #9/14 Coal Liquid  
Coal Liquid = 100 g, Co-Mo-Al = 10 g, T = 410°C, 1000 RPM, Reaction Time = 30 min., Reactor - Autoclave

Pressure, Psig H <sub>2</sub>	1000	1500	2000	2500
H <sub>2</sub> Used, g	0.08	0.13	0.18	0.22
Total Sulfur S <sub>f</sub> , %	0.35	0.30	0.20	0.19
SRC Sulfur, %	0.66	0.57	0.49	0.45
So - Sf				
Se = $\frac{So}{So - Sf}$	4.1	3.3	3.4	2.9
H <sub>2</sub> Used, g				
SRC Conversion, %	22	19	22	21

Table IV. Maximum Selectivity at Different Reaction Conditions Meeting 0.5% SRC Sulfur Content

Temp., °C	Time, Min.	Se	Standard Deviation in Se, %	SCR Conversion, % (Estimated from Fig. 8)
370	114	2.50	6.3	>20.0
385	62	2.80	7.5	>20.0
400	38	3.20	7.2	---
410	27	3.5	7.2	20.5
420	20	3.70	7.0	--
435	13	3.85	7.3	19.5

Table V. Summary of Operating Conditions for Various Maximum SRC Sulfur Contents

SRC Sulfur, %	Total Sulfur, %	Temperature, °C	Time, Min.	Se
0.6	0.29	435	7	5.40
0.5	0.23	435	13	3.85
0.4	0.17	435	21	2.80

Figure 1. Effect of Amount of Catalyst (Co-Mo-Al) on Selectivity

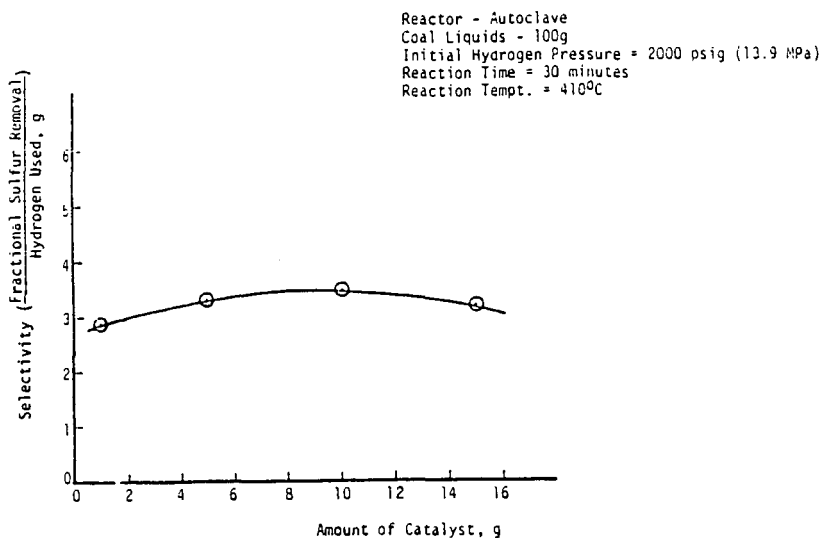


Figure 2. Semi-Log Plot of Total Sulfur (%) vs. Time for Hydrotreating Reaction in The Presence of Co-Mo-Al

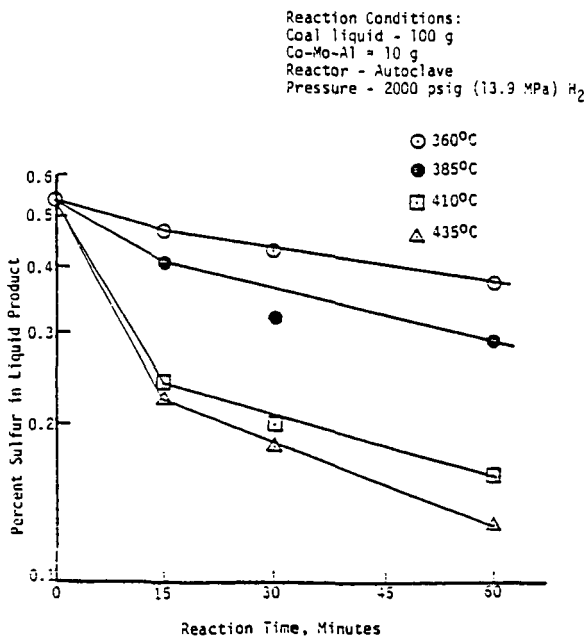


Figure 3. Effect of Hydrotreating Reaction Time on Total Sulfur Content

Reaction Conditions: See Figure 2

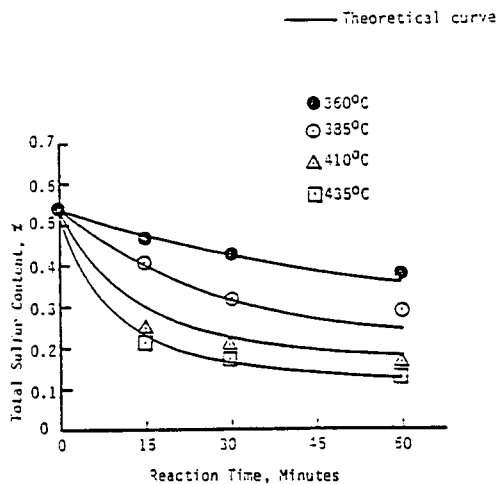


Figure 4. Semi-Log Plot of  $H_g/H_{g0}$  vs. Time for Hydrotreating Reaction in the Presence of Co-Mo-Al

Reaction Conditions: See Figure 2  
 $H_g$  = amount of hydrogen (g) in the reactor at any time  
 $H_{g0}$  = amount of hydrogen (g) initially charged to the reactor

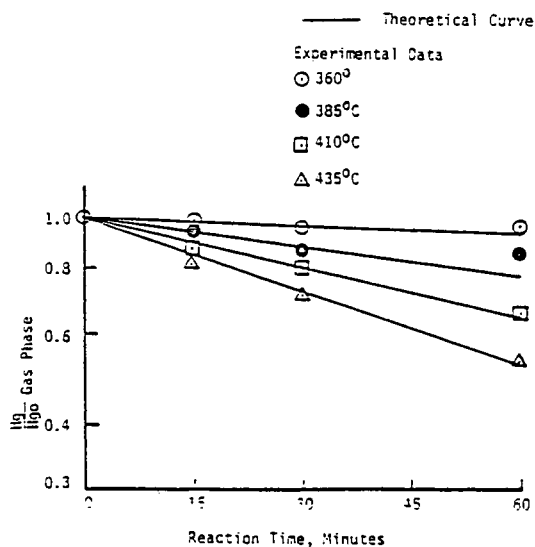


Figure 5. Relationship Between Hydrotreated Total Sulfur Content (%) and SRC Content (%)

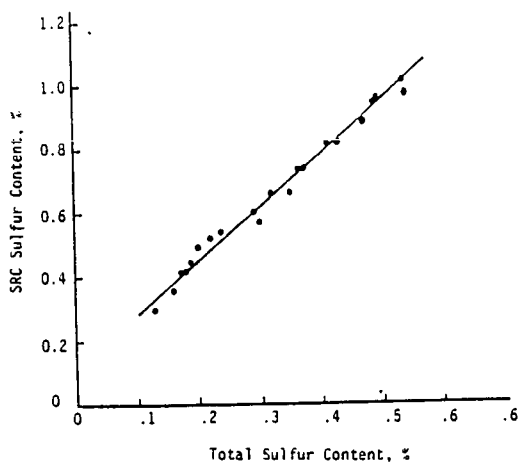


Figure 6. Variation of Total Sulfur Content with Reaction Time and Temperature for Hydrotreating Reaction

SRC Sulfur = 0.50%  
Total Liquid Sulfur = 0.23%

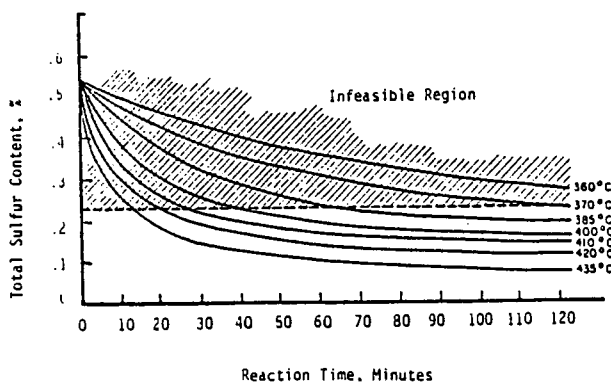


Figure 7. Variation of Selectivity with Reaction Time and Temperature for Hydrotreating Reaction

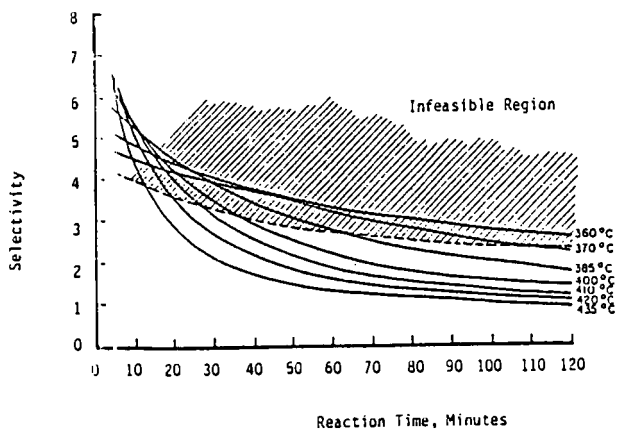
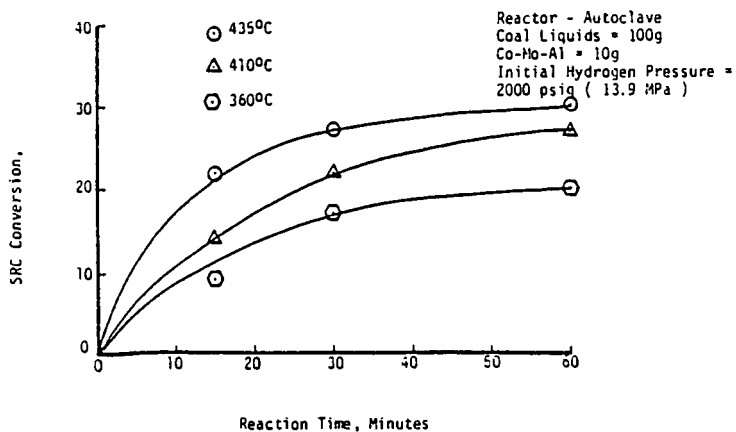


Figure 8. Conversion of SRC with Hydrotreating Reaction Time and Temperature



A COMPARISON OF THE HYDRODESULFURIZATION AND HYDRODENITROGENATION ACTIVITIES  
OF MONOLITH ALUMINA IMPREGNATED WITH Co AND Mo AND NALCOMO 474 CATALYSTS

Dalip S. Soni  
International Research and Technology Corporation  
7655 Old Springhouse Road  
McLean, Virginia 22102

Billy L. Crynes  
Oklahoma State University  
Stillwater, Oklahoma 74074

INTRODUCTION

In the wake of precarious supplies of petroleum, the need to turn to the abundant reserves of coal as an energy base can hardly be overemphasized. However, to accomplish the objective of using coal extensively, much research effort in the field of converting coal to environmentally clean and convenient fuel is required. The work presented here is so directed and is a part of the research program, at Oklahoma State University, which has the goal of tailoring catalysts for upgrading of liquids derived from coal.

In this study, a novel Monolith alumina structure was of interest as a base (or a carrier) material for Co-Mo-Alumina catalysts. The specific interest centered around assessing the suitability of the catalyst prepared by impregnating the novel alumina support with Co and Mo for hydrodesulfurization (HDS) and hydrodenitrogenation (HDN) of a relatively high boiling stock. The Monolith catalyst was also tested on a low boiling coal-derived liquid.

OBJECTIVE

The objective of this work was to study the activity of the Monolith catalyst for removing sulfur and nitrogen from a Synthoil process liquid (heavy stock) and Raw Anthracene Oil (light feedstock), and to make a preliminary assessment of the advantages and/or disadvantages of the Monolith catalyst over a commercial catalyst used in the petroleum industry.

MATERIALS

Feedstocks:

As mentioned before, two coal-derived liquids were used. One was Raw Anthracene Oil obtained from Reilly Tar and Chemical Corporation. The other was a Synthoil liquid obtained from Pittsburgh Energy Research Center. The properties of these two liquids are given in Tables I and II. As is clear from the boiling point ranges of the two liquids, Synthoil is very high boiling as compared to the Raw Anthracene Oil.

Catalysts:

The properties of the two catalysts used in this study are given in Tables III and IV. The Monolith catalyst was prepared in the laboratory at OSU by impregnating Co and Mo on the Monolith alumina support received from the Corning Glass Company. The Nalco 474 catalyst was received from the Nalco Chemical Company. It is a commercial preparation and was used as a reference catalyst in this study.

Figure 1 shows the pore size distribution of the two catalysts as determined from the mercury porosimeter data. The most frequent pore radius of the Monolith catalyst is 80 $\text{\AA}$  as compared to 33 $\text{\AA}$  of the Nalco 474 catalyst. On the other hand, the surface area of the Monolith catalyst is 92.0 m<sup>2</sup>/gm. as compared to 240 m<sup>2</sup>/gm. of the Nalco 474 catalyst. The chemical compositions of the two catalysts also differ widely as shown in Tables III and IV.

TABLE I  
PROPERTIES OF THE RAW ANTHRACENE OIL

	<u>Wt. %</u>	
Carbon	90.3	
Hydrogen	5.57	
Sulfur	0.47	
Nitrogen	1.035	
Oxygen	2.625	
Ash	Nil	
API Gravity	-7	

<u>Boiling Range</u>		
<u>Volume Distilled, Percent</u>	<u>Vapor Temperature, C(F), at 50 mm Hg.</u>	<u>Vapor Temperature, C(F), at 760 mm Hg.</u>
10	138.9 (282)	229.4 (445)
20	169.4 (337)	263.9 (507)
30	186 (367)	283.3 (542)
40	202.7 (397)	302.2 (576)
50	215 (419)	315.5 (600)
60	227.2 (441)	331.1 (628)
70	240.5 (465)	345 (653)
80	256 (493)	362.7 (685)
90	278.9 (534)	387.8 (730)

TABLE II  
PROPERTIES OF THE SYNTHOIL LIQUID

	<u>Wt. %</u>	
Carbon	80.5	
Hydrogen	7.72	
Sulfur	1.02	
Nitrogen	1.19	
Ash	3.4	
Specific Gravity	1.12	

<u>Boiling Range</u>		
<u>Volume Percent Distilled</u>	<u>Vapor Temperature, C(F), at 50 mm Hg.</u>	<u>Weight Percent S.</u>
10	170.5 (339)	0.2
20	211.6 (413)	0.242
30	260 (500)	0.332
33	276.6 (530)	0.366
Bottoms		1.7

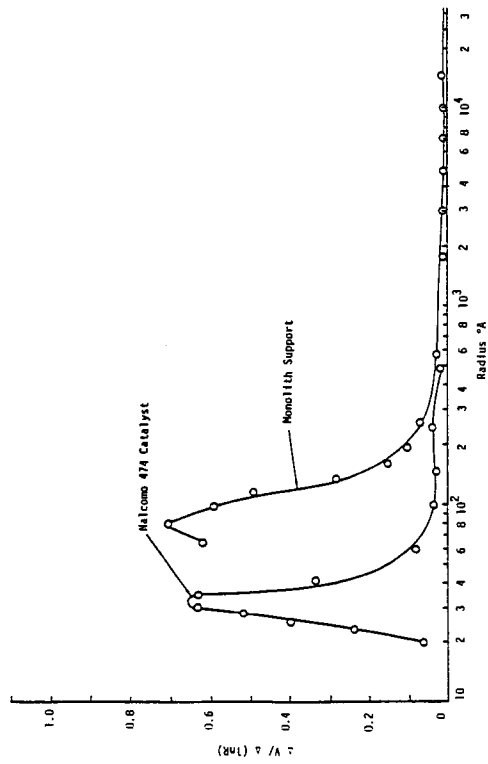
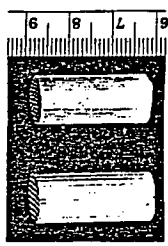
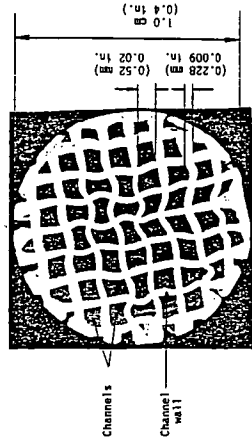


Figure 1: Pure Size Distribution of the Catalysts



Monolith Alumina Segments



Cross Section of a Monolith Alumina Segment

Figure 2: Monolith Alumina Structure

TABLE III  
PROPERTIES OF THE MONOLITH CATALYST

	Wt. %
CoO	3.37
MoO <sub>3</sub>	7.25
Support	Alumina
Surface Area, m <sup>2</sup> /gm.	92.0
Pore Volume, cm <sup>3</sup> /gm.	0.55
Most Frequent Pore Radius, °A	80.0

TABLE IV  
PROPERTIES OF THE NALCOMO 474 CATALYST

	Wt. %
Alumina	82.39
MoO <sub>3</sub>	12.5
CoO	3.5
Na <sub>2</sub> O	0.08
Fe	0.03
SiO <sub>2</sub>	1.5
Surface Area, m <sup>2</sup> /gm.	240.0
Pore Volume, cm <sup>3</sup> /gm.	0.46
Most Frequent Pore Radius, °A	33.0

Figure 2 shows the shape and size of the Monolith alumina supports. These are in the form of cylindrical segments of about 2.54 cm. (1 in.) in length and about 1.0 cm. (0.4 in.) in diameter. These have longitudinal and parallel channels along their length. The size, shape and thickness of the walls of the channels are also shown in Figure 2.

The Monolith structure has about 60 to 80 percent of its cross-sectional area open. Therefore, a bed of regularly stacked Monoliths would offer significantly less pressure drop than that encountered in conventional packed beds. This has been observed by Satterfield and Ozel (1) for water-air systems. Some of the other important advantages listed by them are:

- (1) Where intraparticle diffusion appreciably affects the rate of the reaction, reduction in catalyst particle size would be necessary to increase the effectiveness factor and hence conversion. But this may not be possible due to the pressure drop limitations in conventional packed beds. In such situations, the use of Monoliths would provide the advantage of higher effectiveness factor.
- (2) When processing coal derived liquids which contain fine solid particles, the possibility of bed plugging may be minimized.
- (3) The flow of the liquid through regular channels would provide better gas-liquid contact, liquid distribution and wetting of the catalyst.

- (4) The compressive strength of Monoliths would be much higher than the catalyst particles generally used in packed beds. Therefore, the use of Monoliths would enable deep beds to be constructed without using intermediate supports and gas-liquid distributors.

All of the above advantages stem from the special geometry of the Monoliths as compared to that of the usual catalyst particles.

#### EXPERIMENTAL SETUP AND PROCEDURE

##### Reactor System:

A trickle bed reactor system was employed in this study. A schematic diagram of the experimental system is shown in Figure 3. The reactor was a 12.7 mm (0.5 in.) O.D. stainless steel tube packed with the catalyst. The catalyst bed height was 35.5 cms. (14 in.). When using Monolith catalyst, redistributors were put at intervals of 10.15 cms. (4 in.) each to ensure that the liquid passes through the channels. Figure 4 shows cross-section of the reactor packed with the Monolith and Nalcomo 474 catalysts. The latter catalyst was used in the form of 8-10 mesh (2 mm.) size particles.

The reactor was heated with the help of massive aluminum blocks placed around the reactor. The reactor temperature was measured at every inch of the catalyst height by traversing a thermocouple in a thermowell placed along the reactor bed. The reactor was operated at nearly isothermal conditions.

##### Method of Operation:

After loading the reactor with the catalyst and installing it in the experimental setup, the catalyst was activated. This was done by first calcining the catalyst at 232.2 C (450 F) and then sulfiding it with a mixture of 5.14 volume percent  $H_2S$  in  $H_2$ . The reactor was then brought to the operating conditions and the flow of hydrogen and oil started. After about 32 hours of reactor-in-oil operation, representative product oil samples were taken at specified reactor conditions. The line out time of 32 hours was allowed to stabilize the activity of the catalyst. The product oil samples were analyzed for their sulfur and nitrogen contents with the help of a Leco Model 634-700 automatic sulfur analyzer and Perkin Elmes Model 240 elemental analyzer, respectively.

#### RESULTS

Figure 5 and 6 show the results of this study along with the results of Sooter (2) and Satchell (3) who conducted similar studies using the same experimental setup but with Nalcomo 474 catalyst and Raw Anthracene Oil. The graphs presented here are either weight percent sulfur or nitrogen in the product oil from the reactor vs. the volume hourly space time. Low sulfur or nitrogen in the product oil would correspond to higher activity of the catalyst under consideration.

The results with each feedstock and catalyst were obtained over a single reactor run lasting 105-132 hours. In each reactor experimental run, the start up reactor conditions were repeated at the end to check for loss, if any, of the catalyst activity. No significant decrease in catalyst activity was observed over the conditions studied.

The overall reproducibility of each reactor experimental run was checked by comparing the mode of response of desulfurization and denitrogenation to changes in space time as observed from the two reactor runs on the same feedstock. Figures 5 and 6 show that reactor runs were reproducible.

An estimate of the precision of sulfur and nitrogen analyses was made by analyzing Raw Anthracene Oil and Synthoil liquid a number of times. The results of sulfur

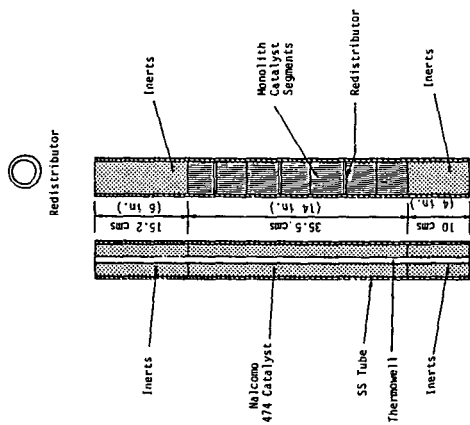


Figure 4: Cross Sections of the Reactors Packed with Nalco 474 and Monolith Catalysts

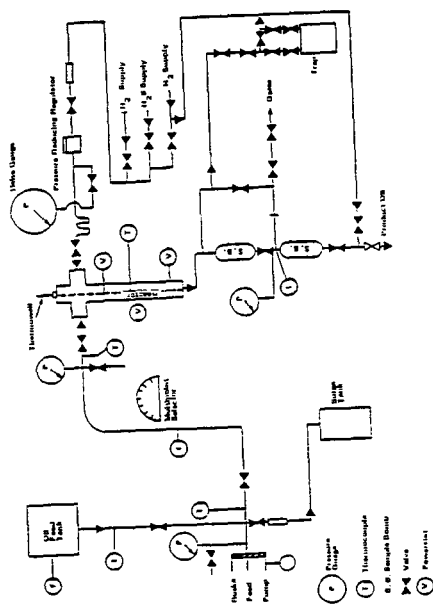


Figure 3: Reactor System

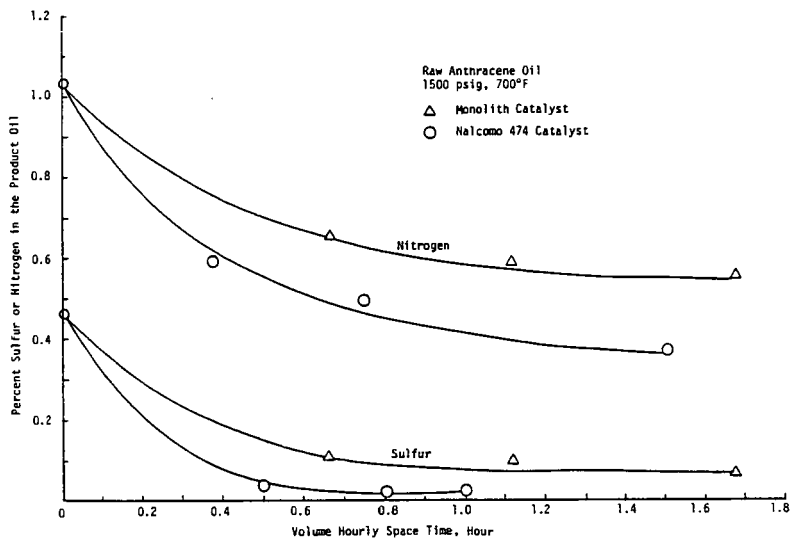


Figure 5: HDS and HDN Responses to the Changes in the Volume Hourly Space Time

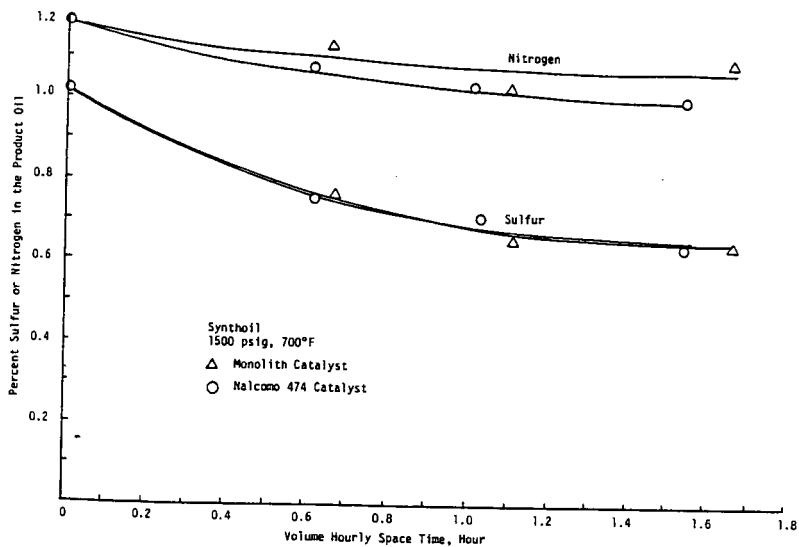


Figure 6: HDS and HDN Responses to the Change in the Volume Hourly Space Time

analysis of Raw Anthracene Oil were found to be precise within 0.25%. But precision of other results was within 5.0%.

#### DISCUSSION

Figure 5 indicates that on volume basis, the activity of the Monolith catalyst is less than the activity of Nalcomo 474 catalyst when Raw Anthracene Oil was the feedstock. Similar behavior was observed when comparison was made on weight basis. Figure 6 shows that when tested on Synthoil, the HDS activity of the two catalysts were almost the same on volume basis. However, when comparison was made on the weight basis, Monolith catalyst was observed to remove more sulfur per unit weight of the catalyst.

Since the surface areas of the two catalysts differed widely, comparison of activities of the two catalysts on unit surface area basis was studied. Figures 7 and 8 represent such a comparison. The abscissa of these graphs is  $S/Q$ , where  $S$  is the total surface area of the catalyst in the reactor and  $Q$  is the volumetric flow rate of oil.  $S/Q$  or  $S/W$  are quite akin to volume hourly or weight hourly space times. Figure 7 shows that for removing sulfur from the Raw Anthracene Oil, essentially same amount of surface areas of the two catalysts would be required. However, with regard to removing nitrogen, surface areas required of two catalysts would be different. This indicates that as far as the desulfurization of lighter stock such as Raw Anthracene Oil is concerned, the unit surface activity of the two catalysts is the same. But the surface activity towards denitrogenation is higher for the Monolith catalyst than for the Nalcomo 474 catalyst.

Figure 8 shows the comparison of the surface activities of the two catalysts on the heavier feedstock, i.e., Synthoil. In this case, the activity of the Monolith catalyst is far greater than that of the Nalcomo 474 catalyst. This behavior is different from that observed on the Raw Anthracene Oil, and as further discussion will show, this difference in the superiorities of the Monolith catalyst on the two feedstocks throws light on some interesting and important observations and conclusions of this study.

To have a quantitative idea of the higher unit surface area activity of the Monolith catalyst, rate constants based on surface area were considered essential to know. To accomplish this, the global reaction kinetics of desulfurization and denitrogenation were determined. For the desulfurization, the following three kinetic models, as suggested in literature, were tested to see as to which one best represented the data of this study.

$$(1) \text{ Second order; } \frac{1}{C_A} = kt + \frac{1}{C_{AO}}$$

- (2) Combination of two first order reactions; one for the lighter and the other for the heavier fractions of the stock;

$$\frac{C_A}{C_{AO}} = \alpha e^{-k_1 t} + (1 - \alpha) e^{-k_2 t}$$

where  $\alpha$  is the fraction of light or heavy component in the feed.

$$(3) \text{ First order; } \frac{C_A}{C_{AO}} = e^{-kt}$$

The second model was discarded because the value of the rate constant  $k_2$  found by the non-linear regression of data was approximately zero which was not considered reasonable on a physical basis. Of the other two models, the first model, i.e., the

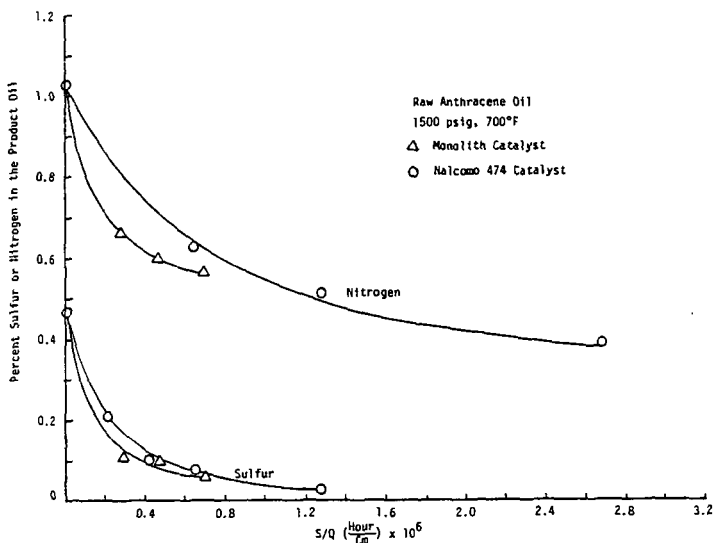


Figure 7: HDS and HDN Responses to the Change in Surface Area/Volumetric Flow Rate of Oil

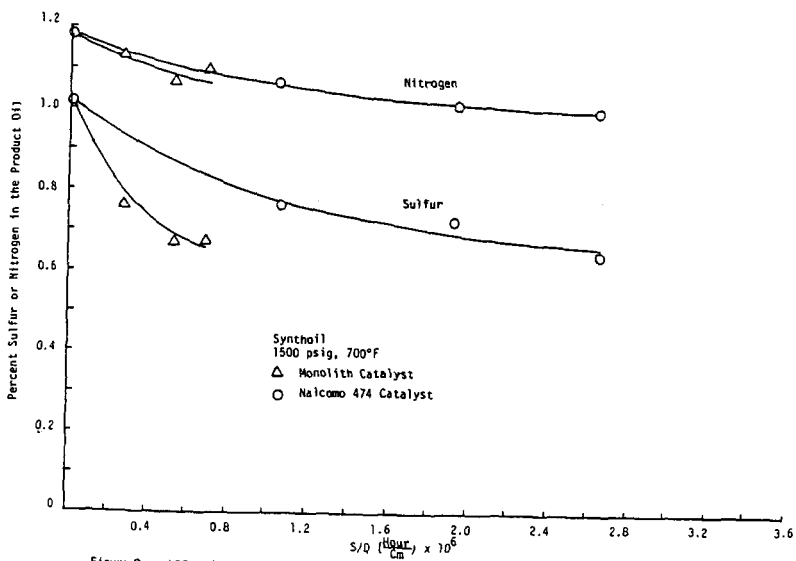


Figure 8: HDS and HDN Responses to the Change in Surface Area/Volumetric Flow Rate of Oil

TABLE V  
SECOND ORDER RATE CONSTANTS (VOLUMETRIC)

$$k, \frac{\text{cm}^3}{(\text{gm.})(\text{hour})}$$

	Raw Anthracene Oil		Synthoil	
	Monolith Catalyst	Nalcomo 474 Catalyst	Monolith Catalyst	Nalcomo 474 Catalyst
Desulfurization	8.68	48.8 <sup>a</sup>	0.427	0.431
Denitrogenation	0.724	1.4 <sup>b</sup>	0.084	0.134

TABLE VI  
SURFACE AREA RATE CONSTANTS

$$k, \frac{\text{cm}^4}{(\text{gm.})(\text{hour})}$$

	Raw Anthracene Oil		Synthoil	
	Monolith Catalyst	Nalcomo 474 Catalyst	Monolith Catalyst	Nalcomo 474 Catalyst
Desulfurization	2282	2400 <sup>a</sup>	108	25
Denitrogenation	190	81 <sup>b</sup>	24	8.5

<sup>a</sup>Corresponds to the volumetric rate constant obtained using Sooter's data (2)

<sup>b</sup>Corresponds to the volumetric rate constant obtained using Stachell's data (3)

second order rate expression was found to fit the data better. For denitrogenation, only the first and second order models were examined, and in this case also the latter model was found to represent the data better.

Table V gives the values of the second order rate constants for the HDS and HDN for both liquids and catalysts studied. The values of the rate constants for HDS and HDN of Raw Anthracene Oil using Nalcomo 474 catalyst were obtained by applying the same non-linear regression analysis technique to the data of Sooter (2) and Satchell (3). The comparison of the rate constants lead one to the same conclusion as shown by Figures 5 and 6.

The rate constant based on surface area,  $k_s$ , was calculated from the volumetric rate constants by using the following equation:

$$k_s = k \frac{V_r}{S}$$

where  $k$  = volumetric rate constant,  $\frac{\text{cm}^3}{(\text{hour})(\text{gm.})}$

$V_r$  = volume of the reactor,  $\text{cm}^3$

$S$  = total surface area of the catalyst,  $\text{cm}^2$

The values of  $k_s$  calculated for the various values of  $k$  are given in Table VI. In the case of Synthoil, the observed surface area rate constants for desulfurization as well as denitrogenation are about 3 to 4 times higher for the Monolith catalyst than those for the Nalcom 474 catalyst. This further confirms that the observed surface activity of the Monolith catalyst for treating heavier liquids is much higher than the commercial Nalcom 474 catalyst. However, in the case of Raw Anthracene Oil, the observed surface area rate constants for desulfurization are about the same for both catalysts and hence they have the same observed surface activity for this lighter feedstock. But the denitrogenation rate constant even on this liquid is higher for the Monolith catalyst than for the Nalcom 474 catalyst.

Thus, the Monolith catalyst seems to have potential superiority over the commercial catalysts used in this study, especially for treating high boiling stocks.

#### Reasons for the Higher Observed Unit Surface Area Activity of the Monolith Catalysts:

There can be three main reasons:

- (1) Intrinsic activity of the Monolith catalyst was higher than that of the Nalcom 474 catalyst.
- (2) Fluid dynamic effects in the reactor when Nalcom 474 catalyst was used did not provide efficient solid-liquid contacting.
- (3) There were severe diffusional limitations in the case of Nalcom 474 catalyst, which had a pore radius of  $33^{\circ}\text{A}$ , due to which its surface area utilization was very low as compared to surface area utilization in the case of Monolith catalyst which had pore radius of  $80^{\circ}\text{A}$ .

If one considers that the Monolith catalyst was intrinsically more active than the Nalcom 474 catalyst then the observed superiority of the Monolith catalyst should be almost the same, or at least have the same order of magnitude, when tested on two different feeds. But as explained earlier, the observed surface activities of the two catalysts for HDS are almost equal in the case of Raw Anthracene Oil, while on Synthoil the observed surface activity of the Monolith is about 4 times that of the Nalcom 474 catalyst. Therefore, there is sufficient ground to believe that the Monolith catalyst used in this study was not intrinsically more active than the Nalcom 474 catalyst as far as the HDS was concerned.

In previous studies, Sooter (2) and Satchell (3) observed that reducing the particle size of the Nalcom 474 catalyst from 8-10 mesh to 40-48 mesh did not have any significant effect on the desulfurization and denitrogenation of Raw Anthracene Oil under similar experimental conditions as employed in this study. This suggests that the fluid distribution and hence the fluid dynamic effects were not important in the trickle bed reactors as operated for this work. If these effects were important,

then the reduction in particle size should increase conversion, or the HDS and HDN, by improving fluid distribution and reducing the intraparticle diffusion resistances.

Under the likelihood that the first two reasons do not explain the results of this study or are not important in the present context, intraparticle diffusion limitations appear to be responsible for differentiating the activities of the two catalysts. Tables I and II show that the Synthoil is a high boiling liquid as compared to Raw Anthracene Oil. This means that the molecules that constitute Synthoil are larger on the average than the molecules that constitute the Raw Anthracene Oil. Therefore, the smaller pore size, 330A, of the Nalco 474 catalyst and its longer diffusion path, which is the radius of the catalyst particle, about 1 mm, would offer much higher intraparticle diffusion resistance to Synthoil molecules than to the Raw Anthracene Oil molecules. This would severely limit surface area utilization of Nalco 474 on Synthoil liquid but not as much on Raw Anthracene Oil. Therefore, observed unit surface area activity of Nalco 474 catalyst on Synthoil would be lowered appreciably as compared to the lowering of the activity of the same catalyst on Raw Anthracene Oil. On the other hand, pores of the Monolith catalyst are approximately two and a half times larger than the pores of the Nalco 474 catalyst. The diffusion path is only 0.114 mm, i.e., half the thickness of the channel wall. This is 1/9 times the diffusion path length of the Nalco 474 catalyst. Due to this, the Monolith catalyst would offer much less diffusion resistance to Synthoil molecules than that offered by Nalco 474 catalyst. Therefore, the percent surface area utilization of the Monolith catalyst would be much higher than the percent surface area utilization of the Nalco 474 catalyst. But the larger pore size and smaller diffusion length of the Monolith catalyst could not have any advantage when a lighter feedstock like Raw Anthracene Oil is processed because, as determined by Sooter (2) and Satchell (3), this feedstock does not have significant diffusion problems with the Nalco 474 catalyst.

To have a quantitative idea of the problem of intraparticle diffusion, "Effectiveness Factors" for the two catalysts were calculated from the observed reaction rates using the relationship between  $\eta$  and  $\eta(5)$  and the "triangle method" suggested by Satterfield (4). The Effectiveness Factors for the Monolith and Nalco 474 catalyst were found to be 0.94 and 0.216, respectively.

#### SUMMARY

The results of this study indicated that at the reactor operating conditions of 371 C and 1500 psig, the observed HDS activity based on unit surface area, was much higher for the Monolith catalyst as compared to the Nalco 474 catalyst when processing the heavier feedstock, i.e., Synthoil. But it was about the same when processing a lighter feedstock like Raw Anthracene Oil. Since the average pore radius and the intraparticle diffusion length of the Monolith catalyst were 87.6A and 0.114 mm against 31A and 1 mm of the Nalco 474 catalyst, the intraparticle diffusion was considered to be responsible for the lower observed activity of the Nalco 474 catalyst on the heavier feedstock. From the observed rates of reaction, the Effectiveness Factors for the Monolith and Nalco 474 catalysts were found to be 0.94 and 0.216, respectively, for the HDS of Synthoil.

#### REFERENCES

1. Satterfield, C.N. and F. Ozel, Paper presented at the American Institute of Chemical Engineers Meeting at Chicago, 17 C, (1976).
2. Sooter, M.C., Ph.D. Thesis, Oklahoma State University, Stillwater, OK. (1974).
3. Satchell, D.P., Ph.D. Thesis, Oklahoma State University, Stillwater, OK. (1974).
4. Satterfield, C.N., Mass Transfer in Heterogeneous Catalysis, M.I.T., Press, Cambridge, Mass. (1970).
5. Thiele, E.W., Industrial and Engineering Chemistry, 31, 7 (1939).

## THE THERMAL CRACKING OF COAL-DERIVED MATERIALS

R.S. Bernhardt, W.R. Ladner, J.O.H. Newman and P.W. Sage

National Coal Board, Coal Research Establishment, Stoke Orchard  
Cheltenham, Glos. GL52 4RZ, England

### SUMMARY

Up to 27% benzene, toluene and xylenes and 24% ethylene were obtained by cracking a highly hydrogenated coal extract, compared to less than 4% of each from unhydrogenated coal, coal extract and anthracene oil. The importance of naphthenes as BTX and ethylene precursors was confirmed.

### INTRODUCTION

Many of the feedstocks for the chemical industry, especially aromatic hydrocarbons, were originally obtained as byproducts from the carbonisation of coal (1,2). However, nowadays most of these chemical feedstocks are derived from petroleum. Nevertheless, it is probable that, within the next few decades, the shortage of world reserves of petroleum will mean that BTX will once again have to be produced from coal, as will ethylene. It is, therefore, appropriate to examine ways in which these materials can be produced from coal; the present investigation was designed to study the formation of BTX and ethylene by the thermal cracking of coal-derived materials from the NCB coal liquefaction/hydrogenation processes (3).

### EXPERIMENTAL

#### Feedstocks

The vapours from the carbonisation of a bituminous, low-rank coal, an anthracene oil and a coal extract in anthracene oil were diluted with nitrogen and cracked; their product yields were compared with those from the cracking of a partially hydrogenated anthracene oil and coal extracts hydrogenated to various extents. The coal was Linby (National Coal Board, Coal Rank Code 802) and the extract was prepared by digestion at 673 K and 8 bar in anthracene oil, filtration to remove mineral matter and dissolved coal, followed by distillation under reduced pressure until the extract contained about 70% coal. The two coal extract hydrogenates were prepared by catalytically reducing a dilute extract from Annesley (NCB, CRC 702) coal in a trickle bed reactor and fractionating the product. The fractions were further reduced in a vapour phase reactor to give two highly hydrogenated liquids.

Four model compounds, n-undecane, tetralin, cis/trans decalin and mesitylene, and a natural gas condensate from the North Sea were also cracked. Analyses and the reference code key of the coal-based feedstocks and the gas condensate are given in Table 1. Paraffin, naphthene and aromatic type analyses were calculated from gas chromatographic analyses of the partially hydrogenated anthracene oil and gas condensate, whereas mass spectrometric analysis was performed on the two coal extract hydrogenates and their further hydrogenated products.

#### Apparatus and Procedure

The experiments with the solid feedstocks and the initial experiments on liquid samples were carried out in the apparatus shown in Figure 1a. The vapours from a stainless steel, stirred-bed carboniser/vaporiser at 873 K were cracked at atmospheric pressure in a tube reactor heated in a platinum-wound furnace.

The reactor was 30 mm ID and had a 100 mm long hot zone within 20 K of the maximum reactor temperature. Solid feedstocks were introduced at about 1 g min<sup>-1</sup> from a vibratory table through a water-cooled port. Liquids were injected at the same point from a mechanically driven syringe at 0.1 to 0.8 ml min<sup>-1</sup>. The amount fed was determined by weighing the feeders.

Liquid products were collected in two glass traps at 258 K and in a glass wool filter. The gas was measured in a dry gas meter and sampled over mercury into glass bottles. The reactor and collection train were weighed and the liquids removed with a known amount of chloroform. The effects of vapour residence time and cracking temperature on the product yields from each feedstock were investigated. The effects of variables such as reactor surface, type and area, feedstock vapour concentration and the addition of steam was also tested over a limited range of conditions with a hydrogenated coal extract. Gaseous and liquid products were analysed by chromatography.

Later experiments with the hydrogenated feedstocks, which were completely vaporisable, were performed by injecting the liquids into the top of the smaller reactor (9 mm ID) shown in Figure 1b: the liquid feed rate was only a tenth of that required for the larger apparatus; the furnace and collection systems were similar. Comparative tests with cis/trans decalin and hydrogenated anthracene oil showed that the smaller reactor gave marginally higher BTX and ethylene yields than the larger reactor.

## RESULTS

### The Effect of Surface, Reactant Concentration and Diluent

Results from the cracking of a hydrogenated coal extract similar to (D) in the larger reactor with and without copper or stainless steel packing, which increased the surface area about threefold whilst decreasing the reactor volume by only 10%, showed that neither copper nor stainless steel significantly affected the yields of BTX and ethylene. An eightfold reduction in the concentration of the feedstock vapour (at constant vapour residence time) also had no significant effect. Replacement of part of the diluent nitrogen to give a 70% steam + 30% nitrogen mixture had a negligible effect on the yields of BTX and ethylene although xylenes were favoured at the expense of benzene.

### Unhydrogenated Coal-derived Materials

Preliminary experiments on cracking the vapour from coal extract (B) at 1133 K for 0.7 to 8 s showed that the BTX yield peaked at 2 s whereas ethylene was favoured by shorter residence times. Figure 2 shows the effect of cracking temperature at 2 s vapour residence time on the yields of BTX, benzene and ethylene from Linby coal (A), coal extract (B) and anthracene oil (C). Yields of BTX and benzene peaked at about 1273 K whereas the maximum ethylene yields were obtained at about 1100 K. The mass balances and yields of the gaseous and liquid products at one condition, 1273 K for 2 s, are given in Table 2.

The yields of BTX and ethylene are low, less than 3.5% BTX and 1.5% ethylene: the highest yields were from Linby coal. Although the BTX yields are greater than the 1% from conventional, high temperature coal carbonisation (2), they are only a fraction of those obtainable from petroleum feedstocks (4).

### Hydrogenated Coal-derived Materials

The yields from the partially hydrogenated anthracene oil (C1), two coal extract hydrogenates (D and E) and their further hydrogenated products (D1 and E1) when cracked at 1133 K, which favoured ethylene formation, are listed in Table 2 together with the yields from the gas condensate at 1158 K. The BTX,

benzene and ethylene yields from the two further hydrogenated materials (D1 and E1) are plotted against cracking temperature in Figure 3.

Table 2 shows that the parent hydrogenates (D and E) gave relatively low yields of BTX and ethylene (<10%) whereas considerable yields of polynuclear aromatics such as naphthalene, methyl naphthalenes, acenaphthylene, fluorene, anthracene and phenanthrene were obtained. In contrast, the further hydrogenated materials (D1 and E1) gave higher yields of BTX and ethylene (>20%) and relatively low yields of polynuclear aromatics. The highest yields of BTX, 27% at 1083 K for 1 s and at 1108 K for 0.4 s, and of ethylene, 24% at 1158 K for 0.4 s, were both obtained from D1. The curves in Figure 3 for a vapour residence time of 0.4 s show broad maxima in BTX and ethylene yields; similar maxima were obtained at 1 and 2 s but at slightly lower cracking temperatures.

The yields from the partially hydrogenated anthracene oil (C1), also given in Table 2, are relatively low, little more than 10% BTX and ethylene being obtained.

#### Natural Gas Condensate

To compare the yields from coal-derived materials with those from a petroleum material, a full range, North Sea gas condensate (F) was cracked at 1158 K for 0.4 s. Its analysis is given in Table 1 and the yields obtained are listed in Table 2. More ethylene (30%) but less BTX (16%) were produced than from the highly hydrogenated coal materials.

#### Model Compounds

Four model compounds (mesitylene for aromatics, tetralin for hydroaromatics, decalin for naphthenes and n-undecane for paraffins) were cracked singly and as mixtures at 1133 K for 1 s. The yields of BTX, ethylene, butadiene and methane are shown as a bar chart in Figure 4. Decalin gave the highest BTX yield, 25%, compared with less than 7% from n-undecane. Mesitylene gave only 8% BTX. Tetralin produced the least BTX, 3%, its major products being polynuclear aromatics. n-Undecane gave 37% ethylene compared to 20% from decalin, 3% from tetralin and 0.2% from mesitylene. Six binary, four ternary and the quaternary mixtures of the four compounds were cracked and the observed product yields were within  $\pm 2\%$  of the values calculated from the constituents' yields.

#### DISCUSSION

The low yields of BTX and ethylene from the unhydrogenated feedstocks reflect the stability of the condensed aromatic structures which constitute much of their volatiles and confirm the findings of a literature review (5). It is interesting that the coal extract (B), which contained 70% coal, yielded even less BTX and ethylene than the coal itself; this is probably due to elimination of reactive constituents and cross-linking during digestion/extraction of the coal.

Yields of BTX and ethylene increased with increasing extent of hydrogenation of coal extract, as indicated by the H/C ratios listed in Table 1. This was reflected in their naphthene contents, which were in the order D1 > E1 > D > E, and confirms the finding (6) that polynuclear aromatic hydrocarbons need to be fully hydrogenated to the naphthenic structure to maximise their conversion to BTX and ethylene. Concomitantly, the yields of tar and polynuclear aromatics decreased with decrease in the (hydroaromatic + aromatic) content of the feedstock, suggesting that the higher aromatics result from the dehydrogenation of hydroaromatics to the parent aromatics and from the survival of those aromatic hydrocarbons already present. 34% of C<sub>2</sub>-C<sub>4</sub>

gaseous hydrocarbons ( $C_2H_6$ ,  $C_2H_4$ ,  $C_3-C_4$  unsaturates and saturates) were obtained from E1 at 1133 K for 0.4 s (up to 17%  $C_3-C_4$  unsaturates were obtained at a lower cracking temperature of 1083 K). The sum of BTX + valuable gaseous hydrocarbons amounted to 55% at 1133 K, 60% at lower temperatures.

Some acetylene and polyacetylenes, which are undesirable, explosive byproducts, were also formed. The amount increased with the severity of cracking but was only 2.5% of the maximum ethylene yield; this value is about that found in the industrial cracking of petroleum naphtha to ethylene (7,8).

Cracking temperature and vapour residence time were the most important parameters controlling the cracking reactions. Within the range of conditions tested, other variables such as type and area of cracking surface, the vapour concentration of the feedstock and presence of steam made little difference to the yields of BTX and ethylene. Steam is used as a diluent and carrier in industrial ethylene crackers, where it reduces carbon laydown in the reactors (9).

The aromatic and hydroaromatic components of coal-derived feedstocks are potential sources of carbon laydown and steam would be needed to reduce reactor fouling.

The high ethylene and moderate BTX yields from the gas condensate are commensurate with its 56% paraffin and 12% naphthene content (see Table 1). This was confirmed by the 37% ethylene and 7% BTX obtained from the model paraffin, n-undecane (see Figure 4).

The model compound studies confirmed that the molecular structure of the hydrogenated coal extract is of paramount importance in determining the product pattern: hydroaromatics dehydrogenate to aromatics, which either survive or polymerise to tars and, eventually, to carbon; naphthenes crack principally to BTX and ethylene; aliphatics mainly give small unsaturates such as ethylene and butadiene. The abnormally low yield of BTX from mesitylene is attributed to its high symmetry and thermal stability.

## CONCLUSIONS

The results from the thermal cracking of unhydrogenated and hydrogenated coal-derived materials, a gas condensate and model compounds led to the conclusions that:

- (i) only low (< 3.5%) BTX and ethylene yields were obtained by cracking the vapours from a bituminous coal, an anthracene oil and the anthracene oil extract of the coal;
- (ii) the BTX and ethylene yields increased with increasing extent of hydrogenation of the extract (which increased the naphthene content); tar was mainly derived from the aromatic and hydro-aromatic components;
- (iii) about 27% BTX and 24% ethylene were obtained from the highly hydrogenated coal extract; in comparison, a paraffinic North Sea gas condensate gave 16% BTX and 30% ethylene;
- (iv) the product yields from mixtures of model compounds were predicted to within  $\pm 2\%$  from those of the constituents.

#### ACKNOWLEDGEMENTS

We thank the National Coal Board for permission to publish this paper and the European Coal and Steel Community for financial support. The views expressed are those of the authors and not necessarily those of the National Coal Board.

#### REFERENCES

1. Lowry, H.H., The Chemistry of Coal Utilisation, Supplementary Volume, John Wiley and Sons Inc., New York, 1963.
2. Dryden, I.G.C., Carbonisation and Hydrogenation of Coal, United Nations, 1973.
3. Thurlow, G.G., The Chemical Engineer, 733, October 1978.
4. Wett, T., The Oil and Gas Journal, 71, 73 November 26, 1973.
5. Ladner, W.R., Newman, J.O.H. and Sage, P.W., to be published in J. Inst. Energy.
6. Korosi, A., Woebecke, H.N. and Virk, P.S., Am. Chem. Soc., Div. Fuel Chem. Preprints, 21 (6), 190 (1976).
7. Krönig, W., Hydrocarbon Processing, 49 (3), 121 (1970).
8. Prescott, J.H., Chem. Eng., 82 (14), 52 (1975).
9. Miller, S.A., Ethylene and Its Industrial Derivatives, Ernest Benn Ltd., London, 1969.

Table 1 Analysis of Feedstocks

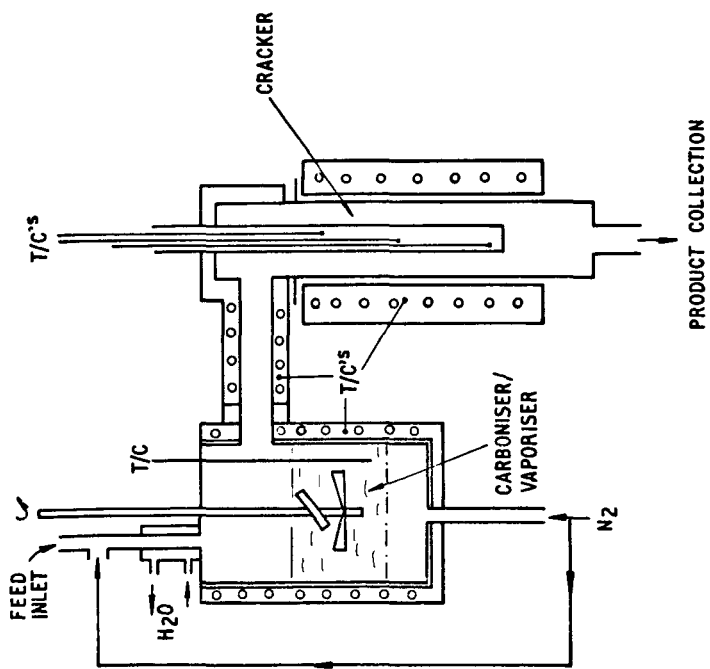
Solid Feedstock	Key	Size, $\mu$ m	Proximate Analysis, % w/w			Ultimate Analysis, % w/w d.a.f.						H/C atomic ratio
			Moisture, a.d.	Ash, a.d.	V.M. d.a.f.	C	H	O	N	S		
Lumpy coal	A	210 to 350	8.3	6.0	39.1	82.4	5.3	9.0	1.95	1.00	0.77	
	B	210 to 350	0.3	0.3	50.5	88.7	4.8	3.8	1.90	0.55	0.65	
Liquid Feedstocks												
Anthracene oil	C	573 to 673										
Partially hydrogenated anthracene oil	D	449 to 505										
Hydrogenated coal extracts	E	523 to 573										
Further hydrogenated coal extracts	G	443 to 570										
Natural gas condensate	F	619 to 625										

N.D. = Not Determined

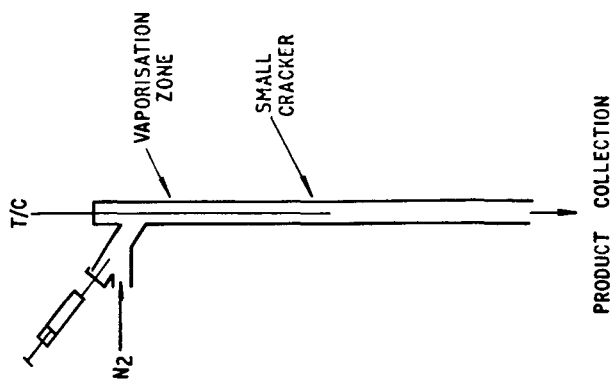
Table 2 Yields from Cracking Coal-derived Feedstocks and a Natural Gas Condensate

Yield		g w/g									
Cracking Temperature, °C		1273		1373		1473		1573		1673	
Vapour Residence Time, s		2.0		1.0		0.4		0.4		0.4	
Feedstock	Product	Anthrane oil linby coal*		Anthrane oil		Partially hydrogenated anthracene oil		Hydrogenated coal extract		Hydrogenated coal extract	
		A	B	C	D	E	F	G	H	I	J
Benzene		3.1	1.8	2.1		6.6		3.5		17.1	13.5
Toluene		0.1	0	0		2.7		1.9		5.3	5.1
Xylene		0	0	0		1.3		1.7		3.0	2.8
Total HTX		3.2	1.8	2.1		10.6		7.1		25.4	21.4
Cl <sub>4</sub>		4.3	2.6	2.7		8.2		6.4		12.0	10.8
C <sub>2</sub> H <sub>6</sub>		0.2	0	0		0.8		1.0		1.5	1.7
C <sub>2</sub> H <sub>4</sub>		0.3	0.1	0.09		10.8		9.1		23.1	21.5
C <sub>2</sub> H <sub>2</sub>		N.D.	N.D.	N.D.		0.3		0.1		0.4	0.1
C <sub>3</sub> -C <sub>4</sub> nats.		0.4	0.1	0		0		0.05		0.1	0.2
C <sub>3</sub> -C <sub>4</sub> unnat.		0	0	0		1.8		3.4		7.9	10.6
H <sub>2</sub>		1.3	1.0	1.3		1.2		1.1		0.9	1.3
CO		7.8	1.7	1.6		0		0		0	0
CO <sub>2</sub>		3.8	0.4	0.4		0		0		0	0
Indene		< 0.01	< 0.01	< 0.01		1.3		3.4		7.2	1.8
Naphthalene		0.3	0.2	1.4		19.5		23.5		15.6	5.3
Methyl naphthalenes		< 0.01	< 0.01	< 0.01		3.1		7.9		8.6	1.3
Diphenyl		0.03	0.01	< 0.01		1.1		3.3		4.1	0.4
Acenaphthylene		0.09	0.06	0.07		1.8		3.9		5.1	0.9
Fluorene		0.01	0	0.07		0.5		0.5		2.2	0.3
Anthracene and phenanthrene		0.2	0.2	1.7		1.4		0.4		6.0	0.2
Fluoranthene		0.06	0.2	0.4		0		0.3		0.2	0
Pyrene		0.06	0.2	0.4		0.5		0.3		0.3	0
Mass Balance											
Gas		21	13	8		28		24		20	57
Liquid/Lar		17	15	56		46		69		82	31
Solid		61	72	23		10		10		5	11
Total		99	100	87		84		103		107	99

\* Carbonation temperature 873 K.  
N.D., Not Determined



1a. CARBONISER/VAPORISER/CRACKER



1b. SMALL VAPORISER/CRACKER

FIGURE 1. CRACKING APPARATUS

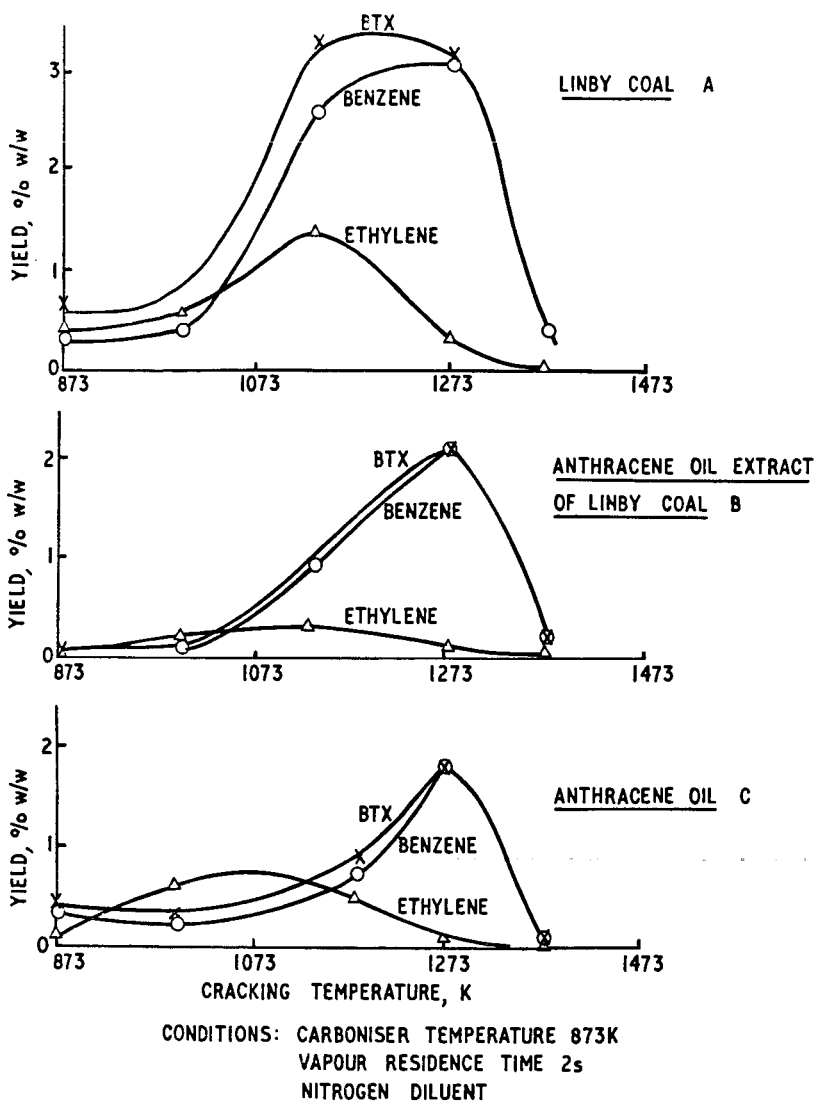
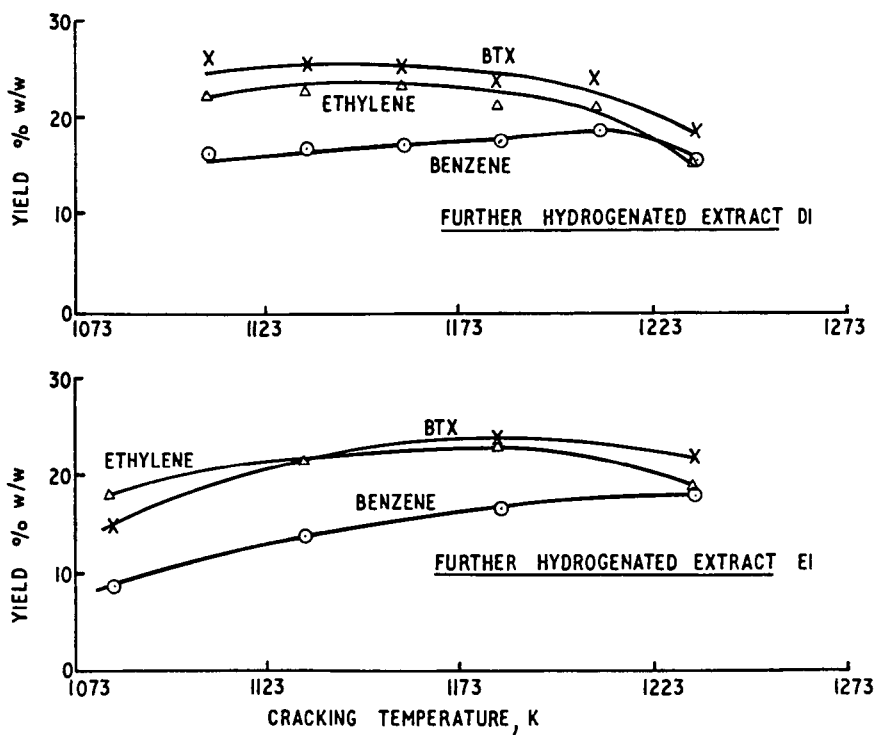
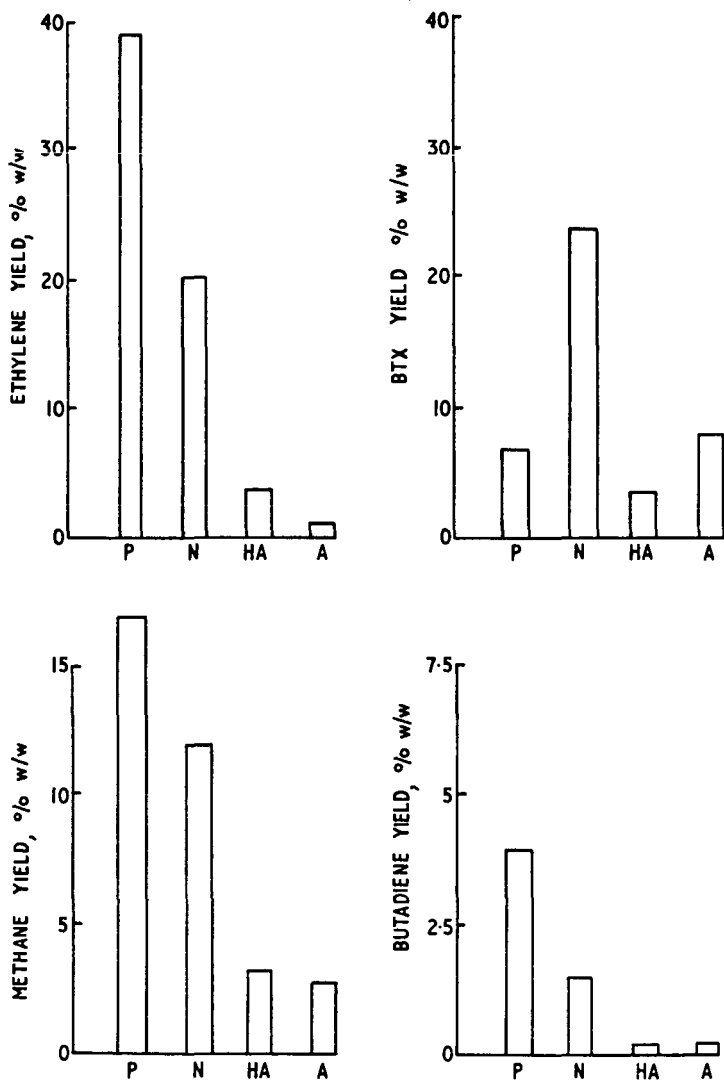


**FIGURE 2. THE EFFECT OF CRACKING TEMPERATURE ON YIELDS OF BTX, BENZENE AND ETHYLENE FROM UNHYDROGENATED COAL MATERIALS.**



CONDITIONS: VAPOUR RESIDENCE TIME 0.4s  
NITROGEN DILUENT

FIGURE 3. THE EFFECT OF CRACKING TEMPERATURE ON YIELDS OF  
BTX, BENZENE AND ETHYLENE FROM FURTHER  
HYDROGENATED EXTRACTS.



CRACKING TEMPERATURE 1133K  
VAPOUR RESIDENCE TIME 1s

KEY: PARAFFIN P=n-UNDECANE; HYDROAROMATIC HA= TETRALIN;  
NAPHTHENE N= CIS/TRANS DECALIN; AROMATIC A=MESITYLENE

FIGURE 4. THE VARIATION OF YIELDS WITH HYDROCARBON TYPE